Selective hydrogenation of acrolein over supported silver

and silver alloy catalysts

BY

HAOJUAN WEI
B.S., Nanjing University, 2004
M.S., Nanjing University, 2007

THESIS

Submitted as partial fulfillment of the requirements
for the degree of Doctor of Philosophy
in Chemical Engineering in the Graduate College of the
University of Illinois at Chicago, 2013

Chicago, Illinois

Defense Committee:
 Randall Meyer, Chair and Advisor
 Jeff Miller, Argonne National Laboratory
 Chris Marshall, Argonne National Laboratory
 Robert Klie, Physics
 Neal Mankad, Chemistry

ACKNOWLEDGMENTS

Looking back on my four and a half year as a graduate student, there were excitement of making breakthroughs, confusion of contradictory results, enjoying running an overnight experiment, tension in a practice for an oral presentation and confidence to present my achievement in public and many memorable moments. I learned that to be a good researcher I needed to be intelligently, mentally and physically ready all the time. This dissertation would not have been possible without the help of several individuals.

First and foremost, I would like to thank my advisor Dr Randall Meyer, who is warm-hearted to people and enthusiastic to work. His strict and meticulous attitude towards research influenced me deeply. I really appreciate the guidance he provided. I also appreciate Dr Jeff Miller. His knowledge in the field of heterogeneous catalysis and brilliant ideas inspired me greatly during my research.

I also would like to thank Dr Chris Marshall for providing precious advice and the resources of his lab. Dr Neng Guo gave a lot of help when I started the project. Dr Rodrigo Lobo, Dr Tianpin Wu and Dr Neil Schweitzer offered help in experiments and valuable discussions. In addition, I want to than Jinjing Liu, Dr Robert McCoy, Dr Richard Pauls and Jeremy Kropf for their amazing technical expertise.

Last but not the least, I want to thank my family as well for their unconditional love and support.

TABLE OF CONTENTS

LIST OF FIGURES

LIST OF TABLES

LIST OF ABBREVIATIONS

acac   Acetylacetonate

APS   Advanced photon source

BEP   Brønsted−Evans−Polanyi

CN   Coordination number

cNEB   climbing nudged elastic band

DFT   Density functional theory

DI   Deionized

DP   Deposition precipitation

EDX   Energy-dispersive X-ray spectroscopy

EXAFS   Extended X-ray absorption fine structure

FID   Flame ionization detector

GC   Gas chromatography

GC-MS   Gas chromatography-Mass spectrometry

GGA   Generalized gradient approximation

HAADF   High angle annular dark field

HREELS   High resolution electron energy loss spectroscopy

HRTEM	High resolution transmission electron microscopy
HTR	High temperature reduction
HTS	High temperature shift
I	Impregnation
ICP	Inductively coupled plasma
ICP-OES	Inductively coupled plasma-optical emission spectrometry
IRA	Infrared absorption
IWI	Incipient wetness impregnation
LTR	Low temperature reduction
LTS	Low temperature shift
mIWI	modified incipient wetness impregnation
ML	Monolayer
MPV	Meerwein-Ponndorf-Verley
MRCAT	Materials research collaborative access team
MSR	Methanol steam reforming
MTP	Multiple twinned particle
NEXAFS	Near edge X-ray absorption fine structure

PAW   Projector-augmented wave

PW   Perdew Wang

RAIRS   Reflection absorption infrared spectroscopy

RRC   Research resources renter

SAA   Single atom alloy

SEA   Strong electrostatic adsorption

SG   Sol gel

SMSI   Strong metal support interaction

SSHC   Single site heterogeneous catalyst

STEM   Scanning transmission electron microscope

TCD   Thermal conductivity detector

TEM   Transmission electron microscopy

TOF   Turnover frequency

TOR   Turnover rate

TPD   Temperature programmed desorption

TPR   Temperature programmed reaction

TS   Transition state

UHV	Ultra high vacuum
VASP	Vienna ab initio simulation package
WGS	Water gas shift
XANES	X-ray absorption near edge structure
XAS	X-ray absorption spectroscopy
XPS	X-ray photoelectron spectroscopy
XRD	X-ray diffraction

Summary

This thesis aims to investigate multiple critical properties of catalysts which can affect the activity and selectivity greatly in heterogeneous catalysis. Two reactions which attract wide and extensive attention were chosen as test reactions for this study: the selective hydrogenation of α,β-unsaturated aldehyde to α,β-unsaturated alcohol (using acrolein as model reactant) and the water gas shift reaction. The former was studied experimentally and the latter was studied theoretically.

For the selective hydrogenation of acrolein to allyl alcohol , it is a particularly difficult reaction to obtain satisfying selectivity towards C=O bond hydrogenation thermodynamically and kinetically. The hydrogenation of C=C bond is about 35 kJ/mol easier than that of C=O bond. In the particular case of acrolein, the lack of substituents at C=C bond makes it especially vulnerable to hydrogenation. Previous research has made great progress in understanding some of the factors (choice of metal, process condition) that may improve selectivity. But no catalyst exists with both high activity and selectivity. Thus we studied this reaction systematically from four aspects: 1) particle size effects; 2) support effects; 3) utilizing single atom alloy to improve the performance of catalysts; 4) employing single site heterogeneous catalysts. Some of the aspects were well understood through our study and others results were preliminary but very intriguing and promising.

For the water gas shift reaction, the effect of alloying was studied for a particular example: PdZn. Previous research showed that Pd-Zn alloy was a promising catalyst for the related steam reforming of methanol and that its electronic structure closely mimics that of Cu, the commercial WGS catalyst. Three mechanisms of water gas shift were

investigated on PdZn(111) and NiZn(111) surfaces. NiZn was expected to be a cheaper substitution for PdZn. But despite its close similarly, NiZn actually shifts the primary mechanism from the carboxyl route to one where both the redox route and the carboxyl route are important.

1   INTRODUCTION

1.1   Factors influencing heterogeneous catalysis

Heterogeneous catalysis plays a crucial role in many industrial processes. In contrast to its counterpart homogeneous catalysis, heterogeneous catalysis excels because less waste is generated (especially toxic organic solvents and reagents) and separation and recycle of the catalysts are easier. As a result, processes catalyzed by heterogeneous catalysts are more easily scalable. A good catalyst should provide satisfactory activity, selectivity and stability. However, among these three essential properties, selectivity is the least well understood in heterogeneous catalysis [1]. It is very important to understand the driving force of the reaction pathways and lead the reaction towards the desired direction, i.e. 100% selectivity to the preferred product is ultimately required. Only in this way can we make the best use of the materials, produce less waste and even save the energy for separation and purification.

There are many factors which influence catalyst performance: choice of metal, particle size, choice of support, process conditions, addition of promoters or alloying. In this thesis each of these factors will be explored for two model reactions: acrolein hydrogenation (all of the factors mentioned above) and water gas shift (alloying). We will begin our discussion of these factors through a review of the relevant literature for acrolein hydrogenation before illustrating the specific effects in detail in the various chapters: Chapter 2 (particle size effects, process conditions), Chapter 3 (support effects), Chapter 4 (alloying effects), and Chapter 5 (choice of metal). In Chapter 6 we will discuss alloying effects in water gas shift before making some summarizing statements

and suggestions for future work in Chapter 7.

The first candidate reaction we chose to examine is the selective hydrogenation of α, β–unsaturated aldehydes. It is of commercial interest because the product α, β–unsaturated alcohols are important intermediates in the production of fine chemicals, flavors, perfumes and pharmaceuticals [2, 3]. For example, cinnamyl alcohol is used in perfumery as a component of various flower compositions and benzyl alcohol is a general solvent for inks, paints and resins [4]. However, selective hydrogenation of the C=C double bond is thermodynamically favored over hydrogenation of the C=O bond of the aldehyde by ~ 35 kJ/mol [5] so kinetic control is required. Thus this reaction is of scientific interest as well. As illustrated in the scheme of reaction pathways in hydrogenation of α, β–unsaturated aldehydes (Fig. 1), there are side reactions, i.e. the hydrogenation of C=C bond and further reduction resulting in a saturated alcohol (or potentially even full hydrogenation to propane). Cracking or aldol condensation may also occur. Therefore, the search for an active and selective catalyst presents a challenging problem.

Generally the hydrogenation of C=O bond in α, β–unsaturated aldehydes can be accomplished by classical solution methods using hydride donors, such as $LiAlH_4$ and $NaBH_4$ [6]. Meerwein-Ponndorf-Verley (MPV) reduction (aluminum catalyzed reduction of aldehydes and ketones by alcohols) is also highly specific for hydrogenation of C=O bonds [7]. Currently, the primary method for the manufacture of allyl alcohol is the alkaline hydrolysis of allyl chloride as developed by Shell and Dow [8]. However, the general low activities, difficulties in separation and recovery of the catalysts, and the subsequent environmental and economic issues limit the application of these

homogeneous reactions on a large scale and therefore replacement processes are desirable. By contrast, processes employing heterogeneous catalysts are more environmentally friendly and cost efficient. Gas phase reactions are particularly easier because no solvent and no product separation is needed. Celanese Corporation [9] reported that allyl alcohol could be produced from hydrogenation of acrolein in vapor phase over Ag-Cd alloy catalysts supported on SiO_2 or Al_2O_3. The best yield was 70% at 100% conversion. However, Cd is very toxic so its use should be avoided. In addition, the yield is still lower than commercial process hydrolysis of allyl chloride (85 - 95% yield). Nonetheless, if a more active and selective catalyst could be developed then it would have the potential to replace the hydrolysis method.
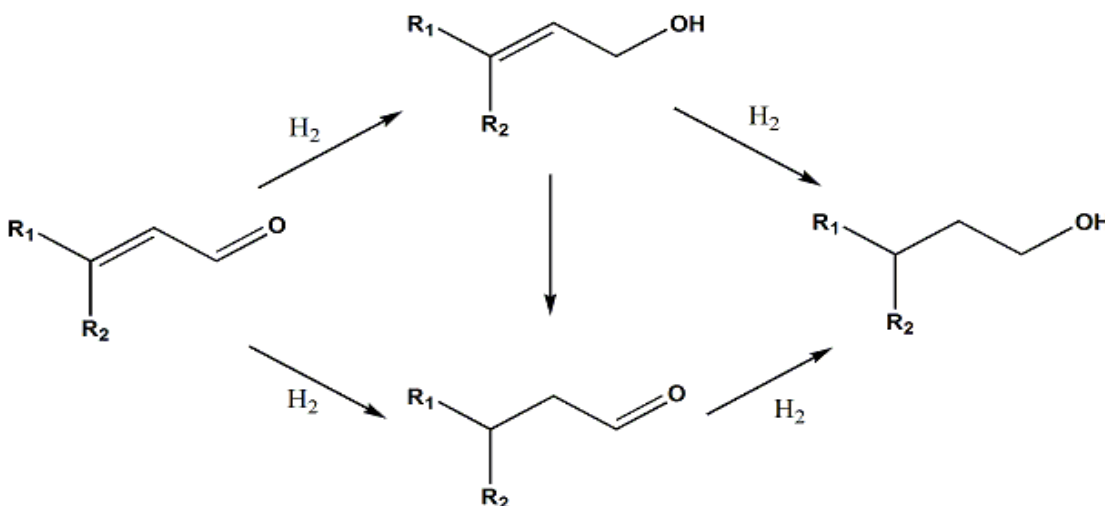
Fig. 1 Reaction scheme for the hydrogenation of α, β–unsaturated aldehydes

In an earlier research of Delbecq and Sautet [10] using semi-empirical extended Hückel calculations to study the adsorption of a variety of α, β–unsaturated aldehydes on Pt and Pd crystal surfaces, the selectivity was determined to be related to electron

3

attraction-repulsion effect between the adsorbates and the metal surface. The binding energy of the C=C bond will decrease as a result of an increase in the repulsive four-election interactions with the metal. i.e., the combination of the presence of substituents on the C=C bond and a metal having extended *d*-orbitals (like Os, Ir) leads to Pauli repulsion.

Acrolein, which is the simplest α, β–unsaturated aldehyde, is an ideal model compound to investigate the selective hydrogenation reaction. Because there are no functional groups on the ethylenic double bond ($R_1=R_2=H$ in Fig. 1), no *trans-* or *cis-* products will be formed during hydrogenation process and analysis of the products is therefore comparatively simple. In addition, acrolein is very volatile (its boiling point is only 53 ℃) and the reaction can be studied in the gas phase. However, it is found in many studies that bulky substituents facilitate high selectivity to unsaturated alcohols [3, 11-13]. The substituents not only sterically hinder the interaction between C=C double bond and the surface of catalyst, but also have an electronic and inductive effect that may deactivate the C=C bond. The simplicity of acrolein (which lacks these substituent groups) ironically makes it the most difficult among all the α, β–unsaturated aldehydes to be selectively hydrogenated.

In this work we focused on developing an understanding of how the nature of the catalyst affects its selectivity and activity. Selective hydrogenation of acrolein to allyl alcohol was employed as our primary test reaction because it is a thorny problem needing improvement and it presents an intriguing selectivity play between hydrogenation of an aldehyde functionality and hydrogenation of a double bond. Such chemistry may also prove important in the upgrading of biomass derivatives to fuels [14]. Any enhancement

4

in raising selectivity in acrolein hydrogenation will benefit the research on any other selective hydrogenation of α, β–unsaturated aldehydes (as well as α, β–unsaturated ketones) and even be inspiring to some other reactions demanding high selectivity. Silver based supported nanoparticle catalysts were chosen as the standard in this thesis for understanding the basic and important properties in favor of producing the desired product allyl alcohol. As mentioned above, we then systematically examined a variety of effects to perturb the reactivity and selectivity to improve the performance with the hope that through increased understanding, new standards for selectivity could be achieved.

1.2 Factors important to selectivity in acrolein hydrogenation

Many factors can influence the activity and selectivity of heterogeneous catalysts, including the metal particle size and shape, the interaction of the metal and support, the reaction conditions and the presence of alloys and promoters. Here we will discuss examples from the literature to highlight several critical factors that are important for a good catalyst for partial hydrogenation of acrolein to allyl alcohol.

1.2.1 Choice of active metal

Conventional hydrogenation catalysts involving late d-band transition metals such as Pd, Pt, Rh, Ru, etc. as active metals usually have poor performance in selective hydrogenation of acrolein. Marinelli [15] *et al.* reported that Pt/Aerosil 200 has only 1.6% selectivity to allyl alcohol when tested at 80 °C in a fixed-bed reactor. Hoang-Van and Zegaoui [16] tried platinum catalysts on different supports. Pt/Al$_2$O$_3$ and Pt/black showed

zero-selectivity to allyl alcohol while Pt/SiO_2 had merely 0.4% selectivity. Co/Al_2O_3, Ni/Al_2O_3 and Ru/ZrO_2 catalysts prepared and tested by Coq [17] *et al.* all showed excellent selectivity initially (43%, 59% and 74% respectively) but the selectivity of these catalysts dropped rapidly to a level of 5-10%. For example, for a Ru/Al_2O_3 catalyst having the initial selectivity of 31.4%, the selectivity to allyl alcohol dropped to about 16% after 30 minutes and to about 7% after an hour. Gyorffy and Paál [18] conducted a detailed investigation of acrolein hydrogenation on a series of PdPt powder catalysts prepared by colloid synthesis. They compared product distribution at different temperatures, but no selectivity to allyl alcohol was observed for any of these catalysts.

Surprisingly two hydrogen-inert metals, silver and gold, have much better selectivity to desired hydrogenation product allyl alcohol [5, 19-25]. While platinum can dissociate H_2 molecules readily, even at temperatures as low as -173 °C, providing atomic hydrogen for reaction, silver and gold barely adsorb and dissociate H_2 on their surfaces and are traditionally considered inert for hydrogenation/ dehydrogenation [26]. Therefore, it is very interesting to observe high selectivity to unsaturated alcohol in the partial hydrogenation reaction of acrolein over coinage metal catalysts.

Although the bulk material is unreactive, highly dispersed supported gold catalysts have garnered much interest due to their unusually high activities in many reactions [20]. Three Au/TiO_2 catalysts were synthesized by Claus' group [19], each by a different method: deposition precipitation (DP), impregnation (I), and sol gel technique (SG). Another gold supported on zirconia (Au/ZrO_2-F) was prepared by co-precipitation. At 180 °C, Au/TiO_2-DP and Au/TiO_2-I showed similar selectivity to the desired unsaturated alcohol, 41% and 43% respectively. However, no allyl alcohol was produced on Au/TiO_2-

SG or Au/ZrO$_2$-F under the same reaction condition. When the temperature was brought up to 240 °C the catalysts exhibited different selectivity in the following series: Au/TiO$_2$-I > Au/TiO$_2$-DP > Au/TiO$_2$-SG = Au/ZrO$_2$-F. The highest selectivity at 240 °C was obtained on Au/TiO$_2$-I (26%). Later a series of zirconia supported gold catalysts were studied by the same group [21]. The most selective Au/ZrO$_2$ catalyst, prepared by precipitation at pH = 5 and reduced at 450 °C, gave 37% selectivity at 5% conversion.

Silver catalysts have also been shown to be good candidates for acrolein hydrogenation. Grünert [23] *et al.* employed Ag/TiO$_2$ catalysts in the gas-phase hydrogenation of acrolein. Catalysts were prepared by incipient wetness impregnation using AgNO$_3$ as the silver precursor on P25 TiO$_2$ followed by calcination and reduction. For example, a Ag/TiO$_2$ catalyst reduced at 200 °C was able to selectively convert 41.8% of acrolein to allyl alcohol at 200 °C and 2 MPa pressure. The activity of this Ag/TiO$_2$ catalyst was 85.3 μmol g_{Ag}^{-1} s^{-1}, which was almost two times of that of the gold catalyst mentioned before (44 μmol g_{Au}^{-1} s^{-1} [21]). Silica supported silver catalysts were also investigated [25]. Other silver catalysts, *i.e.*, silver sputtered on aluminum foil (Ag/Al-S) or on silica (0.2Ag/ SiO$_2$-S), electrochemically deposited silver (Ag/Al-E) and bulk silver (single crystals and foil), were also catalytically tested for comparison with catalysts prepared via more traditional methods such as incipient wetness impregnation (IW) and deposition precipitation (DP). Catalysts were tested at 250 °C and two pressure ranges: low pressure (~ 1 bar) and high pressure (5-20 bar) No conversion was observed over single crystals or electrolytic silver. At 1 atm, Ag/Al-S and 0.2Ag/SiO$_2$-S mainly produced propanal and exhibited less than 5% selectivity to allyl alcohol. Ag/SiO$_2$-IW gave selectivity up to 28% under almost the same conditions. The 0.2Ag/SiO$_2$-S catalyst

had 23% selectivity to allyl alcohol when tested at 20 bar but at a conversion of less than 5%. Under the same conditions, the other two silica supported samples prepared by IW or DP had selectivities of 42% and 39% respectively at conversions of ~25%.

1.2.2   Effect of support

Supports can often participate in the catalytic reactions directly or indirectly by interacting with supported active metals and altering their properties. Volckmar *et al.* has examined the influence of the support acidity on the gas phase hydrogenation of acrolein over Ag/SiO_2-Al_2O_3 catalysts by varying the SiO_2:Al_2O_3 ratio via changes in the Al_2O_3 content from 0 to 100% Al_2O_3 in 20% steps [27]. The acidity of catalysts was measured by temperature programmed desorption of adsorbed ammonia ("NH_3-TPD") and infrared spectroscopic investigation of the adsorption and desorption of pyridine ("pyridine-IR"). The catalytic performances were tested via gas phase hydrogenation of acrolein. TEM images were taken before and after reactions for each catalyst to obtain particle sizes. Although the catalysts had different average particle sizes of silver before reaction, the sizes became almost uniform after reaction (~ 4.8 nm) except the one supported on silica without any alumina (1.9 nm). As a result, the differences in selectivities and activities could be ascribed to the varying support properties for these samples having similar particle sizes of silver. From NH_3-TPD and pyridine-IR results, the highest total acidity with both the most and strongest of Lewis acid sites were achieved at medium Al_2O_3 contents (40% and 60%). These catalysts also showed low TOF and selectivity to allyl alcohol. A conclusion was drawn that a decrease in the total acidity and the number of strong Lewis acid sites would lead to a better selectivity and activity.

Strong metal support interaction (SMSI) is commonly observed when using reducible oxides as support, i.e. TiO_2, CeO_2 and ZrO_2. The performance of Au/TiO_2, Au/ZrO_2 and Au/ZnO were tested in the hydrogenation of acrolein [19, 21]. SiO_2 supported gold catalysts (which do not exhibit SMSI) converted 23.4% acrolein to allyl alcohol [19]. Although TiO_2 exhibited stronger interaction with gold than ZrO_2 [21], better selectivity was obtained on the reducible oxide supports. Different synthesis methods were claimed to have great influence on the gold particle sizes, occurrence of multiple twinned particles (MTPs), and exposed surfaces and sites. Thus TOF and selectivity were both affected.

SMSI has been observed on titania supported silver catalysts. Grünert *et al.* [23] found that Ti suboxide overlayers were formed due to strong metal support interaction at higher temperature. Growth of silver particles was inhibited as a result. While Ag/TiO_2 samples reduced at 200 ℃ (LTR) had ~3 nm mean diameter, the mean diameter of catalysts reduced at 500 ℃ (HTR) was only ~1.5 nm. Higher selectivity (41.8%) and one order of magnitude higher TOF were observed over the catalysts reduced at low temperature.

1.2.3 Effect of alloying

To improve selectivity (and potentially activity as well) a second metal may be alloyed with the active metal. The inherent complexity of the bimetallic systems offers us more possibilities and parameters to tune the reactivity and selectivity of the catalysts. The presence of the alloy can result in a change in the electronic properties of the catalytically active surfaces/sites, the adsorption site preference of the adsorbates, the

reaction ensemble, the thermodynamics of the elementary reaction, the reaction mechanism and accordingly modify the reaction activity and selectivity. Most of the platinum group metals reported on selective hydrogenation of α, β–unsaturated aldehydes have been alloyed with a more electropositive metal in an effort to improve selectivity [2, 3]. The electropositive metal B works as an electron-donor to increase the electron density on host metal A. As mentioned in Section 1.2.1, the selectivity to α, β–unsaturated alcohol can be rationalized to the preference of the catalyst surface for the carbonyl group in α, β–unsaturated aldehyde over the competing olefinic group. The increase in electron density in the active metal is repulsive to the C=C bond and as a result, the binding energy of C=C bond is weakened thus improving the selectivity to α, β–unsaturated alcohol. The metals in the first transition row, such as Fe or Co, and *p*-electron metals like Ge or Sn are often chosen as promoters [15, 28-30].

Gas phase hydrogenation of acrolein was carried out on $PtSn/SiO_2$ by Marinelli *et al*. [15]. Wet co-impregnation of the metal salts was performed in an ethanol solution to create the bimetallic catalyst. With the addition of Sn, the selectivity was improved from 1% to ~18%. In another study of PtSn catalysts, Poltarzewski [29] *et al.* studied the hydrogenation of acrolein over Pt-Sn catalysts supported on Nylon 66 powder in the liquid phase. Final atomic ratios of Pt/(Pt+Sn) varied from 0 to 100%. Addition of 18 % tin enhanced the selectivity to allyl alcohol from 30% to 60% but additional increases in the tin content did not further improve the selectivity. In fact, the rate of reaction dropped drastically if the loading of tin was larger than 50% and finally zero when tin exceeded 80 wt%. The promoting effect of tin on platinum was not only studied for acrolein hydrogenation, but also for the hydrogenation of cinnamaldehyde [29], furfural [28], and

crotonaldehyde [30]. Astonishing increases in selectivity were observed in all cases. SnO_x species were suggested to be a reason why the C=O bond was activated preferentially as compared to the monometallic case [15]. Marinelli et al. [15] also tried Na (alkali metal), V, Ti, Fe (transition metals), Ga, Sn and Ge (nontransition metals) as promoters for silica-supported platinum catalysts for acrolein hydrogenation. Sn and Ga were the best among theses and brought the selectivity to allyl alcohol up to 27.5% and 13.2%, respectively, compared to 1.6% selectivity on pure Pt.

Coq *et al*. [31] investigated alumina-supported ruthenium-based catalysts promoted with various metals (Sn, Fe, Zn, Ge, Sb). However, only Sn had a positive promoting effect. The selectivity was enhanced from 45.2% (on pure ruthenium) to 52.7% (on RuSn), but declined to about 7% on Sb or Zn promoted catalysts. However, the values reported above were observed at initial time and decreased rapidly afterward.

Indium was added through a second-step impregnation to a reduced Au/ZnO sample [21, 24]. The bimetallic Au-In catalyst (0.13 wt% of In, 1.59 wt% of Au) supported on ZnO gave a selectivity to allyl alcohol of 63%. EDX (Energy-dispersive X-ray spectroscopy) investigations showed a relative homogeneous distribution of indium on the gold particles. HRTEM images clearly supported the EDX result since a separate indium layer could be seen outside Au particles so the In did not incorporate as an alloy (although multiple AuIn phases are possible [32]). Images further revealed that the indium decorated the gold surfaces in a way that left the edges uncovered, suggesting that these corner sites may be the active sites for allyl alcohol formation. For silver, indium exhibited a positive promoting effect as well [33]. By a two-step impregnation method, indium was put into the calcined Ag/SiO_2. A bimetallic catalyst with 9 wt% Ag and 0.75%

In was made. At nearly complete conversion (97%), a high selectivity of allyl alcohol (61%) was achieved. This catalyst was also tested in liquid phase. An even higher selectivity of 75% was observed at 93% conversion, giving a total yield of 70%. To our knowledge the In promoted Ag catalyst shows the highest yield for any metal based heterogeneous catalyst on record. No mechanistic level explanation towards the high selectivity and activity was given, but the formation of a Ag_3In alloy was claimed in XRD result [33, 34].

1.2.4 Influence of reaction condition

To have an effective catalyst, one must tune the process conditions appropriately. Obviously the reaction temperature has a clear influence on the rate of individual reactions and therefore the selectivity (as individual elementary steps will have widely varying activation energies). In addition, the reaction pressure is also shown to be a crucial process parameter in the selective hydrogenation of acrolein in gas phase [24, 25]. In their investigation of acrolein hydrogenation over silver catalysts, a detailed map of selectivity vs. reaction pressure was drawn by Schlögl and co-workers over a pressure range from ~2 mbar to 20 bar (Fig. 2). Higher pressure favored the selective production of allyl alcohol. For example, over Ag/SiO_2, no allyl alcohol was formed below 75 mbar. However, the selectivity shot up to 28% when the pressure reached about 1 bar, continued increasing to ~36% at 5 bar, and eventually reached a plateau above 10 bar. It has been speculated that the increase in selectivity may be due to the change of adsorption mode of acrolein under higher pressure (which necessarily results in higher surface coverage).

12
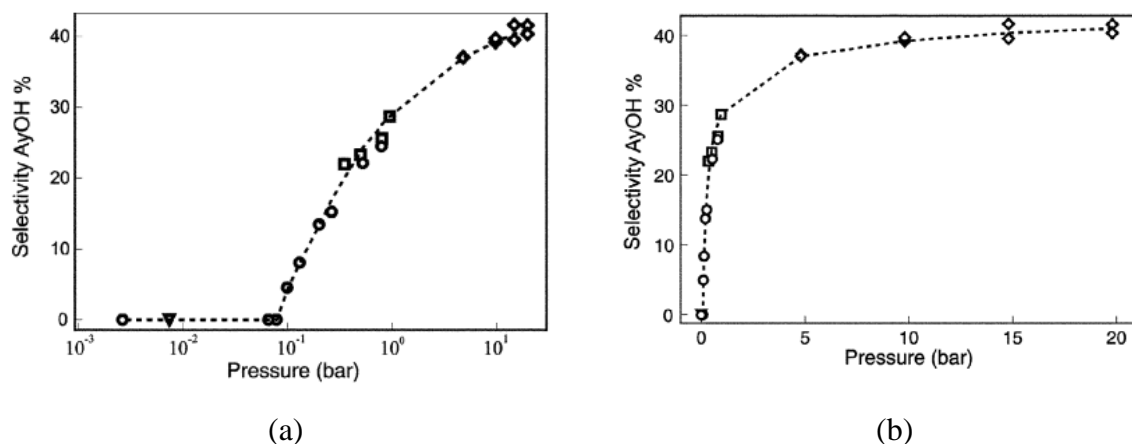
Fig. 2 Dependence of the selectivity of allyl alcohol on the reaction pressure over a Ag/SiO$_2$ catalyst: a) logarithmic range; b) linear range [24].

1.3   Understanding the mechanism of acrolein hydrogenation

1.3.1   Experimental adsorption studies

From prior catalytic studies, the effect of pressure suggests that the adsorption manner of acrolein on the catalyst surface may steer the final selectivity to the desired product allyl alcohol. Logically, if acrolein adsorbs on the surface by C=O bond it is most likely that the C=O bond is hydrogenated by the H atoms on the surface and the unsaturated alcohol is produced, or conversely if the molecule bonds through the C=C double bond then hydrogenation will occur there and the saturated aldehyde will be the primary product. Earlier studies done by Barteau and co-workers investigated the adsorption of acrolein on Rh(111) [35] and Pd(111) [36] surfaces using HREELS and TPD. On Rh(111) acrolein was found to adsorb via η^2(C,O) configuration at 91 K and η^4(C,C,C,O) configuration at 200 K. Decarbonylation was observed between 200~300 K. On the Pd(111) surface, acrolein was re-hybridized and adsorbed as η^4(C,C,C,O) species.

13

Jesús *et al.* studied the adsorption of acrolein on Pt(111) by RAIRS and TPD [37]. The RAIRS data taken at 90 K showed a very weak signal of ν(C=O) mode indicating that C=O bond was parallel to the surface. With higher initial doses (>2 L) τ(CH$_2$) twisting motion occurred, but no ν(C-C) stretching or the in-plane δ_{ip}(CH)$_{aldehyde}$.was observed. This implies acrolein initially adsorbed with its plane parallel to the surface and interacted mainly via the carbonyl group at low coverage.

Acrolein adsorption was also investigated on Au(111), Ag(111) and polycrystalline gold surfaces [38]. Infrared reflection absorption (IRA) spectra were measured at -193 ℃ under UHV conditions. Consistent with Jesús' results, acrolein adsorbed on Au(111) in a parallel configuration. Although the features of parallel adsorbing pattern were still observed, the IRA spectrum of adsorbed acrolein on polycrystalline gold film looked similar to the IR transmission spectrum of liquid acrolein, indicating that the adsorbates at the polycrystalline gold film existed in a disordered liquid-like state. On Ag(111) the IR bands for the adsorbates exhibited broader features were compared to those on Au(111) indicating that acrolein was in a less ordered state than on Au(111). Other powerful techniques like high resolution synchrotron XPS, NEXAFS and temperature programmed reaction were also employed to examine the hydrogenation on Ag(111) surface by Brandt and co-workers [39]. They drew several conclusions based on their study: 1) In the case of no co-adsorbed H(a), at relatively low coverage, the acrolein molecule adsorbed parallel to the surface while at high coverage C=C bond tilted remarkably, kinetically favoring the hydrogenation of C=O bond. 2) At low H(a) coverage, the C=C bond in the newly formed allyl alcohol tilted so that further hydrogenation was avoided. Nonetheless at high H(a) coverage, the C=C bond in allyl alcohol turned parallel to the surface—a

14

vulnerable position to be attacked by H(a). When a 0.6 ML coverage of acrolein and 0.66 ML dose of H_2 were coadsorbed, the selectivities to allyl alcohol and propanal were both 47%. However, with the same coverage of acrolein and an increase in the hydrogen coverage to 1 ML the selectivity to allyl alcohol decreased to 30% while the selectivity to propanal increased to 67%.

1.3.2 Theoretical studies

Hirschl *et al.* investigated various adsorption modes for acrolein on the (111) surface of Pt [40] and $Pt_{80}Fe_{20}$ [13] with spin-polarized density functional theory. On Pt(111) over a large range of coverages, acrolein showed its main interaction with the surface with the C=C bond, with an eventual additional weak interaction with the oxygen atom. This could clearly result in a predominant hydrogenation of the C=C bond, as was seen experimentally. As for the $Pt_{80}Fe_{20}$(111) surface, a strong segregation of platinum atoms towards the surface layer occurred when the surface was clean. However, the significantly larger aldehyde-surface interaction energy upon the formation of O–Fe bonds can change the surface composition (the adsorption energy of acrolein on Pt(111) via a diσ_{CO} configuration was 0.25 eV and its counterpart on $Pt_{80}Fe_{20}$(111) was 0.68 eV) and increase the Fe content in the surface layer. Thus the presence of Fe bears the potential to influence the hydrogenation selectivity in favor of unsaturated alcohols.

Silver is especially interesting because of its outstanding selectivity for selective hydrogenation of acrolein. Rösch and co-workers studied the adsorption of acrolein on flat Ag(110) and stepped Ag(221) surfaces [41]. C=O bond was expected to be activated according to experimental results. However, the calculations showed acrolein to interact only weakly with all adsorption sites under study (by at most 35 kJ mol^{-1}, obtained on

Ag(211) step through a η^4(C,C,C,O) configuration), resulting very limited C=O bond activation. They also mentioned that weaker adsorption was found on denser Ag(111) surface (~ 10 kJ mol^{-1}) with the molecular plane parallel to the surface. Rösch and co-workers went on to examine hydrogenation of acrolein over Ag(110) and Ag(111) with O in the subsurface [42]. The authors found that while hydrogenation of the C=O bond was less favorable over the bare silver (and thus propanal is the favored product) but when O was present in the subsurface, the energetics switched such that the selectivity favors allyl alcohol.

Notwithstanding the results of Rosch, Ferullo *et al.* [43] showed that there was a coverage dependence of the structure of adsorbed acrolein on Ag(111) surface. They calculated the adsorption modes of acrolein at different coverages by changing the sizes of Ag(111) supercells. $p(4\times4)$ and $p(2\times2)$ were used in the case of "head to tail" adsorption, representing low and high coverages. In this situation, all acrolein molecules were oriented in the same way. Yet another possibility of acrolein arrangement exists. Acrolein can adsorb in a "head to head" adsorption configuration, meaning the C=O bond of one acrolein molecule is adjacent to C=O of another molecule. Thus supercells $p(5\times3)$ and $p(4\times2)$ were employed to examine the "head-to -head" adsorption mode. When acrolein molecules were oriented in head-to-tail manner, varying coverage basically did not alter the adsorption mode. Acrolein remained parallel to the Ag(111) surface at both low and high coverages. For the $p(5\times3)$ supercell, the adsorbates form almost isolated dimers and adsorbed parallel to the surface. However, for the $p(4\times2)$ structure, a totally different picture of adsorption emerged as the molecular network involved chains of adsorbed acrolein in a zigzag pattern, where each molecule interacted with two nearest

neighbors through O···H contacts (Fig. 3). It is obvious that in one row of the zigzag structure the molecules were almost perpendicular to the surface. Thus oxygen atoms from the carboxyl group were much closer to the surface and should react more easily with adsorbed atomic hydrogen. This result gives an explanation of the phenomena [25] mentioned in Section 1.2.4 that increasing reaction pressure could improve the selectivity to allyl alcohol.
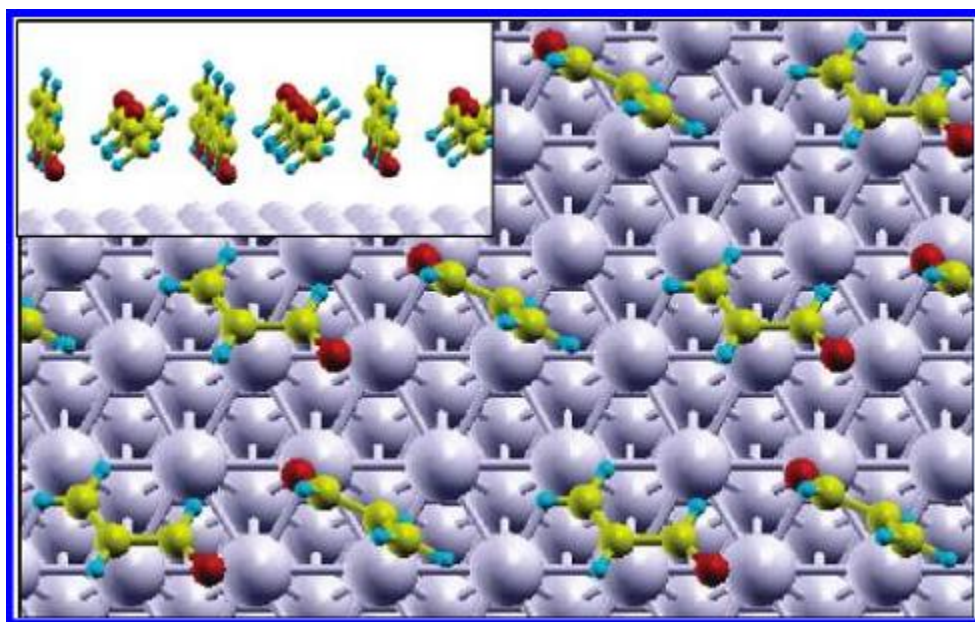
Fig. 3 Optimized geometry of the network of adsorbed acrolein on Ag(111)
corresponding to the $p(4 \times 2)$ supercell [43].

1.4   Preview of experiments

To clarify the factors governing the selectivity in the hydrogenation of acrolein, we have attempted to perform a systematic experimental study. Since silver has been found

to be one of the most promising candidates (as well as gold) for this reaction so far, it was chosen as the primary catalyst of interest here. In the first part of this work, we wish to understand how this reaction proceeds over Ag catalysts so the particle size effect and support effects over Ag catalysts are examined. Second, we tried to improve the selectivity and activity by using an unconventional type of alloy, single atom alloy (SAA). Third, we also attempted to use another type of nontraditional catalyst single site heterogeneous catalyst (SSHC).

1.4.1 Experimental methodology: kinetics study and pathway analysis

Reaction kinetics is the study of rates of chemical process and highly important to heterogeneous catalysis research. Important kinetics parameters of the reaction which can be derived include the reaction order, the rate constant and the activation energy. The establishment of the rate law can help in our understanding of the reaction mechanism and accordingly help improve the chemical process by redesign to develop a better catalyst and optimize the reaction condition.

1.4.1.1 Kinetics study

Since the kinetics study is based on the measurement of the reaction rate, it is crucial to make sure the reaction rate is measured accurately and also there is no mass transfer limitation during the rate measurement, i.e. the measurement should be carried out in the kinetics-control regime. Reproducibility is required as well. Only when the

above two criteria reached, can we be confident about the accuracy and precision of the rate measurement.

First of all, we must establish that we are in the limit of differential conversion. Since we are using a plug reactor to test the catalyst, one must be careful to recognize that the rate is changing continuously down the length of the reactor. Therefore, to derive the rate, one must examine the reaction at very low conversion where the concentration is nearly constant. We test this by showing that a linear relationship must exist between the conversion and 1/F (F is flow rate). By repeating this test of the rate for several times, we can check the reproducibility of our measurements. In Fig. 4, we show a conversion vs. 1/F plot for the 8%Ag/SiO$_2$_R325 sample. The slope is the rate of reaction (black solid lines). The rate of the total reaction is 0.139±0.007 mol/(h*g$_{Ag}$) at 5 atm. The error is only within 5%, which is very satisfying.

When using porous materials as supports, it is possible that the diffusion of the reactant molecules into the support pores is the rate limiting step, which then masks the intrinsic reaction kinetics. One way to evaluate the effect of mass transfer is through the use of a dimensionless variable, $\Phi=\sqrt{kR^2/D}$, known as the Thiele modulus, where k is the intrinsic rate constant, R is the characteristic diffusion length (i.e. the catalyst pellet radius) and D is the diffusion coefficient. For a large value of the Thiele modulus (generally $\Phi \gg 1$), we are in the mass transfer limited regime. However, in the limit of a low Thiele modulus ($\Phi \ll 1$), we are under kinetics control. To prove our rate measurement is within the kinetics-control regime, we grind this catalyst to larger mesh size (60 to 325 mesh; R changes from 250 to 44 μm) and retested it. When the catalyst grain is reduced, the Thiele modulus decreases as it is easier for the reactant molecules to

19

travel in or out the pores. If the intrinsic rate changes with the pellet radius, then the reaction is not under kinetics control. As seen in Fig. 4, the rate of the ground sample (represented by red solid line) is 0.134 mol/(h*g$_{Ag}$) and it falls exactly into the error region of the original sample, i.e. the rate of reaction does not change after the catalyst is ground, suggesting no internal mass transfer limit exists in both case.
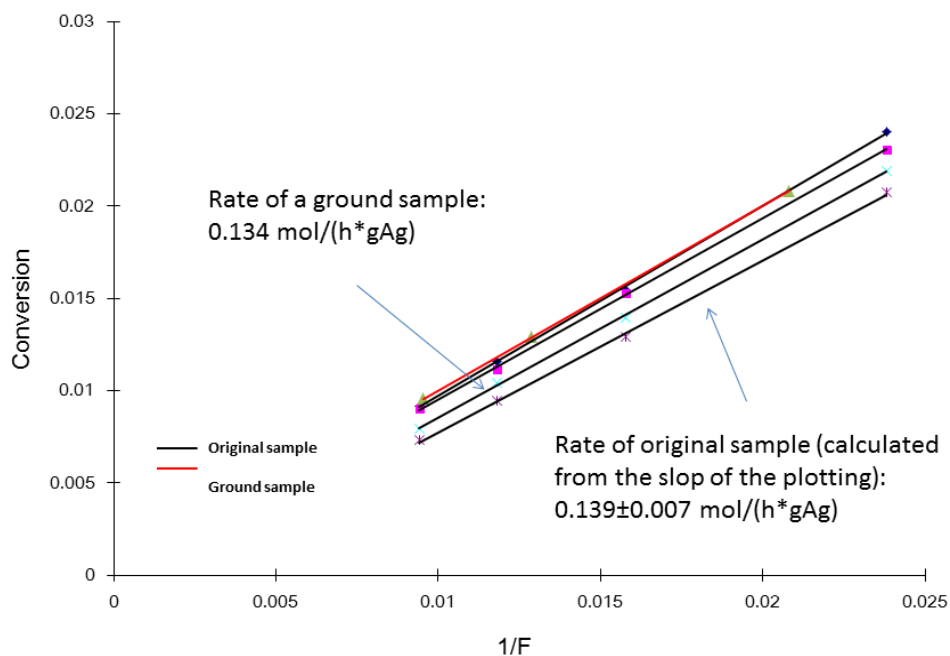
Fig. 4 Reproducibility of the rate measurement and the comparison with a ground catalyst

Once we have successfully proven that we can measure intrinsic kinetics with high reliability, we can proceed to evaluate the kinetic parameters . We begin with a simple rate law: $r = k[Acrolein]^m[H_2]^n$ where k is the intrinsic rate constant. By varying the concentration of each reactant, m and n can be calculated. A linear relationship between

ln(r) and ln[Acrolein] will evolve by taking the natural logarithm of the rate equation as following equation:

$$\ln(r) = \ln(k) + m\ln[Acrolein] + n\ln[H_2]$$

Since k is a constant at a certain temperature, the slope of plotting ln(r) against ln[acrolein] is m when keeping the concentration of H_2 constant. n can be achieved in the same manner. At the same time we can also calculate the reaction constant k. As a result the pre-exponential factor A in Arrhenius Equation is found.

According to Arrhenius Equation: $k = A\exp(-E_a/RT)$, taking the natural logarithm of it yields: $\ln(k) = -\dfrac{E_a}{RT} + \ln(A)$. Ploting ln(k) against 1/T generates a straight line, the slope of it is $-E_a/R$. Thus the activation energy can be calculated.

1.4.1.2 Pathway analysis

In a complex reaction network, elucidation of the reaction pathway is a challenging task. A pathway analysis has also been done for $8Ag/SiO_2\_IWI\_R325$. This method was developed by Bhore et al. [44] for discernment of the rank (i.e., primary, secondary, etc.) of a reaction product. We begin by examining a first rank plot whereby the selectivity to various products as a function of conversion. The first-rank delplot method, allows one to separate the primary product from nonprimary products. One only needs to extrapolate the plot to zero conversion. If the intercept is nonzero, the product is primary. If the intercept is zero, the product is nonprimary. Higher rank products can be determined by a higher rank deplot. For example, secondary products can be separated by plotting (component selectivity)/(conversion) against conversion. At zero conversion,

primary products have infinite intercepts, secondary products have finite intercepts and higher-order ones have zero intercepts.

The advantage of doing the first-rank plotting is not only to tell the primary products from the others, but also to provide a relationship between selectivity and conversion so that the selectivity for a specific conversion can be read via the curve. One can expect that the selectivity changes along with conversion. The selectivity at 10% conversion and that at 90% could be totally different even for one single catalyst as the surface concentrations could be highly different. Once the relationship between selectivity and conversion is established (holding temperature constant and varying conversion via changes in space velocity), one can evaluate the conversion for all the catalysts and read out the value of selectivies at a given conversion. In this way, a fair performance comparison of different catalysts can be conducted. The first-rank plotting also provides the information for optimizing reaction condition.

1.4.2   Particle size effects

Previous studies have shown that particle size plays an important role in both selectivity and activity. A study on hydrogenation of crotonaldehyde by Claus and Hofmeister [45], a very similar reaction to hydrogenation of acrolein, revealed that larger particle sizes lead to higher selectivity. In the range of 1.4~2.8 nm, the selectivity to crotyl alcohol increased from 28% to 53%. When the particle sizes dropped into a region of 3.7~6.3 nm, it was observed that the selectivity was independence of particle size (all about $(59 \pm 3)\%$). However, the smaller samples (1.4~2.8 nm) were supported on titania

while the larger samples (3.7~6.3 nm) were supported on silica. Thus the support effects could not be excluded.

As mentioned in section 1.1.2, two titania supported silver catalysts having particle sizes of 2.8 nm and 1.4 nm respectively were compared. The larger particle size sample had not only higher selectivity (42% vs. 27%) but also better activity (TOF: 20.1×10^{-3} s^{-1} vs. 1.5×10^{-3} s^{-1}). Nonetheless, TiO_2 very likely interacted with silver particles and affected the properties. As a result, support effect needed to be considered and it was very difficult to distinguish whether the contribution of selectivity was from particle size change or the nature of support.

It is apparent that although hydrogenation of α, β-unsaturated aldehydes are considered to be structure sensitive, a systematic and detailed study on particle size effect is still need. We propose to prepare a series of silver catalysts supported on identical support (SiO_2 was chosen because weak interaction with metals), vary the particle size in a fairly broad range and compare their selectivity at the same conversion. As a result, we are only varying one parameter at a time so that we can be confident that any changes we observe are due to the change of particle size.

1.4.3   Support effects

As described in the previous sections, support effects have been observed in previous studies as well. However, similarly to the situation of the studies on particle size effects a systematic study comparing the support effects and considering the size effects simultaneously was lacking.

Malathi and Viswanath [46] studied hydrogenation of citral on platinum catalysts supported over several different supports: TiO_2 (commercial), TiO_2 (synthesized by gel), mixed oxide (titania and alumina) and CeO_2 (commercial). 100% selectivity to only one of the unsaturated alcohols, geraniol (E isomer), was observed. So the catalysts were different only in the activity. When the catalysts were all reduced at low temperature (300 °C), Pt/TiO_2-Al_2O_3 showed higher conversion (by ~15% absolutely) than all the other catalysts, especially for the first four hours. When reducing the catalysts at 500 °C, Pt/TiO_2(gel) became the most active one. The authors explained the different behavior under different reduction temperatures by SMSI effect. However, as is sometimes typical in these earlier studies, the particle sizes of the catalysts were not mentioned at all in this report.

Our study on support effects attempts to systematically examine these effects over a range of sizes so that clear trends may be elucidated. We chose three different metal oxide supports: SiO_2, Al_2O_3 and TiO_2. On each support various mean particle size of silver nanoparticles were loaded by adjusting synthesis and treatment methods. Therefore, a trend line can be drawn illustrating the relationship between activity/selectivity and the particle size. When the trend lines of all the supports were compared, a clear conclusion can be reached safely.

1.4.4   Single atom alloys (SSA)

The creation of uniform active sites in heterogeneous catalysis remains a long standing dream of the catalysis community. Previous stategies for the development of

single site catalysis have typically relied on the heterogenization of homogenous catalysts. In contrast, the single atom alloy is a new concept in heterogeneous catalysis which stems from typical heterogeneous catalysis by supported nanoparticles. It describes a special case in which one metal is completely dispersed into another host metal, i.e. it exists in a form of individual atoms of an active in the host metal (which is considerably less active). The loading of the inserted metal is generally low in order to avoid having metal islands or particles and changing the structure of the host metal. By doing so, the structure of the host metal should remain the same as the monometallic catalyst so that the existing active sites and their properties should not be altered. This is different from the traditional alloy catalysts in that only a single atom of the active metal participates in the catalysis. Instead of changing the electronic and/or structural characters of the whole metal, those of the host metal of a single atom alloy are basically unaffected. In addition, new properties which can be essential to a catalytic reaction are added into the monometallic system by doping individual atoms of a second metal.

Skyes' group has recently shown an excellent example of a single atom alloy using Pd@Cu SSA for selective hydrogenation of acetylene and styrene [47]. Pd atoms were alloyed into Cu(111) surface. Pd remained as isolated atoms on the copper surface up to 0.1 ML (0.01, 0.1 and 1 ML of Pd was deposited on Cu surface). 0.01Pd@Cu had > 95% selectivity for selective hydrogenation of both acetylene and styrene. It was claimed that the high selectivity benefit from a total effect of the weak interaction between the adsorbants and Cu surface plus the ease of H_2 association on Pd atoms. We will demonstrate another example of a SAA in this work. In our case, we show that this type of alloy can be created in high surface area nanoparticle catalysis creating single atom Pd

sites in Ag nanoparticles. From the preliminary results, the small amount of Pd boosted both selectivity and activity compared to monometallic Ag/SiO$_2$ catalyst with same particle size.

1.4.5   Single site catalysts

Conventional heterogeneous nanoparticle catalysts consist of various active sites that are very diverse in energetics, activity and selectivity. For example, on a metal particle surface there can be terraces, edges, kinks and even surface vacancies with the ratios of these sites varying with the particle size and shape. They all have their own energetics of interacting with reactant adsorbates. Even on a single crystal surface there exits multiple adsorption sites [48] and the situation is more complex for alloy surfaces [49]. In addition, the particles are not identical and there is always a distribution in size (narrow or broad). Due to the high degree of heterogeneity the active sites of nanoparticle catalysts are nearly impossible to identify and characterize. In contrast, the counterpart of supported nanoparticle catalysts, homogeneous and supported homogeneous catalysts, are structurally uniform. It is easier to characterize a specific site, understand what steric and electronic properties are important for the reaction and tune the properties by changing the combination of metals and ligands accordingly. However, the thermal stability of homogeneous catalysts is usually not as good as supported nanoparticle catalysts and an understanding of how the support participates is still in the nascent phase.

A classic example of a SSHC is H-ZSM-5 for the catalytic cracking of *n*-hexane [50]. ZSM-5 has a very low concentration of aluminum in a level of ppm compared to X

and Y zeolites. However, the very diluted tetrahedral aluminum atoms were identified to be the highly reactive ingredients. The actual active sites were the protons associated with tetrahedral Al atoms serving as solid acid. The turnover rates were comparable or better than enzymatic turnover numbers.

Shannon *et al.* [51] grafted isolated Mo (VI) active sites onto the inner surface of MCM-41 and tested the catalysts for oxidative dehydrogenation of methanol to formaldehyde. It was shown by Mo K-edge EXAFS results that when the loading of Mo was low (~ 1 mol%) isolated MoO_4 species existed on the surface. Nonetheless polymeric oxomolybdenum species formed in a higher (~ 4 mol%) sample. When examined for oxidative dehydrogenation of methanol, the lower the Mo loading, the better the selectivity to formaldehyde. The selectivity towards formaldehyde was 63.3% over 0.03 mol% Mo/MCM-41. It decreased to 15.3% when the loading of Mo was raised to 1.0% and became zero on 2.0 mol% Mo/MCM-41. The main products for the two higher loading samples were dimethoxymethane and dimethyl ether. The catalyst having most diluted Mo, 0.03 mol% Mo/MCM-41, was not only the most selective but also the most active. The authors believed that higher dispersion of active sites benefited the reaction rate. The reason for lower activity of higher Mo loading samples was formation of volatile oxides of Mo that also result in leaching of molybdenum.

Single site catalysts have a special advantage of simplicity and specificity due to the highly dispersed uniformed active sites. We want to take advantage of unique properties of SSHC because once we have finely tuned active single sites favoring hydrogenation of C=O bond in acrolein we should obtain a very high selectivity. In this work, a thermo-stable single site Zn/SiO_2 was synthesized and tested. Although the

nature of the active site and the mechanism are still mysterious, we do obtain very high selectivity (albeit with poor stability) Based on this initial study, we believe better catalysts can be made by changing the active metal and changing/modifying the support.

1.5 Density functional theory (DFT) study on water gas shift (WGS) over PdZn(111) and NiZn(111) alloy surfaces

In addition to our study of alloy effects in acrolein hydrogenation, we have also examined the effect of alloying on another common industrial reaction: water gas shift. In this case, we investigate this effect solely through the use of density functional theory calculations. Water gas shift is a mature and significant reaction widely used in many industrial processes such as methanol steam reforming (MSR), methanol synthesis, and Fischer–Tropsch synthesis. In industry, water gas shift for increasing hydrogen content in synthesis gas is typically performed in two stages, a low temperature shift and a high temperature shift. The catalyst for low temperature shift is $Cu/ZnO/Al_2O_3$. The results from Schumacher et al. [52] indicated that Cu was close to the optimal of the rate calculation although improved kinetics are still desirable. However, Cu catalysts sinter easily because the melting point of Cu is low. In addition there are some concerns with the pyrophoric nature of the catalyst. Thus modification or substitution to Cu catalyst for better activity and stability represents a continuing goal.

It was found by Iwasa et al. that Pd-Zn alloy had better or comparable performance to Cu catalyst for methanol steam reforming (MSR). They compared supported Pd catalysts for MSR over various supports (Pd/SiO_2, Pd/Al_2O_3, Pd/La_2O_3, Pd/Nb_2O_3,

Pd/Nd$_2$O$_3$, Pd/ZrO$_2$, Pd/ZnO and unsupported Pd) and found the selectivity and activity of Pd/ZnO were extraordinary [53]. The rate of H$_2$ production over Pd/ZnO was at least twice as high as that over any other Pd catalysts. The selectivity to CO$_2$ was 97% while none of others surpassed 20%. In the successive study, they claimed that the great improvement by using ZnO as support was because Pd-Zn alloy was formed when reducing the catalyst [54]. XRD and XPS results clearly demonstrated the existence of Pd-Zn alloy phase. It was also noticed that higher reduction temperature facilitated the formation of alloy phase and promoted the selectivity and activity of the catalyst. For example, the selectivity was 98% for the Pd/ZnO catalyst pre-reduced at 773 K which the one reduced at 493 K only had about 61% selectivity.

In order unravel the reason for the outstanding performance of Pd-Zn, Rösch and co-workers performed a density functional study to investigate the electronic structure of Pd-Zn and Cu for comparison. They demonstrated the similarity of local valence d-band density of states of Pd in the 1:1 Pd-Zn alloy and that of Cu [55] suggesting a similar catalytic performance of Pd-Zn alloy to Cu catalyst. In addition, the d-band of Pd reduced by 2.5 eV after alloying with Zn. Therefore we would like to extend the study to WGS which is closely related to MSR. We investigated two popular reaction mechanisms by DFT calculations for WGS on PdZn (111) surface to demonstrate the feasibility of using PdZn alloy as a promising catalyst for WGS. We also carried out the reaction on NiZn(111) surface which could potentially be a cheaper substitution for PdZn since Pd is very expensive.

2   A KINETICS STUDY OF PARTICLE SIZE EFFECTS ON SELECTIVE HYDROGENATION OF ACROLEIN

2.1   Introduction

Selective hydrogenation of acrolein was selected as the test reaction because of its commercial and research attraction as described in Chapter 1. As mentioned in Section 1.2.1, the commonly used hydrogenation catalysts including Pd, Pt, Rh, etc. are too active for selective hydrogenation of acrolein. They often lead to the unwanted product propanal and propanol and even cleave the carbon skeleton of acrolein molecule. Marinelli [15] *et al.* reported that Pt/Aerosil 200 has only 1.6% selectivity to allyl alcohol at 80 ℃ in a fixed-bed reactor. Hoang-Van and Zegaoui [16] examined Pt/Al$_2$O$_3$, Pt/C and Pt/SiO$_2$ which all displayed poor selectivity (< 1%). Gyorffy and Paál [18] conducted a detailed investigation of acrolein hydrogenation on a series of unsupported PdPt powder catalysts prepared by colloid synthesis. They compared product distribution at high conversion (> 80%) and at different temperatures (from 293 K to 473 K) and hydrogen partial pressures (varied between 10 and 400 Torr), but observed no selectivity to allyl alcohol for any of these catalysts.

In contrast to the poor selectivities reported above, silver and gold have been shown to exhibit much higher selectivity to desired hydrogenation product allyl alcohol [5, 19-25] than other *d*-band transition metals. Highly dispersed supported gold catalysts have garnered much interest due to their unusually high activities in many reactions [20]. One Au/ZrO$_2$ and three Au/TiO$_2$ catalysts were synthesized by Claus' group [19], by different methods. Co-precipitation was used for the ZrO$_2$ supported catalyst; deposition

precipitation (DP), impregnation (I), coprecipitation (F) and a sol gel technique (SG) were used to synthesize the TiO_2 supported catalysts. At 180 °C, Au/TiO_2-DP and Au/TiO_2-I showed similar selectivities to the desired unsaturated alcohol, 41% and 43% respectively. Given that the gold particle sizes of these two samples is 5.3 nm for Au/TiO_2-DP and 2 nm for Au/TiO_2-I, they claimed that the hydrogenation of acrolein on Au/TiO_2 is structure-insensitive, at least for this specific range of particle size (2-5 nm). However, no allyl alcohol was produced on Au/TiO_2-SG or Au/ZrO_2-F under the same reaction conditions. Later a series of zirconia supported gold catalysts were studied by the same group [21] showing similar behavior. An increase in selectivity to allyl alcohol with increasing particle size was observed with a maximum selectivity of 35% at 5% conversion over Au/ZrO_2-DP22 (d_{mean} = 7.7 nm) while the selectivity over Au/ZrO_2-DP24 (d_{mean} = 4.0 nm) was 28% at the same conversion. The group investigated the influence of the gold nanoparticle structure from two aspects, the occurrence of multiply twinned particles (MTPs) and the degree of rounding. The authors concluded that higher MTPs resulted in lower selectivity to allyl alcohol and TOF while a higher degree of rounding improved the selectivity.

Silver catalysts have also been shown to be good candidates for acrolein hydrogenation. Grünert [23] *et al.* employed Ag/TiO_2 catalysts in the gas-phase hydrogenation of acrolein. The catalysts were prepared by incipient wetness impregnation using $AgNO_3$ as the silver precursor on P25 TiO_2 followed by calcination and reduction. Higher selectivity was achieved than over similar supported gold catalysts. For example, a Ag/TiO_2 catalyst reduced at 200 °C selectively converted acrolein to allyl alcohol with a 41.8% selectivity at 200 °C and 2 MPa pressure. The

activity of this Ag/TiO$_2$ catalyst was 85.3 μmol g$_{Ag}^{-1}$ s^{-1}, which was almost twice of that of the gold catalyst mentioned above (44 μmol g$_{Au}^{-1}$ s^{-1} [21]). Grunert and co-workers also observed an SMSI effect for these Ag/TiO$_2$ catalysts. The samples reduced at lower temperature (200 ℃) had higher selectivity to allyl alcohol (41.8% vs. 27.2%) and one order of magnitude higher TOF than one reduced at higher temperature (500 ℃). These results suggest that Ti suboxide overlayers may have formed at higher temperature which blocked Ag sites or inhibited the growth of silver particles resulting in a decrease of both activity and selectivity.

Silica supported silver catalysts were also investigated [25]. Two silica supported samples prepared by IW or DP had selectivities of 42% and 39% respectively at conversions of ~ 25% tested under 20 bar. The sample prepared by IW Ag/SiO$_2$-IW (d$_{mean}$ ~ 2-3 nm) had the best performance. These authors concluded that smaller particles with more edge and kink sites favored the formation of allyl alcohol. Nonetheless, this conclusion seems insufficient to explain why Ag/SiO$_2$-DP with a much larger mean particle size (~ 15 nm) had similar catalytic performance

Since silver has been found to be one of the most promising candidates for this reaction so far, we would like to have a deeper understanding of its mechanism in catalyzing the selective hydrogenation of acrolein and the particle size effect of the catalysts. The results of Claus and Schlögl and co-workers suggest that particle size may be a crucial factor governing the selectivity. However, the range of sizes previously examined may not have been sufficient to provide a definitive answer. Herein we report the results of a detailed systematic study on the particle size effect of Ag/SiO$_2$ catalysts.

2.2   Experimental

2.2.1   Preparation of catalysts

Various supported silver samples were prepared using $Ag(NO)_3$ as the silver precursor and silica as the support. Direct or modified incipient wetness impregnation (IWI) was employed in aqueous solution to synthesize silver catalyst samples. Here modified incipient wetness impregnation is referred to a special treatment that is inspired by strong electrostatic adsorption (SEA) [56]. According to the theory of SEA, controlling the pH of the impregnating liquid helps improve the interaction between metal (or metal complex) and support surface, so that better dispersion can be obtained. In the modified IWI, all the steps are the same as normal IWI except that one needs to adjust the pH value of the solution first. We first used a 5 ml water to dissolve the $Ag(NO)_3$ (amount varies depending on loading; for 8 wt% Ag, 0.63 g $Ag(NO)_3$ is required) and then added 30% ammonia hydroxide drop by drop until precipitation disappeared. Water and ammonium hydroxide were added to make a suitable amount of solution for impregnation depending on the pore volume (typically 5-6 ml) and make sure the pH is around 11. After impregnation, catalysts are dried in a vacuum oven at 100 ℃ before different treatments were applied (calcination, reduction and/or steaming) to obtain different particle sizes of silver. The notation for naming the catalysts includes metal loading, support, preparation method and treatment. For example, sample 8Ag/SiO2_mIWI_C250R250S250 is a 8 wt% (designed loading) silica supported silver catalyst prepared by modified incipient wetness impregnation and calcined at 250 ℃, reduced at 250 ℃ and steamed at 250 ℃. The calcination treatments were performed for 2 hours in a furnace open to the atmosphere but without flow. The reduction treatments

33

were performed in a tube furnace with a 50 mL/min flow of 3.5% H_2 for 2 hours. The steaming treatments were performed by flowing 50 ml/min of He over a stainless steel bubbler which was preheated to 55 ℃, so there was about 15% water vapor in the total flow. The flow was brought to the reactor at the steaming temperature. Steaming treatments were performed for 1-3 hours to vary particle size.

2.2.2   Characterization

ICP   The loading of silver was determined by ICP-OES (inductively coupled plasma optical emission spectroscopy) (PerkinElmer, OPTIMA 2000DV). A suitable amount of catalyst (eg. 20 mg for the 8 wt% Ag sample) was wetted first with 2 mL of DI water. 5 mL of concentrated nitric acid was added and the mixture was vigorously shaken for 3 hours to dissolve the silver from the support. It was then diluted to 25 mL with DI water, filtered and tested to determine the amount of Ag present.

EXAFS   Since our target is to understand particle size effect, EXAFS (Extended X-ray absorption fine structure) was adopted as a powerful and efficient tool to estimate particle size. EXAFS experiments were taken at the beamline of the Materials Research Collaborative Access Team (MRCAT, 10-ID and 10-BM) at the Advanced Photon Source (APS), Argonne National Laboratory. The samples were grounded and packed into the sample holder. The amount of sample (10-80 mg) was chosen based on the sample loading to ensure appropriate total absorbance at Ag K edge (25.51 keV). All the samples were reduced in 3.5% H_2/He at 200 ℃ for one hour then cooled in He and scanned at room temperature in an environmental cell in transmission mode. Ag foil was also scanned for energy calibration. The WINXAS 3.1 program was used to fit the data to

obtain coordination number and bond distance between neighboring Ag atoms, using a k^2-weighted Fourier transform. The Ag-Ag phase and amplitude functions were obtained from the first coordination shell of Ag foil (N_{Ag-Ag} = 12 at 2.889 Å). An empirical relationship between the coordination number and particle size previously extracted from a series of platinum samples was used since both silver and platinum are fcc (face centered cubic) metals [26]. However, since there is no specific rule to choose Debye-Waller factor some error is introduced in our size estimation. Therefore, TEM results are needed to calibrate the relationship of particle size vs. coordination number. Once we have established a relationship between the observed particle sizes (TEM) and the estimated sizes (EXAFS), particle sizes can be easily achieved by interpolation and tedious TEM data processing can be avoided.

XANES L$_3$-edge (3351 eV) XANES (X-ray near edge absorption spectroscopy) spectra were measured at beamline 9-BM of Advanced Photon Source (APS) at Argonne National Laboratory. The samples were ground and packed in a specially designed sample holder where the sample pellet was positioned 45° facing the incident beam. Samples are reduced and measured in a flow cell which is air-tight and allows heating and cooling. Samples were reduced first at 200 ℃. The spectra were collected in fluorescence mode without cooling down the samples to avoid re-oxidation. Three spectra were taken on each sample and averaged to ensure the data quality.

STEM STEM (scanning transmission electron microscopy) images were taken at RRC (Research Resources Center), UIC on a TEM/STEM microscope equipped with HAADF (high angle annular dark field) detector (JEOL JEM-2010F). The particle sizes

were analyzed using software Comptage de particule (V2). About 100~250 particles were typically counted in 10 randomly chosen fields for each catalyst.

2.2.3   Catalysis

Catalyst testing was performed in a 1/2 inch OD stainless steel fixed-bed continuous gas flow reactor. Mass flow controllers were used to control gas flow. In an earlier version of experiment setup, acrolein (Fluka $\geq$ 95%) was carried out by argon gas passing through a glass saturator which was kept at 0 ℃ by immersing in ice-water bath. However, limited by the pressure rating of the saturator and the fact that the partial pressure of acrolein at 0 ℃ could not provide high enough concentration for high pressure reaction, a liquid pump was then used. Acrolein was delivered by a liquid pump (VICI M6), evaporated at 70 ℃ in a heat tape traced four way cross packed with quartz wool, and carried in to the system by reaction feed gas (argon and hydrogen). The quartz wool filter was also used to prevent acrolein polymerization products from plugging the reactor. The gas phase concentration of acrolein was checked for every run by via a reactor bypass line that connects directly to the gas chromatograph. The molar ratio of H_2 to acrolein is held constant at 20:1 unless otherwise noted. 30-400 mg of catalyst was used for each test depending on the activity. Catalyst samples were reduced in 20% H_2/Ar flow at 200 ℃ for an hour. For the sake of comparison with previous work by the Claus' group[25], several catalysts were tested under atmosphere pressure and at a pressure of 5 atm. The other process conditions are the same as those under atmospheric pressure. The reactor effluent was analyzed by an on-line gas chromatography (Agilent 6890) equipped with a dual column formed by a RT-Msieve 5A and a RT-QPLOT (Restek) for lighter

36

gaseous species and a EC-Wax (Alltech) for less volatile species such as alcohols. TCD (thermal conductive detector) and FID (flame ionization detector) were both used for detecting H_2 and other organic/flammable compounds, respectively. A trap was installed at the end of the stream to collect condensed products. Product identification was later confirmed via GC/MS in a separate system. All potential products were calibrated for their retention times by the GC/MS (including impurities of acetone and acetaldehyde) using the same column setup in various trial runs involving calibrated mixtures products (acrolein, propanal etc.). The whole system was built with stainless steel parts to handle high pressure and was heat-traced to avoid condensation of any product. The diagram of the reaction system is illustrated in Fig. 5.

2.3   Results and discussion

A series of silica supported silver catalysts with various particle sizes were successfully made by using different synthesis and treatment methods. A Ag K edge EXAFS spectrum of each sample was taken to estimate the particle size. The Fourier transformation in R space of the data taken on a big particle sample ($8Ag/SiO_2\_IWI\_R325$) and a small particle sample ($2Ag/SiO_2\_mIWI\_C500R200$) as well as a Ag foil are shown in Fig.6. For the larger sample, two peaks at 2.70 Å and 2.15 Å appear in the spectra with a shoulder at 1.9 Å. From Fig 6, it is apparent that the same features appear for foil and therefore the smaller scattering distances are not associated with atoms at different distances but rather with the scattering of the photoelectron off electrons of different energy in the Ag atom. For the smaller particle size, these peaks are shifted to slightly smaller scattering distances due to lattice contraction with decreasing
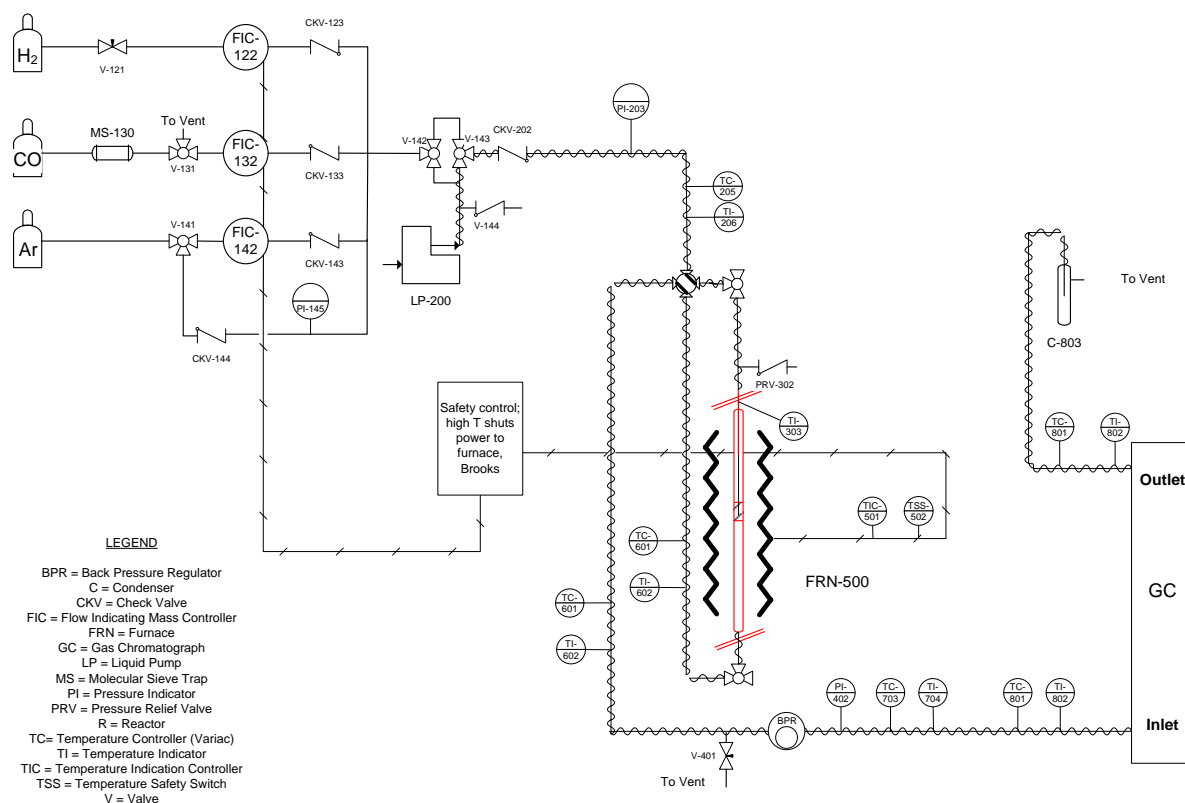
Fig. 5 Flow diagram of the plug flow reactor configuration

particle size[57]. Both the XANES and EXAFS are consistent with metallic Ag and there is no Ag(+1) oxide at detectable levels, typically within a few per cent. STEM was used to help establish the relationship of coordination number and particle size and also confirm the results from EXAFS. The equation used to estimate mean particle sizes in angstrom is:

$$d_{mean} = 10^{0.1319 \times CN + 0.4237} \qquad \text{(Eq. 1)}$$

where CN is coordination number.

We found that it was difficult to make large particles on SiO_2 when the modified IWI was employed and the silver loading was low. In this case steaming had to be carried

out to sinter the small particles so larger particles could be created. By increasing the concentration of silver nitrate and using direct IWI, larger particles were formed without steam treatment. Among all the catalysts, a few with representative particle sizes were chosen (shown in Table I) to test their catalytic performance. The sample treatments, their coordination numbers and corresponding particle sizes are listed in Table I and the relationship between coordination number and particle size is plotted in Fig. 7.

The mean particle sizes that we obtained by analyzing STEM images and by fitting EXAFS coordination numbers are very consistent, proving that EXAFS is an efficient and effective way to analyze particle size. However, there is an obvious disadvantage of using EXAFS to estimate particle size in that it gives a single number for the average particle size and does not reveal the particle size distribution. STEM images showed that the particles were fully consistent with the sizes indicated by EXAFS. For example, using STEM, the $2Ag/SiO_2\_mIWI\_C500R200$ was found to have an average particle size of $d_{mean} = 1.1 \pm 0.3$nm as shown in Fig.8, in agreement with the slightly smaller size reported by EXAFS ($d_{mean} = 0.9$ nm) when considering the estimated error.

Sample name	N_{Ag-Ag}	R/Å	Est. Size/ nm
$2Ag/SiO_2\_mIWI\_C500R200$	3.8	2.74	0.8
$0.5Ag/SiO_2\_mIWI\_C150R200$	7.0	2.82	2.2
$2Ag/SiO_2\_mIWI\_C250R250S350$	10.1	2.88	5.7
$2Ag/SiO_2\_mIWI\_C250R250S500$	10.6	2.88	6.6
$8Ag/SiO2\_IWI\_C250R250S300$	11.2	2.88	8.0
$8Ag/SiO_2\_IWI\_R325$	11.5	2.89	8.7

Table I Samples, their coordination number (N_{Ag-Ag}), distance to neighbor atom (R), and estimated particle size in Å as determined from Ag K edge EXAFS
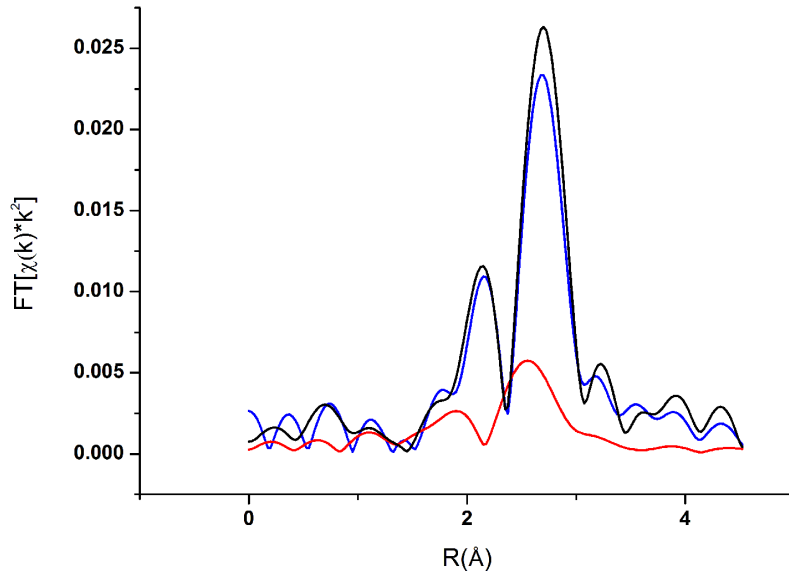
Fig. 6 Fourier transform of the Ag K edge data in R space (k^2: $\Delta k = 2.4 - 10.9$ Å^{-1}). Black line ▬: silver foil; blue line ▬: 8Ag/SiO2_IWI_C250R250S300; red line ▬: 2Ag/SiO$_2$_mIWI_C500R200.
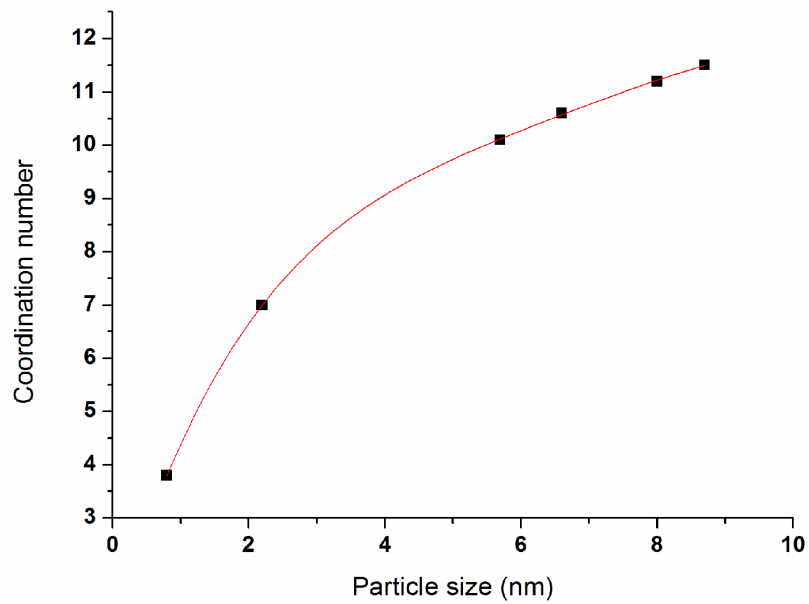
Fig. 7 Coordination number vs. particle size

Silver L$_3$ edge XANES spectra also indicate clear changes according to increasing the particle size. When the particle size is small (sample 2Ag/SiO$_2$_mIWI_C500R200 and 0.5Ag/SiO$_2$_mIWI_C150R200), a small peak arises in the middle of edge at about 3353 eV as marked by solid line in the insert of Fig. 9. This edge peak appears in Ag$^+$ compounds spectra and was assigned to 2p $\rightarrow$ 5s transition [58]. Miyamoto *et al.* [58] suggested that the intensity of the peak for the 4d is a result of 5s-4d hybridization and related to the covalency between silver and its ligand. However, our K edge spectra indicate that the particles are fully metallic, so we ascribe this peak to changes in the hybridization of the Ag-Ag bonds as the coordination decreases[57]. In our case, the peak size shrank with increasing particle size from 0.8 nm (2Ag/SiO$_2$_mIWI_C500R200) to 2.2 nm (0.5Ag/SiO$_2$_mIWI_C150R200). No edge peak was observed in the spectrum of the large particle size sample 8Ag/SiO$_2$_IWI_R325 (8.7 nm). For 8Ag/SiO$_2$_IWI_R325 there are two peaks right after the edge (3363 eV and 3370 eV, marked by dash line in Fig. 9), while no peaks appears at the same energy position for the other two samples. We also observe that the bigger the particles are, the sharper EXAFS oscillation is, because Ag atoms have more neighboring atoms.

Selectivity at 10% conversion versus particle size is plotted in Fig. 10(a). The results indicate that the selectivity to allyl alcohol goes up with increasing the particle size from 1-9 nm. At lower pressure (1 atm) the selectivity obtained over the smallest particle sample 2Ag/SiO$_2$_mIWI_C500_R200 (0.8 nm) is only about 7%. It steadily increases with increasing particle size over the range that we investigated. The best selectivity achieved at 1 atm is 27% on 8Ag/SiO$_2$_IWI_R325. Claus and co-workers previously prepared catalysts in a similar manner with an average particle size of 2.5 nm
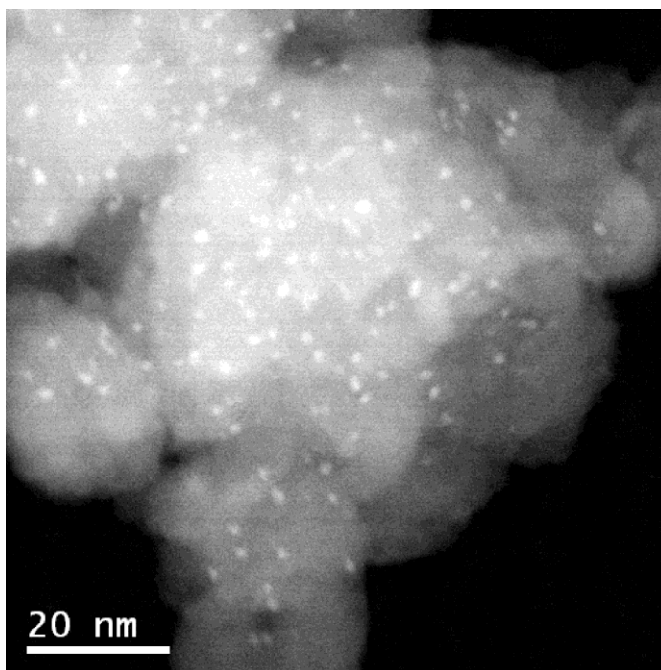
Fig. 8 TEM image of 2Ag/SiO$_2$_mIWI_C500R200

demonstrated a selectivity of 29% at 1 atm[25]. It should be mentioned that the TEM

analysis in Claus' work indicated that at least some of the particles were in the size range

of 12 nm. At higher pressure (5 atm) the selectivity shows the same trend with the

smallest nanoparticles showing a selectivity of 15% and the largest showing a selectivity

of 37%. In contrast to some earlier reports[23, 25], our results unambiguously indicate

that increasing particle size results in increasing selectivity.

The selectivity results indicate that the Ag(111) sites are likely responsible for the

selective hydrogenation of the carbonyl. However, one might suppose that catalysts with

smaller particle size may be more active because the smaller the particles possess more

undercoordinated metal atoms which could act as active sites. Therefore, we estimated a

TOF for the catalysts based on a hemispherical model for particle size whereby only

surface atoms are considered. The number of surface atoms is given by the following
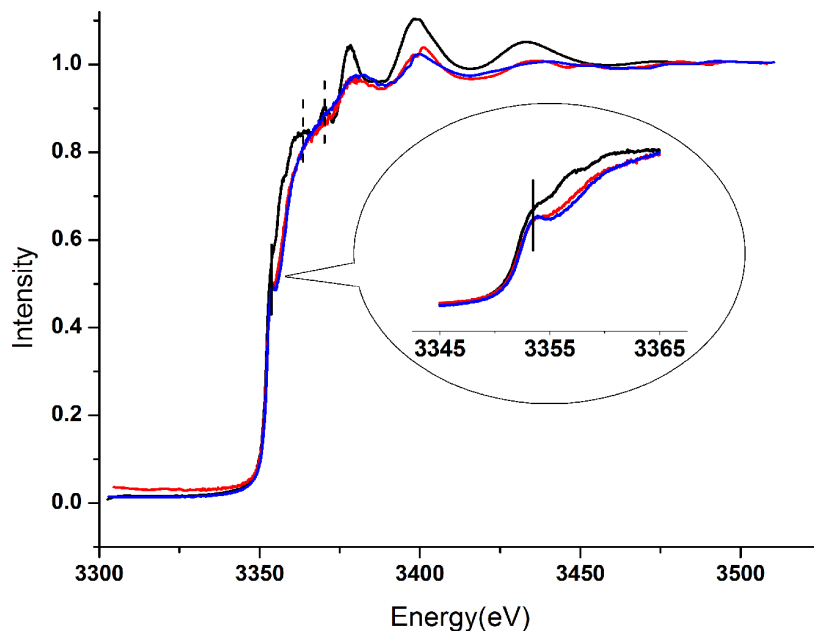
Fig. 9 Ag L_3-edge XANES spectrum of three samples with representative particle sizes: (a) 2Ag/SiO$_2$_mIWI_C500R200 (0.8 nm), solid blue line ▬▬; (b) 0.5Ag/SiO$_2$_mIWI_C150R200 (2.2 nm), solid red line ▬▬; (c) 8Ag/SiO$_2$_IWI_R325 (8.7 nm), solid black line ▬▬.

equation, in which D is the radius of a silver particle and d represents the diameter of Ag atom (0.289 nm in bulk). The rate measurement is reproducible within an error of 4.2%.

$$n = \frac{\pi D^2}{\sqrt{3}d^2} \qquad (Eq.2)$$

Surprisingly, the catalysts having larger particle sizes tended to have higher turnover frequencies. Examining the TOFs of samples at 5 atm total pressure as an example, as illustrated in Fig. 10(b) marked by red dots, the TOF of the silver catalyst having smallest particle size (2Ag/SiO$_2$_mIWI_C500_R200) is 0.06×10^{-2} s^{-1} whereas the TOF improves to 0.53×10^{-2} s^{-1} for the 6.6 nm particle size (2Ag/SiO$_2$_mIWI_C250R250S500), an increase by almost a full order of magnitude. The TOF of the largest particle sample

43

8Ag/SiO$_2$_IWI_R325 rises even more sharply to 2.6×10^{-2} s^{-1}. The TOF results are slightly surprising since they indicate that the most active catalyst is also the most selective one. We have also examined the effect of pressure on the reaction kinetics. First from the results shown in Fig. 10(a) one can notice that increasing the pressure results in better selectivity to allyl alcohol, consistent with the results of Claus' group. We also find that the TOF is enhanced by raising reaction pressure. TOFs at 5 atm are about one order of magnitude higher than at 1 atm.

We extended our study of gas phase acrolein hydrogenation over Ag/SiO$_2$ catalysts by performing a more in-depth analysis of the kinetics. We focus here on one particular catalyst, 8Ag/SiO$_2$_IWI_R325, which we found to have the highest selectivity among the samples we measured. Measurements of reaction kinetics were made for a variety of process conditions under both low (1 atm) or high (5 atm) pressure. For a complete kinetics study we assumed a simple power rate law:

$$r = k[Acrolein]^m[H_2]^n$$

We varied the concentration/partial pressure of acrolein or H$_2$ to attain the reaction orders of both reactants. Taking the logarithm yields:

$$\ln(r) = \ln(k) + m\ln[Acrolein] + n\ln[H_2]$$

Since k is only a function of temperature here, at fixed T the slope from plotting ln(r) against ln[acrolein] is m when keeping the concentration of H$_2$ constant. n can be determined in an analogous manner. The reaction orders under two different pressures and other kinetic parameters are presented in Table II.
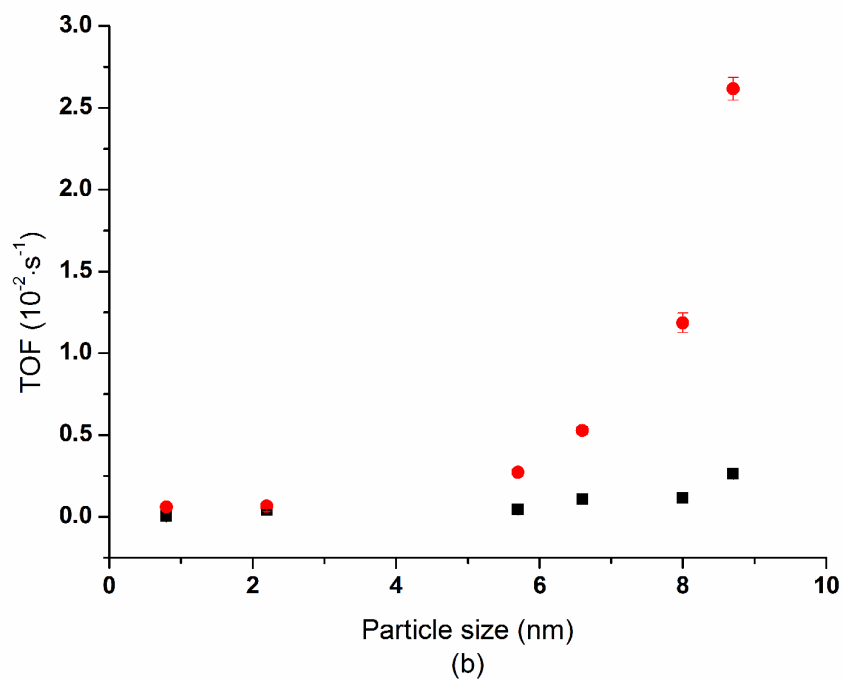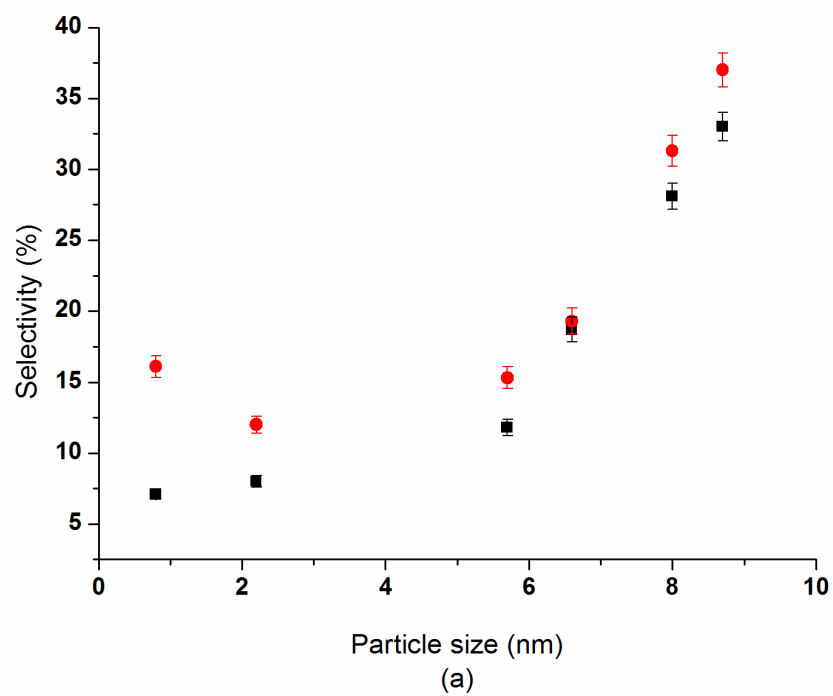
Fig. 10 Particle size effects under two different pressures. Black square ■: 1 atm; red circle ●: 5 atm. (a) Selectivity at 10% conversion vs. particle size; (b) TOF vs. particle size effect.

Pressure [atm]	rate [mol h^{-1}g$_{Ag}$$^{-1}$]	E$_a$ [kJ/mol]	m	n	k [mol/gAg·hr·atm$^{1.5}$]	A
1	0.014	53	0.93	0.58	0.43	3.3×10^5
5	0.139	42	0.77	0.65	0.25	1.0×10^4

Table. II Reaction rate, activation energy E$_a$, reaction order m and n, rate constant k and pre-exponential factor A of Arrhenius Equation at different pressures acquired on 8Ag/SiO$_2$_IWI_R325 given the rate law equation $r = k[Acrolein]^m[H_2]^n$.

Assuming an Arrhenius expression for the rate law, ploting ln(k) against 1/T generates a straight line, with a slope of –E$_{act}$/R. The Arrhenius plots under low and high pressures are shown in Fig. 11. The apparent activation energy of acrolein conversion is
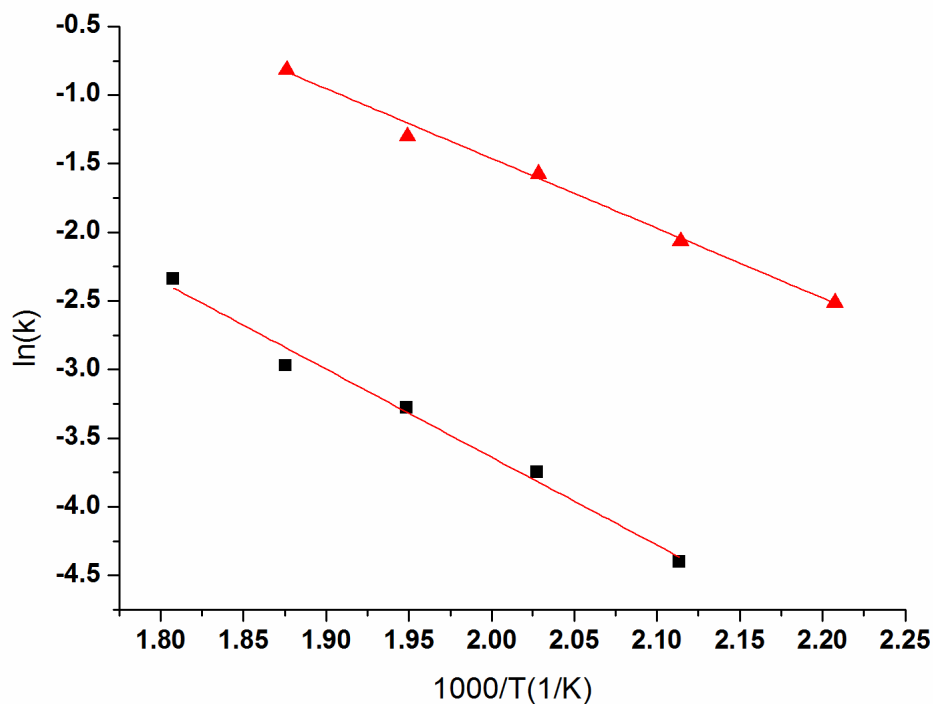
Fig. 11 Arrhenius plot of hydrogenation of acrolein over 8Ag/SiO$_2$_IWI_R325 at 1 atm (black square ■) and 5 atm (red circle ●).

53 kJ/mol at 1 atm but is slightly lower to (42 kJ/mol) at 5 atm. Higher pressure seems to lowers the reaction barrier and also lowers the reaction order for acrolein.

Our results are consistent with Claus' group's result using Ag/TiO$_2$ catalysts for selective hydrogenation of crotonaldehyde[45], although their use of a TiO$_2$ support prevents us from a direct comparison. The structure sensitivity of our silver catalysts (*i.e.* increasing particle size increasing the selectivity towards allyl alcohol) are also similar to what they obtained on a series of gold catalysts [19]. It seems very likely that the increased selectivity and activity with particle size is related to larger portion of (111) surface on larger particles, where acrolein adsorbs especially through C=O bond and its activation are favored. It is not currently clear why the presence of undercoordinated atoms on the surface is unfavorable to acrolein hydrogenation.

In contrast, the effect of pressure is easier to understand when we return to previous fundamental studies. Both the experimental studies of Brandt *et al.* and the computational efforts of Ferullo *et al.* [43] support the notion that the adsorption mode of acrolein is highly sensitive to coverage. At low coverage (low pressure), the molecule may adsorb parallel to the surface but as the coverage (pressure) increases, the adsorption geometry shifts to present the C=O bond to the surface. From our results of reaction order (Table. II), the reaction of order of acrolein is smaller at higher pressure, clearly indicating that raising reaction pressure leads to a higher coverage of acrolein. In addition, Rösch and co-workers have previously found that dissociation of hydrogen on Ag surfaces is a difficult process requiring both high temperature and high pressure to accomplish at high rates[59-61]. One may anticipate that continuing to increase the pressure may enhance the selectivity and activity further.

47

To probe the reaction kinetics further, a pathway analysis has been performed for 8Ag/SiO$_2$_IWI_R325. This method was developed by Bhore *et al.* [44, 62] for discernment of the rank (*i.e.*, primary, secondary, etc.) of a reaction product. We consistently observe four products: propanal, allyl alcohol, propanol, and propene. The first-rank delplot method (a plot of selectivity of a product vs. reactant conversion) allows the separation of primary products from non-primary products. By extrapolating the plot of selectivity vs. conversion to zero conversion, one finds that for primary products that the intercept is non-zero. However, if the intercept is zero, the product is nonprimary. Higher rank products can be determined by a higher rank delplot. For example, secondary products can be identified by plotting (component selectivity)/(conversion) against conversion. At zero conversion, primary products have infinite intercepts, secondary products have finite intercepts and higher-order ones have zero intercepts.

Fig. 12 is the delplot for the primary and secondary product determination at atmosphere pressure. As illustrated in Fig. 12 (a), propanal and allyl alcohol are clearly first rank, and propanol and propene are of higher rank. In Fig.12 (b) the fitting curves for propanal and allyl alcohol diverge at zero conversion confirming they are primary products. The intercept of propanol is nonzero, implying it is a secondary product, while propene may be a higher rank product due to its zero intercept. However, the selectivity to propene may be too low to make an accurate evaluation so one must use some caution. Similar plotting was done on the same catalyst at high pressure (5 atm) as shown in Fig.13. Over this range, one can clearly see that all the product ranks remain the same as at atmosphere pressure.

The advantage of doing the first-rank plotting is not only to tell the primary

48
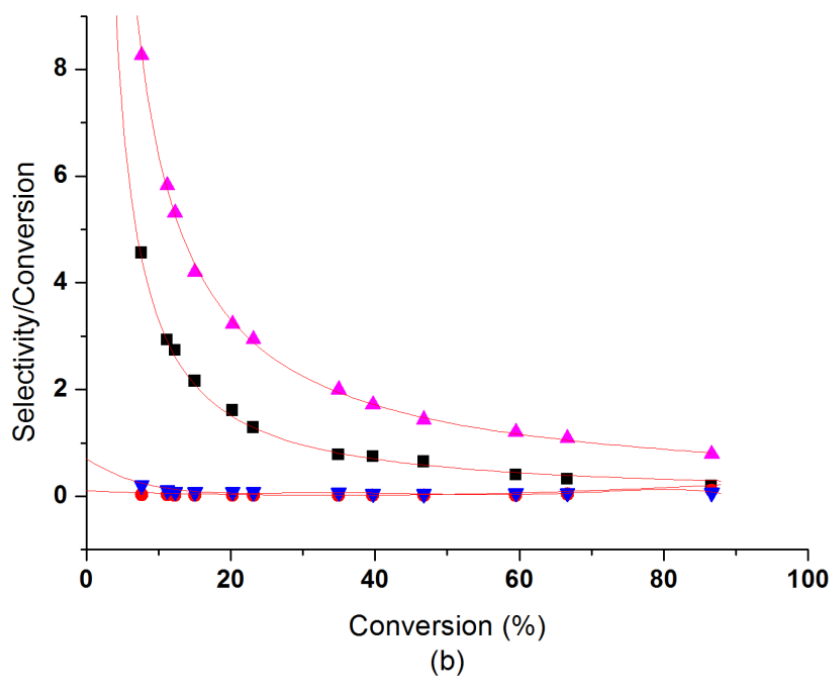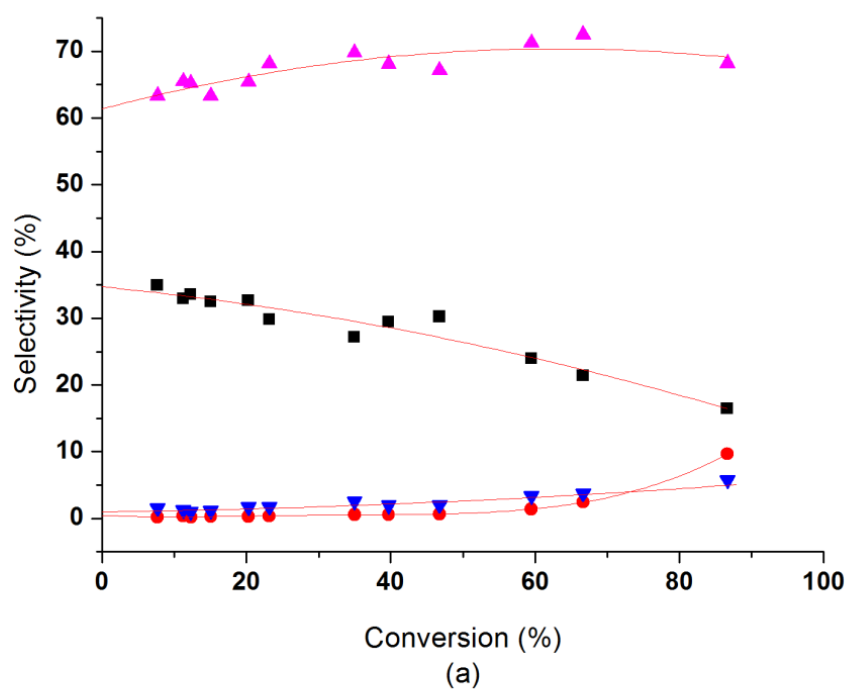
Fig. 12 Pathway analysis under 1 atm: (a) first-rank delplot; (b) second-rank delplot.
Magenta triangle ▲: propanal; black square ■: allyl alcohol; blue up-side-down triangle
▼: propanol; red circle ●: propene

49
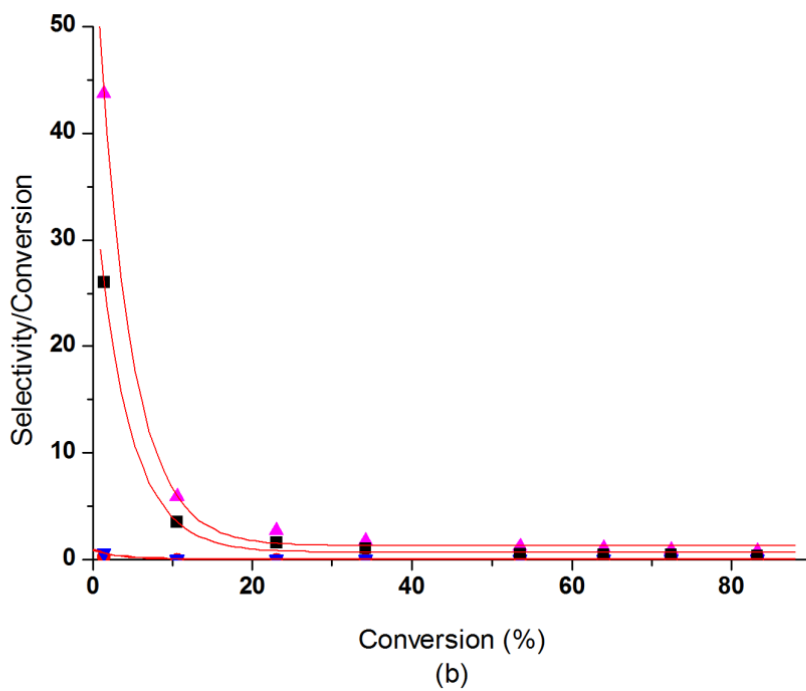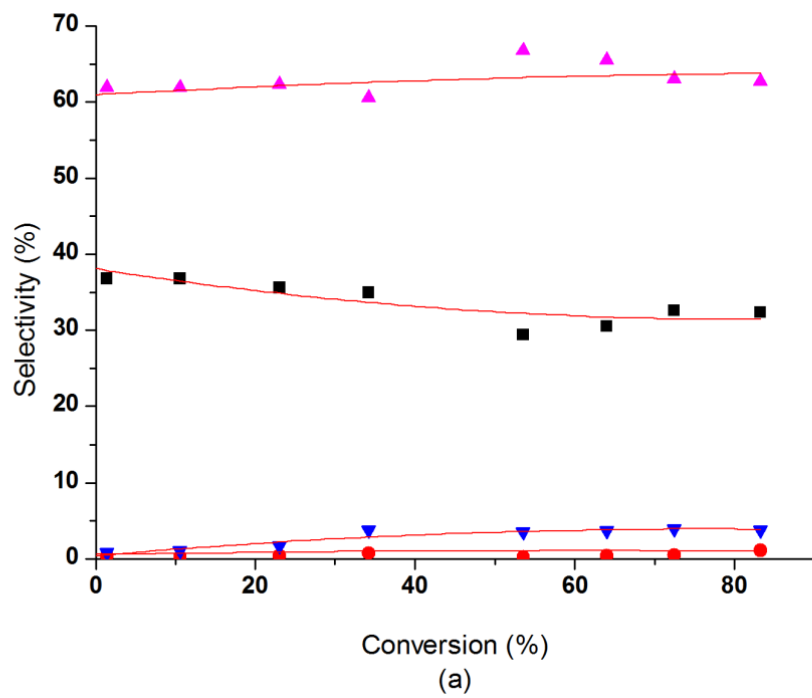
Fig. 13 Pathway analysis under 5 atm: (a) first-rank delplot; (b) second-rank delplot.
Magenta triangle ▲: propanal; black square ■: allyl alcohol; blue up-side-down triangle
▼: propanol; red circle ●: propene.

products from the others, but also to provide a relationship between selectivity and conversion so that the selectivity for a specific conversion can be read via the curve. Thus a fair performance comparison of different catalysts can be conducted. Comparing the first-rank delplot under 1 atm and 5 atm, the selectivity at higher pressure at the initial conversion is higher but not by a large extent (37% at 5 atm vs 33% at 1 atm), in agreement with Claus' result. However, with increasing conversion the selectivity at atmospheric pressure apparently decreases. The allyl alcohol selectivity is 27% at 35% conversion and decreases with increasing the conversion. However at higher pressure the selectivity remains virtually constant. The selectivity only decreased by 2% to 35% when the conversion is 35%. Higher pressure seems to not only improve the selectivity of the catalyst but prevents deleterious side reactions that can occur at high conversion.

As mentioned earlier, for minority products it may be difficult to precisely determine the product rank from the delplot analysis. To overcome this obstacle, additional secondary pathway analysis was performed using the primary products propanal and allyl alcohol as reactants in the feed instead of acrolein. When propanal is used as the feed (Fig. 14(a)), propanol is the only product that we observed. This implies that propanal is stable. However, when we use allyl alcohol as the feed, three products are observed: propene, propanol and propanal (Fig. 14(b)). The selectivity to propene is 5%, the selectivity to propanol is 25%, while the primary product is propanal (70%). This experiment suggests that propene is a second-rank product produced from hydrodeoxygenation of allyl alcohol (we did not attempt to analyze water, the other likely product from the hydrodeoxygenation reaction). To our knowledge propene has not been previously observed as a product of acrolein hydrogenation over Ag

51
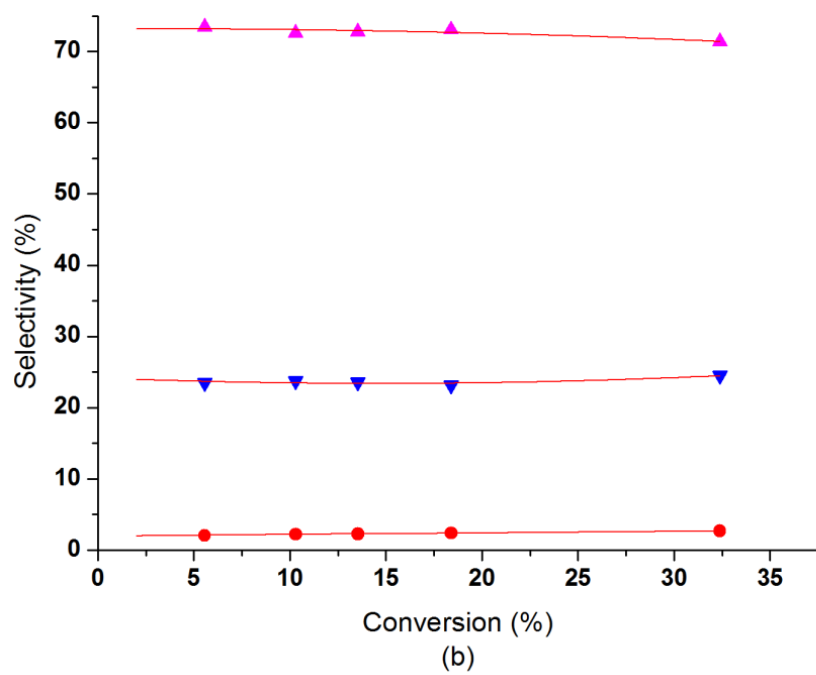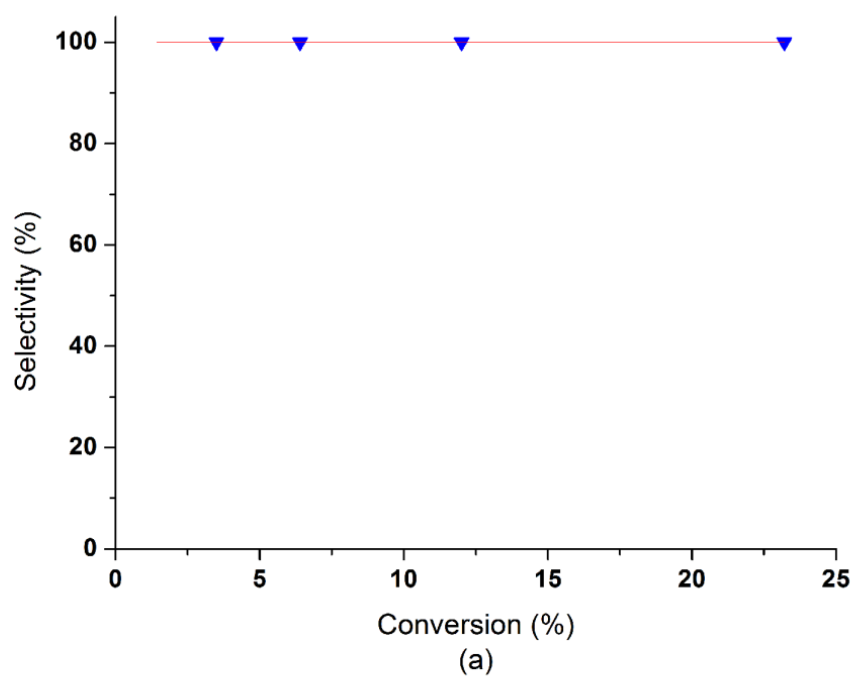
Fig. 14 Secondary pathway analysis from (a) propanal; (b) allyl alcohol. Magenta triangle ▲: propanal; blue up-side-down triangle ▼: propanol; red circle ●: propene.

catalysts. However propane has been previously observed in trace amounts by some researchers over Pt/SiO_2 [16, 63] and silver is typically used to prevent overhydrogenation of alkenes to alkanes [64-66].

In our case, propene does not appear in substantial amounts until relatively high conversion so other researchers may not have attempted to quantify it at low conversion. In addition, allyl alcohol could be fully hydrogenated to propanol, which is not surprising. Finally, we observe that allyl alcohol is easily isomerized to propanal but propanal cannot be isomerized to allyl alcohol on silver catalyst under our reaction condition. Additional tests of the support material in the absence of Ag show no activity for isomerization of allyl alcohol. Our result implies propanal may be produced not only from hydrogenation of acrolein but also from the isomerization reaction. Therefore a successful catalyst for the selective hydrogenation of acrolein must not only hydrogenate C=O bond, but also prevent the isomerization from allyl alcohol to propanal. However, when the isomerization has not been eliminated, one cannot obtain high selectivity at high conversion and the reaction needs to be run at low conversion to achieve high selectivity to allyl alcohol.

2.4   Conclusion

For silver nanoparticle on silica catalysts, larger particle size favors higher rate and selectivity to desired allyl alcohol product. The higher selectivity may be the result of the adsorption geometry of acrolein on larger particles, suggesting that low Miller index surfaces are important for selective hydrogenation of acrolein. As observed by Claus' group, higher pressure yields higher selectivity. The pathway analysis shows that allyl

53

alcohol and major part of propanal are first-rank products and propanol and propene are second-rand products. A small part of propanal is secondary product from allyl alcohol. The isomerization from allyl alcohol to propanal lowers the yield at higher conversion. An ideal catalyst requires selective hydrogenation of C=O bond without allyl alcohol isomerization to propanal.

3   SUPPORT EFFECTS ON SELECTIVE HYDROGENATION OF ACROLEIN

3.1   Introduction

Regioselective hydrogenation of α, β–unsaturated aldehydes to allylic alcohols is challenging because the hydrogenation of the olefinic bond is thermodynamically easier than the carbonyl group by ca. 35 kJ/mol [5]. The reaction network is shown in Fig. 1. The desired products, unsaturated alcohols, are used in drugs, perfumes and synthesis of fine chemicals thus are of commercial interest.

Acrolein is the simplest homologue of α, β–unsaturated aldehydes but also the hardest one to be selectively hydrogenated because of no substituents on C=C bond. A good selectivity to the desired product allyl alcohol has never obtained on conventional hydrogenation catalysts like Ru, Pd and Pt [15-18]. Instead the best reported selectivites have been over Ag and Ag alloy catalysts. This is surprising since Ag is usually considered inert to H_2 chemisorption and therefore not to be able to provide large surface concentrations of atomic hydrogen for hydrogenation reactions [26, 59]. To combat the low activity of Ag for H_2 dissociation, Bron *et al.* [25] examined acrolein hydrogenation at 250 ℃ over Ag/SiO$_2$ catalysts at pressures of up to 20 bar and found that higher pressure favored the selective production of allyl alcohol. For example, no allyl alcohol was formed below 75 mbar. However, the selectivity increased rapidly to 28% when the pressure reached about 1 bar, continued increasing to ~36% at 5 bar, and eventually reached a plateau of ~42% above 10 bar.

Particle size effects have also been reported for this system. Grünert *et al.* reported a combined particle size effect and SMSI effect based on a comparison of two Ag/TiO$_2$ catalysts [23]. While Ag/TiO$_2$ samples reduced at 200 °C (LTR) had ~3 nm mean diameter, the mean diameter of catalysts reduced at 500 °C (HTR) was ~1.5 nm. Higher selectivity (LTR: 42%; HTR: 27%) and one order of magnitude higher TOF was observed over the catalysts reduced at low temperature. Grünert *et al.* explained that Ti suboxide overlayers were formed due to SMSI at higher reduction temperature. As a result, growth of silver particles was inhibited and a truncated particle morphology deviating from spherical shape was formed. Accordingly, both activity and selectivity were hampered. Recently our group has performed our own systematic study on particle size effects for acrolein hydrogenation examining a series of Ag/SiO$_2$ catalysts [67]. We investigated a series of silica supported silver catalysts and have demonstrated that larger particles led to both higher TOF and higher selectivity to allyl alcohol. Although the size effects and pressure effects appear clear over Ag/SiO$_2$, it is not yet determined if the trends are universal.

In addition to particle size effects, support effects are also a well-known and widely studied phenomenon in heterogeneous catalysis [68-72]. Not only do supports act as high surface area thermostable carriers of active metals, they also play an important role in improving the activity and selectivity of catalysts by interacting with metals. Support effects have been previously recognized for the selective hydrogenation of α, β–unsaturated aldehydes. Coq and co-workers [69] studied liquid phase hydrogenation of cinnamaldehyde over supported Ru based catalysts. Among γ-Al$_2$O$_3$, SiO$_2$, TiO$_2$ (anatase), graphite and ZrO$_2$, ZrO$_2$ had the best performance in terms of selectivity.

Although the particle sizes of the catalysts loaded on different supports were various, a plot of selectivity to cinnamyl alcohol versus hydrogen uptake (H/Ru) was developed in order to discriminate between the support effect and particle size effect. Ru/Al_2O_3, Ru/SiO_2 and Ru/graphite demonstrated similar behavior, indicating that the support effect was negligible on these three supports and the selectivity was merely size dependent. In contrast, Ru/TiO_2 and Ru/ZrO_2 catalysts had much higher selectivity than what H/Ru values could predict. The abnormal behavior of these supports was attributed to an SMSI effect. The authors also proposed that a RuZr phase could be formed during the reduction of ZrO_2 and enhance the selectivity or that partially reduced sites ZrO_2 may play a role in the reaction.

Vannice *et al.* examined the hydrogenation of CO [70], acetone [71] and crotonaldehyde [72] over platinum catalysts attempting to capture a clear picture of how the nature of supports influenced the interaction between the carbonyl group and the catalysts, using molecules of increasing complexity. The use of TiO_2 as a support enhanced C=O bond hydrogenation in all cases, no matter whether C=O bond was conjugated with C=C bond or not. When examining the hydrogenation of crotonaldhyde, no unsaturated alcohol product was detected on silica or alumina supported catalysts, while the most selective titania supported catalyst provided 37% selectivity to crotyl alcohol when tested at 318 K and 1 atm pressure. It was believed that new sites, i.e., Ti^{3+} (or Ti^{2+}) or oxygen vacancy were created at the metal-support interface and led to the activation of C=O bonds. The authors discounted the supposition that hydrogen spill-over was responsible for the selectivity improvement because no enhancement was observed in physical mixtures of Pt and TiO_2 for the hydrogenation of CO [73] and acetone [71].

57

Hidalgo-Carrillo *et al.* [74] studied liquid phase crotonaldehyde hydrogenation over Pt catalysts loaded on various partially reducible supports including Fe_2O_3, Fe_3O_4, ZrO_2, ZnO, TiO_2 and SnO_2. When the catalysts were tested at 30 ℃ with initial hydrogen pressure of 0.414 kPa for 8 hours using the mixture 1.4-dioxane as solvent, the highest selectivity was 75% obtained on Pt/ZnO which was reduced at 175 ℃. The extraordinary performance was suggested to result from the formation of ZnO_xCl_y around Pt particles. The ZnO_xCl_y phase which was detected by XPS may serve as Lewis acid sites and anchor the carbonyl bond in crotonaldehyde during adsorption, resulting in better selectivity to crotyl alcohol.

Bron *et al.* did perform an examination of support specifically for acrolein hydrogenation over Ag catalysts [24]. Silver catalysts supported on SiO_2, Al_2O_3 and ZnO were synthesized in the same way by incipient wetness impregnation and tested in similar reaction conditions. SiO_2, Al_2O_3 gave similar selectivities 39% and 42%, respectively, while Ag/ZnO showed a best selectivity of 50%. However, the particle sizes of those catalysts were prominently different. The mean particle size of Ag/SiO_2 was only 2.5 nm; that of Ag/Al_2O_3 was a lot bigger, 11 nm; Ag/ZnO had very broad size distribution and the particle size of it could not be estimated. Thus the difference in particle size may also contribute to the difference in catalytic activity and selectivity.

In addition, Volckmar *et al.* systematically varied the support acidity in a series of SiO_2-Al_2O_3 catalysts [27]. The SiO_2:Al_2O_3 ratio was changed in the Al_2O_3 content from 0 to 100% Al_2O_3 in 20% steps. From NH_3-TPD and pyridine-IR results, the highest total acidity with both the most and strongest of Lewis acid sites were achieved at medium Al_2O_3 contents (40% and 60%). These catalysts showed lower TOF (by a factor of 3-4)

and only a 30 % selectivity to allyl alcohol as compared to the >40% selectivity for Ag/Al$_2$O$_3$ and Ag/SiO$_2$ catalysts. A conclusion was drawn that a decrease in the total acidity and the number of strong Lewis acid sites would lead to a better selectivity and activity. Still it is not clear if other types of support effects are possible beyond tuning of acid/base properties.

An extended support effect study on acrolein hydrogenation is still lacking. Therefore, here we propose a systematic study on how the nature of supports affect the catalyst performance, choosing some of the most prominent examples of metal oxide supports: SiO$_2$, Al$_2$O$_3$ and TiO$_2$. Since we have already examined a series of silica supported silver catalysts from our previous study of particle size effects [67], these data are employed to aid comparisons across supports since particle sizes are difficult to tailor precisely. The trends can be elucidated by examining a series of different sizes on each of the three supports.

3.2   Experimental

3.2.1   Preparation of catalysts

Al$_2$O$_3$ (γ- Al$_2$O$_3$, 210 m^2/g) and TiO$_2$ (p25, Degussa, 32 m^2/g) were chosen to be the carriers of silver nanoparticles in order to study the support effects and the catalysis was compared with SiO$_2$ (silica gel, Sigma-Aldrich, 35-60 mesh, 285 m^2/g) supported catalysts, the synthesis and the catalytic performance of which were described elsewhere [67]. TiO$_2$ was preheated to 550 °C to guarantee good thermal stability before use. To develop the proper comparisons and mitigate particle size effects, samples with different

59

silver particle sizes were created on all three supports. Particle sizes could be directed via, different synthesis approaches and variation of subsequent treatments, of calcination, reduction and steaming. When large particle size was desired, direct incipient wetness impregnation (IWI) using $AgNO_3$ neutral aqueous solution as the precursor and inclement treatments were utilized; when small particle size was targeted, modified incipient wetness impregnation (mIWI) and mild treatments were preferred. mIWI is a revision of normal IWI inspired by strong electrostatic adsorption (SEA) [56] whereby the pH of the solution is adjusted to enhance interaction of the precursor with the support. For example, instead of using silver nitrate solution as is, ammonia hydroxide was added to adjust pH value. We typically used 1 mL of water to dissolve silver nitrate and added 30% ammonia hydroxide drop by drop until the precipitate was fully dissolved. Water and ammonia hydroxide were added so that the total volume of the solution equaled the amount that was required to fill up the support pores and ensure the final pH was around 11. Under these conditions, the $AgNO_3$ precursor reacts to become $Ag(NH_3)_2NO_3$. The basic solution could deprotonate the hydroxyl groups on the support surfaces and served to help disperse the precursor well. After impregnation, catalysts were first dried at room temperature for an hour then at 125 ℃ overnight. Further a combination of treatments, i.e., calcination, reduction and steaming, were carried out on each sample. The calcination treatments were performed for 2 hours in a furnace open to the atmosphere but without flow. The reduction treatments were performed in a tube furnace with a 50 mL/min flow of 3.5% H_2 for 2 hours. The steaming treatments were performed by flowing 50 ml/min of He over a stainless steel bubbler which was preheated to 55 ℃, so there was about 15% water vapor in the total flow. The flow was brought to the reactor at

60

the steaming temperature. Steaming treatments were performed for 1-3 hours to vary particle size. The sample name includes the information of metal loading, support, preparation method and treatment. For instance, 8%Ag/Al$_2$O$_3$_IWI_R325S550 represents an alumina supported silver catalyst loaded with 8 wt% of silver by direct incipient wetness impregnation, reduced at 325 ℃ and steamed at 550 ℃.

3.2.2   Characterization

EXAFS   As proven before [57, 67], EXAFS (extended X-ray absorption fine structure) is a powerful and efficient tool to estimate particle size. In this work it was used as the only method to estimate the particle sizes. Ag K edge EXAFS spectra were taken at the beamline of the Materials Research Collaborative Access Team (MRCAT, 10-ID and 10-BM) at the Advanced Photon Source (APS), Argonne National Laboratory. All the samples were grounded before packed into sample holder. They were then reduced in 3.5% H$_2$/He at 200 ℃ for one hour, cooled in He and scanned at room temperature in He in an environmental cell in transmission mode. Ag foil was scanned at the same time for energy calibration. Data was processed using WINXAS 3.1 and coordination number and bond distance were achieved for particle size estimation. One should notice that the particle size obtained by EXAFS fitting is an averaged number and no distribution is given as by TEM.

3.2.3   Catalysis

Acrolein hydrogenation was performed in gas phase in a 1/2 inch OD stainless steel fixed-bed plug flow reactor. Reaction feed gas (hydrogen and argon) flow was controlled by mass flow controllers. Acrolein (Fluka ≥ 95%) was delivered by a liquid pump (VICI M6), evaporated at 70 °C in a heat tape traced four way cross packed with quartz wool, and carried in to the system by reaction feed gas (argon and hydrogen). The ratio of acrolein and H_2 is 1:20. 60-400 mg of catalyst was used for each test depending on the activity. The gas phase concentration of acrolein was checked for every run by via a reactor bypass line that connects directly to the gas chromatograph. Catalyst samples were reduced *in-situ* in 20% H_2/Ar flow at 200 °C for an hour before testing. The reaction temperature was also 200 °C and pressure was 5 atm. The reactor effluent was analyzed by an on-line gas chromatography (Agilent 6890) equipped with a dual column formed by a RT-Msieve 5A and a RT-QPLOT (Restek) for lighter gaseous species and a EC-Wax (Alltech) for less volatile species such as alcohols. TCD (thermal conductive detector) and FID (flame ionization detector) were both used for detecting H_2 and other organic/flammable compounds, respectively. High-pressure-tolerant stainless steel parts were utilized to build the system. The whole system was heat-traced to avoid condensation of any product. Product identification was later confirmed via GC/MS in a separate system. All potential products were calibrated for their retention times by the GC/MS using the same column setup in various trial runs involving calibrated mixtures of acetaldehyde and other products (acrolein, propanal etc.)

3.3   Results and discussion

Various particle sizes on different supports were desired because a trend for each type of support can be derived and an equitable comparison can be made based on the trends. During synthesis, we clearly observed that the different supports interact with the loaded silver in their own unique ways. On Al_2O_3, the particles tended to be smaller than those on SiO_2 or TiO_2. For example, by following the exactly same procedure, the mean particle size of 8Ag/Al_2O_3_IWI_R325 was 6.4 nm, while 8Ag/SiO_2_IWI_R325 had a particle size of 8.9 nm. In contrast, direct incipient wetness impregnation made huge particles on TiO_2 even followed by mild treatments. As a result, modified IWI was used for all titania supported samples. The sample sizes, their coordination numbers and Ag-Ag bond distances are listed in Table III. We are also showing the normalized EXAFS spectra of the middle size samples on each support in Fig. 15. The edges are all of the same position and shape compared to silver foil, indicating all samples were fully reduced.

Sample name	N_{Ag-Ag}	R(Å)	Est. Size (nm)
2Ag/Al_2O_3_IWI_C200R200	6.9	2.83	2.2
8Ag/Al_2O_3_IWI_R325	10.5	2.87	6.4
8Ag/Al_2O_3_IWI_R325_S550	11.3	2.88	8.2
2Ag/TiO_2_mIWI_C250_R100	9.6	2.87	4.8
3Ag/TiO_2_mIWI_C500_R120	10.7	2.88	6.8

Table III Samples, their coordination number (N_{Ag-Ag}), distance to neighbor atom (R) in Å, and estimated particle size in nm.

Acrolein hydrogenation was carried out over all catalysts. Propanal and allyl alcohol were found to be two major products (~95% total). We compared the selectivity to allyl alcohol (the desired unsaturated alcohol) at same conversion (10%) to avoid drawing any arbitrary conclusions as the selectivity changes with the conversion. The relationship of selectivity versus particle size are plotted in Fig. 16. The particle size effect on selectivity that we observed on silica supported silver catalysts, i.e., the bigger the particle size the higher the selectivity, appears universal across the supports studied.
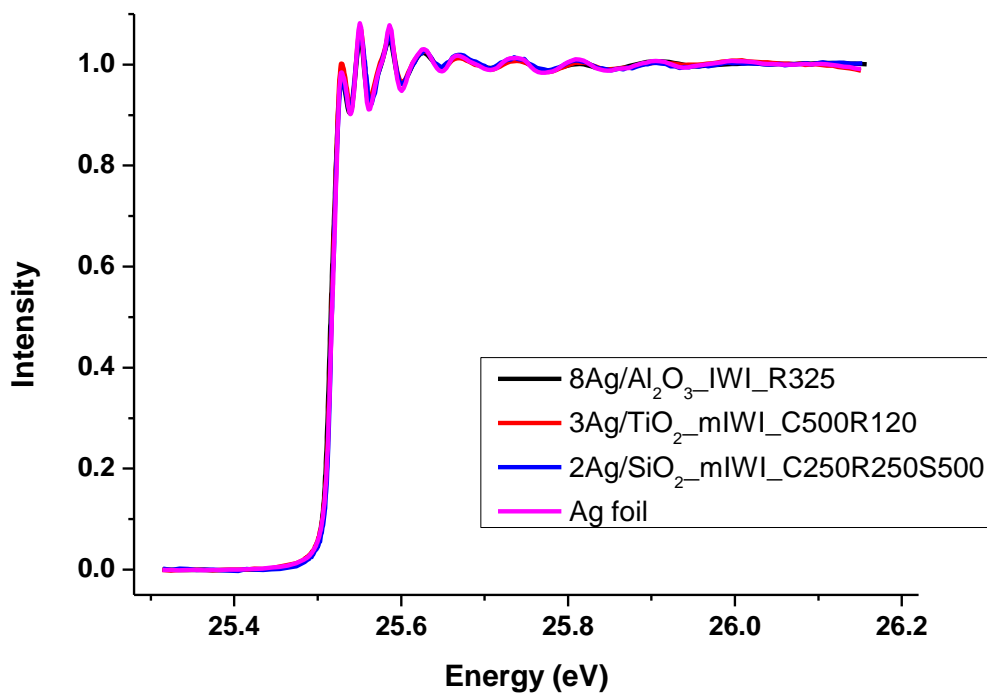
(a)
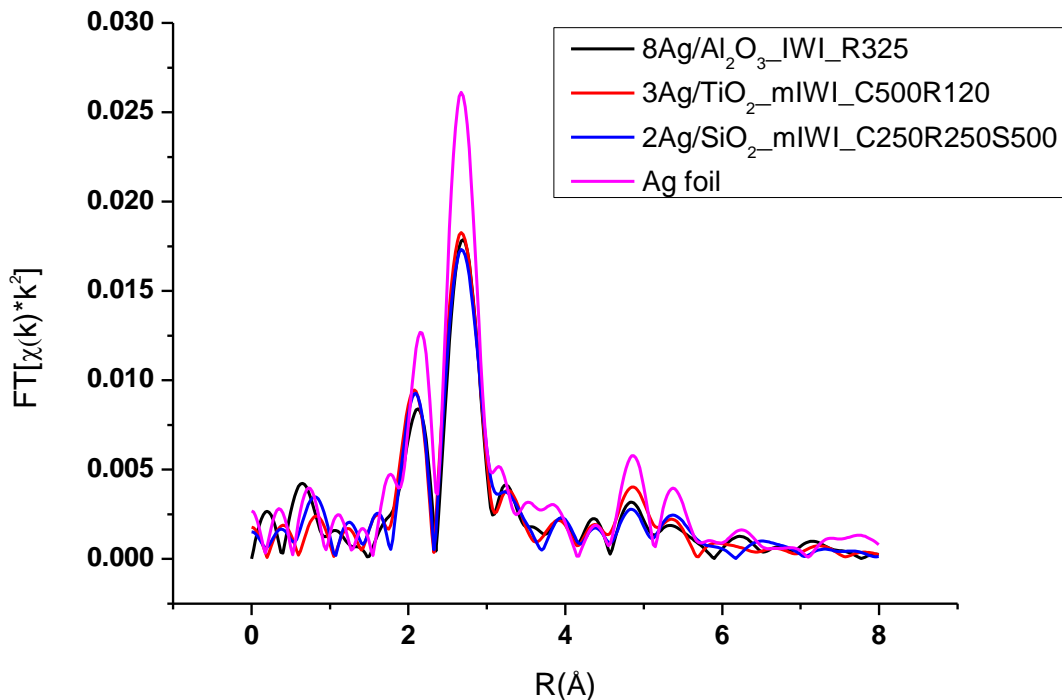
(b)

Fig. 15 Ag K edge spectra of Ag foil and three samples with similar medium particle size on different supports: 8Ag/Al_2O_3_IWI_R325 (6.4 nm), 3Ag/TiO_2_mIWI_C500R120 (6.8 nm), and 2Ag/SiO_2_mIWI_C250R250S500 (6.6 nm). (a) normalized data, (b) Fourier transform of the experimental data in R space.

The result suggests that larger particles with a higher percentage of flat terrace sites favor the hydrogenation of C=O bond over the conjugated C=C bond, consistent with our previous results and those of other researchers [23, 25, 75, 76]. Alumina supported samples more or less fell in the same trend line with silica supported samples. The sample with smallest particle size (2Al_2O_3_IWI_C200R200, 2.2 nm) had same selectivity as the silica supported sample with same particle size. The medium size (6.4 nm) one showed slightly better selectivity to allyl alcohol (22% on Al_2O_3 vs. 18% on SiO_2). However, the

65

selectivity did not continue increasing significantly like when SiO_2 was used as support. It increased by only 2% with increasing the particle size from 6.4 nm to 8.2 nm. The titania supported catalysts showed much higher selectivity than either silica supported or alumina supported catalysts. The trend line of selectivity vs. conversion for titania supported samples was obviously above that for either silica or alumina (i.e. beyond typical experimental errors which might be on the order of $\pm 2\%$ based on repeated runs of the same catalyst). The selectivity of the medium size sample 2AgTiO_2_mIWI_C250R100 (4.8 nm) was 29%. This was about twice as big as the selectivity on the same-size silica-supported sample. The sample 3AgTiO_2_mIWI_C500R120, which had a particle size of 6.8 nm, gave 39% selectivity while silica supported sample having the same size could only provide about 20% selectivity according to the trend line of silica samples. In all sizes within the range we studied, titania doubled the selectivity compared with SiO_2.

It has been previously reported that partially reducible supports, such as TiO_2, CeO_2 and SnO_2 can improve the catalytic performance. There are various explanations for that but they generally fall into three categories: (i) new sites created at the metal-support interface, including creation of alloy phase by the loaded metal and the reduced support [70, 72, 77]; (ii) formation of support overlayer on the metal particles [23] or structural change of the metal particles[20]; (iii) electron transfer between the metal and support [78, 79]. One or more of the effects may be the origin to the apparent support effect in selectivity and/or activity. In our case, since all TiO_2 supported catalysts were reduced at low temperature 100-120 ℃, migration of support onto silver particles seems unlikely. Thus we propose that TiO_2 changes the properties of Ag through effect (i) or/and (iii). As

shown in Fig. 17, not only the selectivity to allyl alcohol but also the TOF was enhanced by using TiO_2 as support. Formation of new sites, for example partially reduced Ti^{3+} species which can serve as a Lewis acid sites, could favor the adsorption of acrolein and especially through C=O bond and result in better selectivity and activity. It is also suggested that the selectivity of acrolein hydrogenation increases when the interaction with the substrate decreases. If there is a strong interaction between the Ag and the TiO_2 support, then the TiO_2 supported nanoparticle may be less reactive (*i.e.* the *d*-band of the Ag nanoparticle moves further away from the Fermi level when supported on TiO_2 vs. Al_2O_3 or SiO_2). Campbell and co-workers have applied this analysis to the changes in the heats of adsorption of silver on various substrates [80-82]. When the particle size of
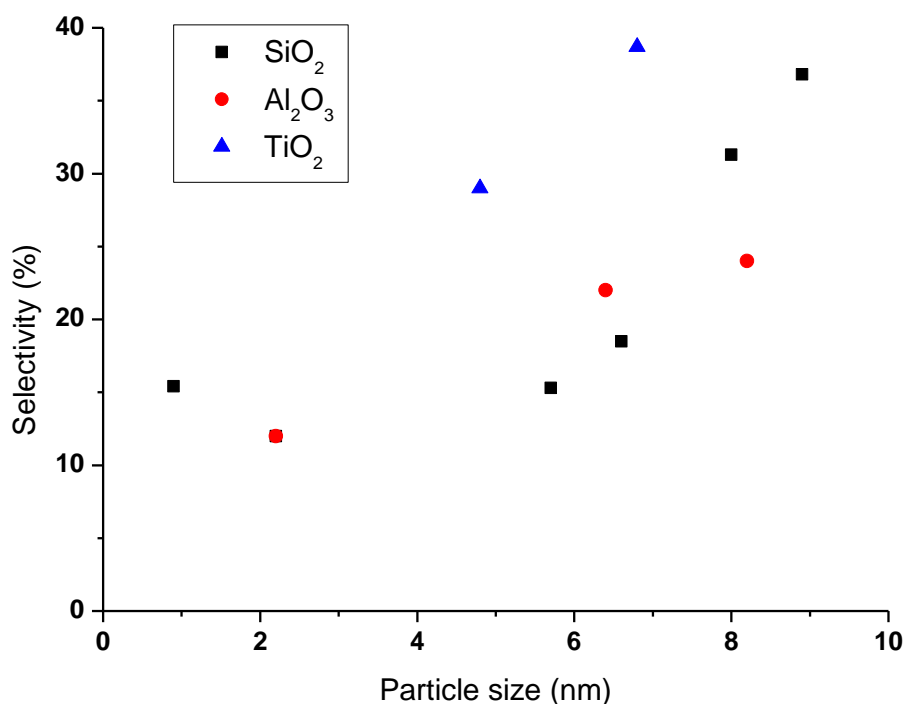
Fig. 16 Support effect on selectivity

silver was smaller than 4 nm, the heat of adsorption on slightly reduced $CeO_2(111)$ and $Fe_3O_4(111)$ were much higher than that on MgO(110). As a result, it was concluded that reducible supports had stronger interactions with silver than non-reducible supports. Campbell, et al. have further suggested that adsorption of molecules on the metal nanoparticles should be sensitive to the bond strength between the particle and the support. Using a simple bond order conservation argument, an adsorbate would bind strongest to a metal nanoparticle on a weak interacting support but the adsorbate would have a weaker interaction with a metal nanoparticle supported on a highly reducible support where a strong metal support interaction exists [82]. In our case, a decrease in the adsorption strength of acrolein on TiO_2 supported Ag vs. SiO_2 or Al_2O_3 supported Ag (which possess a weaker interaction) may therefore increase the selectivity.

In contrast, the behavior of Al_2O_3 supported catalysts do not follow the same trend as the TiO_2 and SiO_2 supported catalysts with respect to their activity. Over SiO_2 and TiO_2 catalysts turnover frequency all increased with increasing the particle size, while the trend was inverted over Al_2O_3 supported catalysts. TOF decreased steadily with the particle size increasing from 2.2 nm to 8.2 nm. When particle size was small on Al_2O_3 TOF of catalyst was 1.6×10^{-2} s^{-1}, about 15 times as large as that over silica supported sample having same particle size. For a medium size Al_2O_3 sample 8Ag/Al_2O_3_IWI_R325, TOF decreased to 1.2×10^{-2} s^{-1}. For 8Ag/Al_2O_3_IWI_R325_S550, TOF was 0.5×10^{-2} s^{-1}, only 1/5 that of the TOF over the largest silica supported catalyst. As Ag does not activate H_2 well, one could speculate that hydrogen activation is actually occurring over the support. If hydrogen is activated on the support, then it can migrate to the Ag nanoparticles via reverse spillover. Previously, Hohmeyer et al. [59] found that
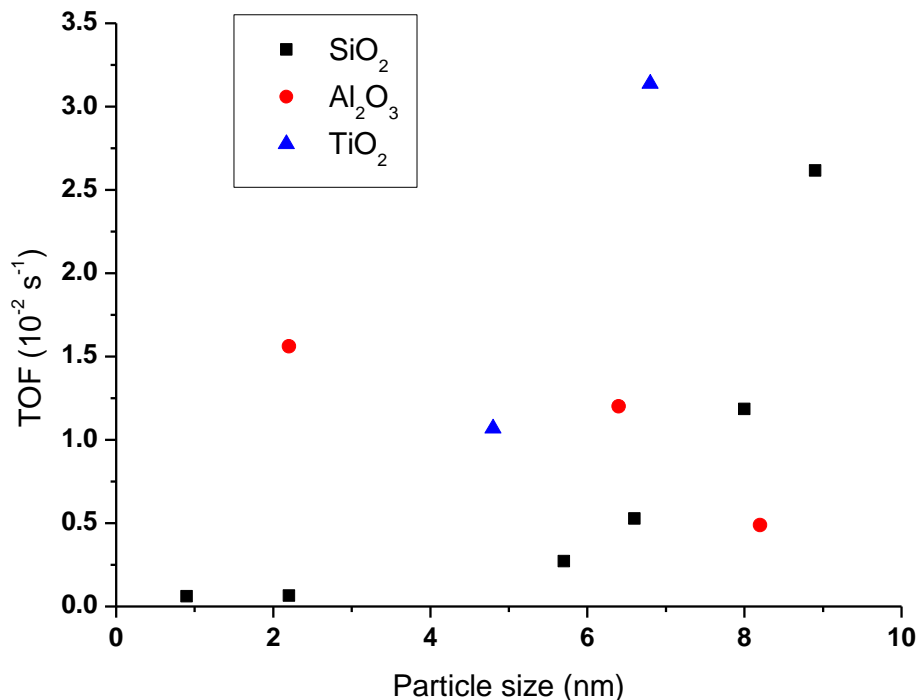
Fig. 17 Support effect on TOF

activation of hydrogen could be achieved over both Ag and the SiO_2 support but that

activation over SiO_2 was much slower than that over Ag. In addition, the formation of

hydroxyl on the surface was determined to be limited by the barrier for diffusion of H

across the silica surface (or diffusion across the interface) as opposed to H_2 activation.

Hohmeyer et al. argue that hydrogen atoms may migrate to the metal support interface

after dissociation where they are still available for reaction (in our case with acrolein). In

the case of alumina, the presence of such interface sites could be very important to the

reaction rate as the activity decreases as particle size increases (i.e. the rate drops as the

perimeter area: volume ratio decreases). In contrast, the rate over TiO_2 may not be dependent upon the presence of such interface OH groups.

In order to further probe the support effect, secondary reaction, (i.e., hydrogenation and isomerization of allyl alcohol) were also studied on Ag catalysts with each of the three supports. One sample for each support having the best selectivity was selected to run a reaction using allyl alcohol as feed under the same conditions for acrolein hydrogenation. The rates of allyl alcohol conversion and rates of acrolein conversion are listed and compared in Table. IV. The ratio of acrolein consumption rate to allyl alcohol consumption rate was 2.8 over $3Ag/TiO_2\_mIWI\_C500R120$ and 2.3 over $8Ag/SiO_2\_IWI\_R325$, which was consistent with their high selectivity for acrolein hydrogenation to allyl alcohol. However, the unwanted secondary reaction rate on $8Ag/Al_2O_3\_IWI\_R325\_S550$ was actually faster than acrolein hydrogenation. In this case, the allyl alcohol concentration was high (~3%) when running it as feed. However, the depletion of allyl alcohol created by acrolein hydrogenation is not as extreme since the alcohol concentration under acrolein hydrogenation conditions is much lower(only about 1/15 of the isomerization test). In real acrolein hydrogenation condition, when having a large amount of acrolein around, the secondary reaction of allyl alcohol should not be so significant, but the ratio in Table IV gave a rough idea to explain the support effect.

Sample name	Particle Size	Acrolein consumption rate R_{Ac}	Allyl alcohol consumption rate R_{Aol}	R_{Ac}: R_{Aol}
8Ag/Al$_2$O$_3$_IWI_R325_S550	8.2	0.026	0.087	0.30
8Ag/SiO$_2$_IWI_R325	8.9	0.14	0.062	2.3
3Ag/TiO$_2$_mIWI_C500R120	6.8	0.23	0.083	2.8

Table IV Comparison of acrolein and allyl alcohol consumption rates in mol $h^{-1}g_{Ag}^{-1}$.

3.4 Conclusion

SiO$_2$, Al$_2$O$_3$ and TiO$_2$ were selected as supports to investigate the support effect of silver catalysts for acrolein hydrogenation. On each support, a similar particle size effect in selectivity (bigger particle size, better selectivity) was observed. TiO$_2$ showed best performance in terms of both selectivity and activity. Formation of Ti^{3+} sites may favor the adsorption of acrolein through carbonyl group. Selectivity of alumina supported catalysts was similar to that of silica supported ones. However, increasing Ag particle size on alumina lowered the activity and this may be due to the reverse spillover of hydrogen.

4 ALLOYING EFFECT ON SELECTIVE HYDROGENATION OF ACROLEIN: SINGAL ATOM ALLOY, A NONCONVENTIONAL CASE

4.1 Introduction

The creation of atomically uniform sites in heterogeneous catalysis remains a long standing dream of the catalysis community. To this end, several groups have recently attempted to heterogenize homogenous catalysts either through tethering to the support or by exchanging ligands with active center-support bonds that tune the electronic structure of the active site. Another strategy for atomically uniform sites comes from the example of Sykes *et al.*, who recently showed that single Pd atoms could be embedded in a Cu(111) surface and act as active sites for the selective hydrogenation of acetylene to ethylene and the hydrogenation of styrene to ethylbenzene [47]. The creation of single atom alloys is based upon the creation of a metal nanoparticle (of a relatively inert metal) with an active metal embedded in the particle. Here we exploit this idea to show an enhancement in another selective hydrogenation reaction: the hydrogenation of acrolein.

Acrolein is an α, β–unsaturated aldehyde which is particularly difficult to selectively hydrogenat to produce α, β–unsaturated alcohol compared to all the other higher homologues due to a lack of substituents on C=C bond. Typical hydrogenation catalysts using platinum, palladium, or ruthenium as active element are very active but not selective to allyl alcohol (desired product). Instead the primary metal of choice is Ag[24, 25, 67], which has been shown to exhibit higher selectivity but low activitiy. Their low activity is not surprising since silver is known to be poor for hydrogen activation. For example, we have found using density functional theory calculations that the activation energy of H_2 dissociation on Ag (111) surface (1.4 eV) was found to be the

72

highest in all elementary steps indicating that the chemisorption of H_2 should be the rate limiting step for acrolein hydrogenation [83]. This result suggests that to expedite the reaction, the dissociation of H_2 must be facilitated. However, there is a trade-off between high selectivity and high activity in that high selectivity to allyl alcohol is a result of the weak binding of acrolein (which is favored over Ag) whereas the efficient dissociation of H_2 takes place over metals such as Pd and Pt which are too reactive for molecular adsorption of acrolein and selectivity shifts towards undesired products.

Bimetallic alloy catalysts have been shown to demonstrate improved performance for many catalytic reactions because the addition of the second metal modifies the electronic and structural properties of the monometallic catalysts allowing the activity and selectivity to be finely controlled [84]. The observed changes in reactivity due to alloy creation include both electronic and geometric effects[85]. Electronic effects that arise from changes in the bonding resulting from replacement of one metal with another include charge transfer between the metals and changes in bonding hybridization[86]. In contrast, structural variation can lead to ensemble effects in catalysis whereby the adsorbate(s) will adsorb in a particular geometry due to the arrangement of the surface atoms of the alloy. In many cases, deciphering which of these two effects (if not both) are controlling the kinetics is difficult (if not impossible).

Alloys have been employed previously for the selective hydrogenation of *α, β*–unsaturated aldehydes. For example, Rh-Cu/SiO$_2$ alloy catalysts showed both higher selectivity and activity to crotyl alcohol in the selective hydrogenation of crotonaldehyde [87]. The addition of Cu enhanced both selectivity and activity to crotyl alcohol. While the selectivity to crotyl alcohol was 55% and 18% on pure Cu and pure Rh catalyst,

respectively, the selectivity to crotyl alcohol increased to 74% over a Rh-Cu alloy (having 33% atomic ratio of Rh) catalyst . Similarly, the TOF was increased from 7.6×10^{-3} s^{-1} over pure Rh/SiO$_2$ to 11.7×10^{-3} s^{-1} over 0.33RuCu/SiO$_2$. It was claimed that the improvement of catalyst performance was due to better Rh dispersion when Cu was present.

In another study of alloy effects in selective hydrogenation, Marinelli and Ponec examined Sn for its ability to improve the selectivity of Pt catalysts for acrolein hydrogenation and found that selectivity to allyl alcohol jumped from 1% to 27% after addition of tin [63]. The authors suggested that tin was in fact not present as an alloy (based on the fact that PtCu systems did not show enhanced selectivity) but rather as SnO$_x$. However, Sautet and coworkers used density functional theory studies of the adsorption of crotonaldehyde and acrolein on PtSn surfaces to show that perhaps reactive ensembles could be important [88, 89]. The hydrogenation of acrolein, crotonaldehyde and prenal was studied over two Pt-Sn alloy surfaces, p(2×2) Pt$_3$Sn(111) and ($\sqrt{3} \times \sqrt{3}$) R30° Pt$_2$Sn(111) [88]. The adsorption energies on alloy surfaces were smaller than on pure Pt for each of the unsaturated aldehydes studied in every configuration. However, the changes in the adsorption energies varied such that the adsorption of the unsaturated aldehyde in the proper configuration for selective hydrogenation was favored on the Pt$_3$Sn and Pt$_2$Sn surfaces due to charge transfer from Sn to Pt, leading to a Sn$^+$ site which allows for bonding with the aldehyde functionality. The repulsive effect of the substituents on the C=C bond was also found to increase as the molecular size increased, so the selectivity enhancement was most prominent for prenal.

In the later experimental results reported by Haubrich *et al.* on the adsorption and thermal decomposition of crotonaldehyde on the same Pt-Sn alloy surfaces, i.e. $Pt_3Sn/Pt(111)$ and $Pt_2Sn/Pt(111)$, and Pt (111) surface as comparison [89]. The higher the surface composition of Sn, the smaller desorption peak of crotonaldehyde observed in the TPD spectra, implying weaker interaction between crotonaldehyde and the surface with addition of Sn. Crotonaldehyde was observed to decompose on both Pt(111) and $Pt_3Sn/Pt(111)$, but it remained intact on $Pt_2Sn/Pt(111)$ up to 500 K. Accompanying DFT calculations suggest that the saturation coverage of crotonaldehyde on Pt_3Sn and Pt_2Sn, involves the favorable η^1-top-OSn configuration which could explain better selectivity to unsaturated alcohol over Pt-Sn alloys.

In the PtSn system, it was not clear if the improvement in selectivity was due to electronic or geometric effects since one could also note that the presence of Sn greatly weakened the adsorption energy of acrolein to the surface and therefore prevented deleterious C-C bond cleavage reactions from occurring. Bimetallic alloys can also adopt core-shell configurations whereby the surface is uniform but the presence of the alloying metal in the subsurface affects its reactivity. One unique version of a core-shell type alloy is a sandwich alloy by which a single layer of one metal is inserted into the second layer of a slab of the second host metal. Chen and co-workers have examined the effect of a Pt sandwich alloy with Ni present in the subsurface [90, 91]. Acrolein would not bond to Pt(111) and Ni/Pt(111) via the di-σ-C=O configuration, but does bond in this configuration to the Pt/Ni/Pt(111) surface. The authors speculate that the selectivity could be further improved with proper tuning of the electronic structure of the surface to shift the binding energy difference between different adsorption configurations of acrolein.

In another study of selective acrolein hydrogenation showing a different type of geometric effect, Claus and co-workers studied Au catalysts that were coated with indium [5]. High resolution TEM images showed that the indium coated the terraces of the Au nanoparticles leaving only the edges exposed. The gold particles covered with indium were still half as reactive as those not covered by indium with a much better selectivity to allyl alcohol (63% vs. 34%). This led the authors to conclude that the exposed corners and edges must be the reactive site for the selective hydrogenation of the C=O group.

Ag alloys have been previously considered for acrolein hydrogenation. In a prominent example of improved selectivity, Lucas and Claus reported that a 9Ag-0.75In/SiO$_2$ (9 wt% of Ag, 0.75wt% of In) catalyst had a selectivity of 61% to allyl alcohol even when acrolein was fully converted (conversion = 97%) [33, 34]. X-ray diffraction (XRD) measurement showed that an Ag$_3$In alloy phase was formed when the catalyst was reduced at 603 K, which might provide the active sites for the outstanding performance. In this case, the presence of In is speculated to serve as a binding site for the C=O bond of acrolein in a manner echoing the calculations of Delbecq and Sautet [88].

An extreme version of ensemble effects would be the creation of an isolated atom in a matrix of another element termed by Sykes et al as a single atom alloy (SAA) [47, 92-94]. In their combined temperature programmed desorption/scanning tunneling microscopy study, Kyriakou *et al.* deposited 0.01 ML, and 0.1 ML of Pd on Cu (111) surface to form structures where individual Pd atoms were alloyed into Cu (111) surface. Hydrogenation of acetylene and styrene were employed as test reactions to investigate the catalytic properties of the Pd@Cu SSA. The presence of hydrogen atoms was clearly

observed on 0.01 ML Pd/Cu(111) surface in STM images indicating that isolated Pd atoms was able to dissociate hydrogen molecules to H atoms which then spilled over to the Cu surface. DFT calculations predicted that the barrier for hydrogen dissociation was reduced from 0.40 eV to 0.02 eV but that the adsorption enthalpy (-0.35 eV on the alloy but -0.20 eV on Cu(111)) was not strongly affected. In agreement with this prediction, the desorption temperature (manifested as the barrier to association- the reverse of the dissociation process) dropped dramatically from 310 K on Cu(111) to about 220 K on 0.01 ML Pd/Cu(111) (and even lower to ~180 K on 0.1 ML Pd/Cu(111). Temperature programmed reaction (TPR) results showed the selectivity of acetylene hydrogenation to ethene (as opposed to overhydrogenation to ethane) were greatly improved on Pd@Cu SAA surface. The selectivity to ethene for acetylene hydrogenation was >95% on 0.01 ML Pd/Cu(111) while the selectivity to ethene was only 33% on 1 ML Pd/Cu(111). Similar results were obtained for the selective hydrogenation of styrene to ethylbenzene (i.e. minimal hydrogenation of the aromatic ring).

Here we present results for the selective hydrogenation of acrolein over a Pd-Ag bimetallic system with dilute Pd in Ag as a host metal. The situation is similar to the Pd@Cu SAA descried by Kyriakou and co-workers but we extend this to high surface area supported nanoparticles. We have chosen the selective hydrogenation of acrolein as our test reaction since hydrogen activation appears to be a critical step in the reaction mechanism. The activity and selectivity (considering particle size effect) are both improved by addition of Pd compared to monometallic silver catalyst.

4.2 Experimental

4.2.1 Preparation of catalysts

Catalysts were synthesized by sequential incipient wetness impregnation (IWI) using $AgNO_3$ and $Pd(NO_3)_2$ as precursors and SiO_2 as the support. Metal salts were dissolved in water separately and impregnated successively. Palladium aqueous solution was impregnated first and the catalysts were dried at room temperature for an hour then at 125 ℃ overnight. Calcination was then performed at 250 ℃ for 2 hours in a furnace open to the atmosphere but without flow. Silver solution was impregnated after calcination. The catalysts were dried again and reduced at 325 ℃ without being calcined. The reduction treatments were performed in a tube furnace with a 50 mL/min flow of 3.5% H_2 for 2 hours. Two low Pd loading samples were made following the same procedure, $0.01\%Pd+8\%Ag/SiO_2$ and $0.05\%Pd+8\%Ag/SiO_2$. Because particle size was approved to be crucial to the catalytic ability of silver catalysts, the performances of bimetallic catalysts were compared with a relationship drawn from a series of silica supported silver catalysts with various particle sizes, the details of which were described elsewhere [67]. A palladium catalyst prepared by strong electrostatic adsorption (SEA) was also used for comparison [95].

4.2.2 Characterization

EXAFS Ag K edge EXAFS was employed to estimate the particle sizes because the loading of palladium was very low and would not change the coordination number noticeably. Pd K edge EXAFS was used to investigate the environment of palladium. EXAFS spectra were taken at the beamline of the Materials Research Collaborative

78

Access Team (MRCAT, 10-ID) at the Advanced Photon Source (APS), Argonne National Laboratory. All the samples were ground and packed into a sample holder. They were then reduced in 3.5% H_2/He at 200°C for one hour, cooled in He and scanned at room temperature in He in an environmental cell. Samples were scanned in transmission mode at Ag edge and in fluorescence mode at Pd edge. Metal foils were scanned at the same time for energy calibration. Data was processed using WINXAS 3.1 and coordination number and bond distance were achieved. Particle size estimation was performed using a pre-established empirical relationship [57]. One should notice that the particle size obtained by EXAFS fitting is an averaged number and no distribution is given as by TEM.

4.2.3 Catalysis

Gas phase acrolein hydrogenation was performed in a 1/2 inch OD stainless steel fixed-bed continuous flow reactor. Controlling of reaction feed gas (hydrogen and argon) flow was done by mass flow controllers. Acrolein (Fluka ≥ 95%) was delivered by a liquid pump (VICI M6), evaporated at 70 °C in a heat tape traced four way cross packed with quartz wool, and carried in to the system by reaction feed gas. The ratio of acrolein and H_2 is 1:20. 15-25 mg of catalyst was used for each test depending on the activity. Before each run the concentration of acrolein was checked via a reactor bypass line that connects directly to the gas chromatograph (GC). Catalyst samples were reduced *in-situ* in 20% H_2/Ar flow at 200 °C for an hour before testing to ensure metallic state. The reaction temperature was also 200 °C and pressure was 5 atm. The reactor effluent was analyzed by an on-line GC (Agilent 6890) equipped with a dual column formed by a RT-

Msieve 5A and a RT-QPLOT (Restek) for lighter gaseous species and a EC-Wax (Alltech) for less volatile species such as alcohols. TCD (thermal conductive detector) and FID (flame ionization detector) were both utilized for detecting H_2 and other organic/flammable compounds, respectively. The whole system was built by high-pressure-tolerant stainless steel parts and heat-traced to avoid condensation of any product.

4.3   Results and discussion

Our initial study involves the creation of a series of PdAg alloy nanoparticle catalysts in varying Ag:Pd ratios (8:1, 160:1, 800:1) as well as their monometallic counterparts. The selectivities of the catalysts at 10% conversion and reaction rates of the four catalysts (the 8:1 Ag:Pd sample is excluded because its activity and selectivity are essentially identical to Pd) are illustrated in Fig. 18. As expected, Pd is tremendously active but not at all selective to allyl alcohol even under extremely mild reaction conditions. The reaction rate at room temperature and 1 atm pressure is 8.72×10^3 mmol/(h g_{Pd}) and selectivity towards allyl alcohol is zero. In contrast, the 8%Ag/SiO$_2$ catalyst was the best catalyst in terms of both selectivity and activity. For this Ag catalyst, the selectivity can reach 37% at 200 ℃ and at 5 atm total pressure.

Surprisingly, the 0.05%Pd+8%Ag/SiO$_2$ catalyst behaves more like Pd than Ag. Its activity approaches that of Pd alone (at T=100 ℃, the rate was 2.28×10^3 mmol/(h g_{metal}) and its selectivity is only about 1%. Our result implies that even at this dilute ratio, the Pd is so much more active than Ag, that its presence completely dominates the observed reactivity. In contrast, the selectivity of 0.01%Pd+8%Ag/SiO$_2$ to allyl alcohol is 31%,

80

only slightly lower than 8%Ag/SiO$_2$. In addition, the activity was twice that of

8%Ag/SiO$_2$ (303 vs. 148 mmol/(h g$_{metal}$)). Our result demonstrates that Pd atoms must be

having a strong effect on the catalysis, although the amount of Pd present is very small.
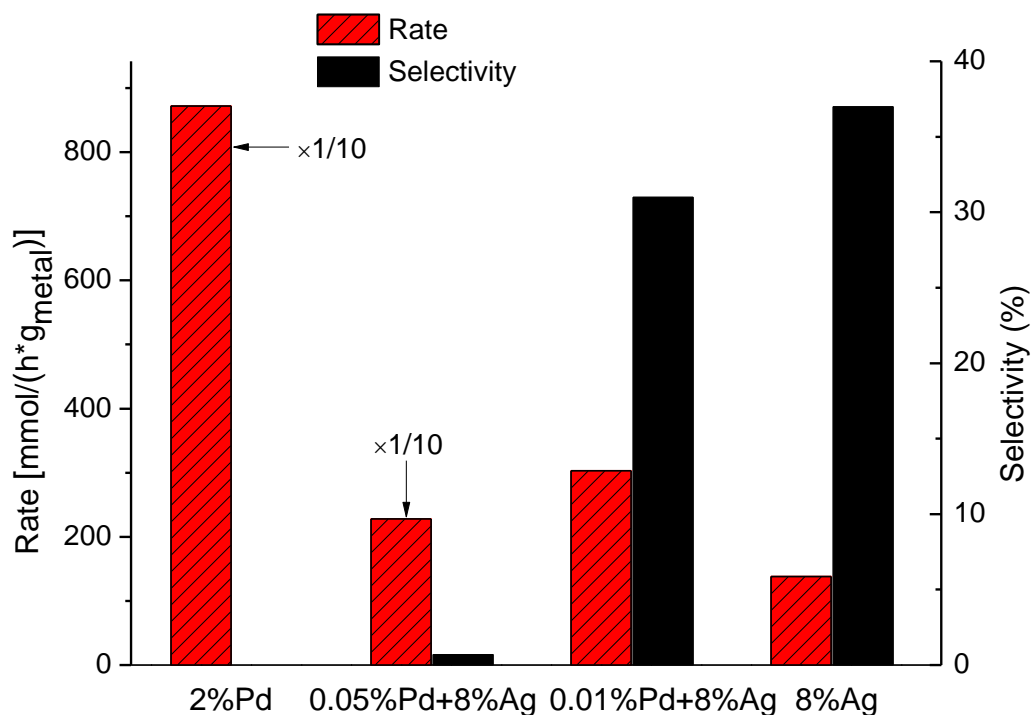
Fig 18. Reaction rates and selectivities to allyl alcohol of Pd, Ag, and Pd-Ag catalysts. All samples are supported on SiO$_2$. 2% Pd/SiO$_2$ was tested at room temperature and atmospheric pressure; 0.05%Pd+8%Ag/SiO$_2$ was tested at 100 ℃ and 5 atm pressure; the reaction temperature of 0.01%Pd+8%Ag/SiO$_2$ and 8%/SiO$_2$ was 200 ℃ and the reaction pressure of them was 5 atm.
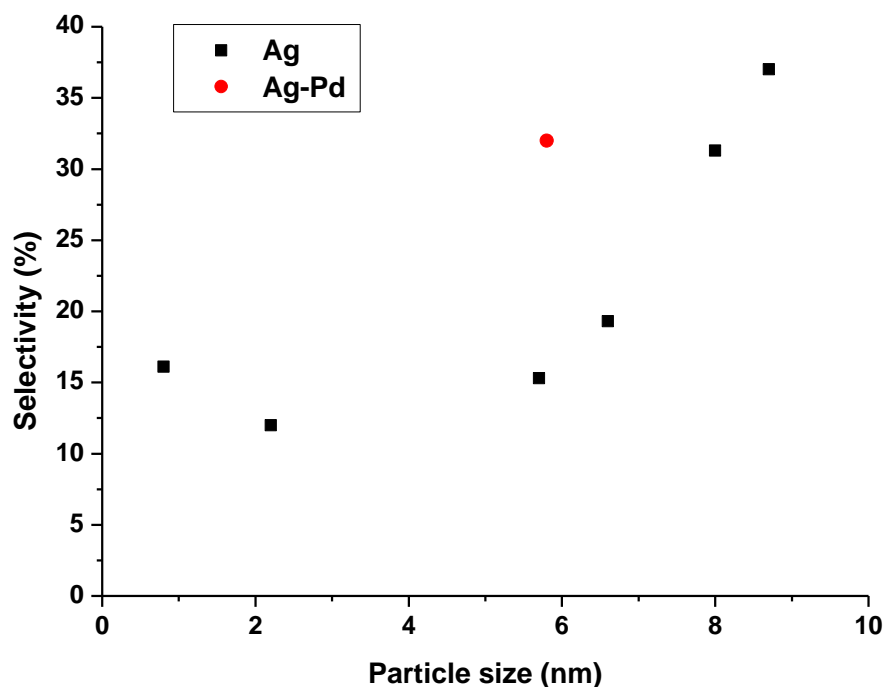
Fig.19 Comparison of Pd-Ag alloys and pure Ag catalysts with various particle sizes.

	Ag edge		Pd edge	
	Bond distance/Å	Coordination No.	Bond distance/Å	Coordination No.
0.01%Pd+8%Ag/SiO$_2$	2.87	10.2	2.82	10.5
Bulk Ag	2.89	12	-	-
Bulk Pd	-	-	2.74	12

Table V   Bond distances and coordination numbers for two Pd-Ag bimetallic catalysts compared with bulk Ag and Pd.

In order to understand the remarkable activity and selectivity of the dilute alloy catalyst, we performed EXAFS experiments at the Advanced Photon Source at Argonne

National Lab at beamline 10-ID (details of the experiments are mentioned in Section 4.3). By fitting EXAFS spectra, the coordination numbers and bond distances of the 0.01%Pd+8%Ag/SiO$_2$ catalyst at both Pd K edge and Ag K edge were obtained and listed in Table V The numbers for bulk metals were also given for comparison. The coordination numbers at silver K edge were used to estimate particle size. The particle size of 0.01%Pd+8%Ag/SiO$_2$ and 0.05%Pd+8%Ag/SiO$_2$ is 5.8 nm and 9.9 nm respectively. Although these two catalysts were synthesized in the same way that we prepared a pure silver catalyst (d = 8.7 nm) [67], the particle sizes of bimetallic samples are smaller than the monometallic sample. The addition of palladium seems to help disperse the silver nanoparticles probably due to the creation of nucleation centers of Pd upon which Ag aggregates. As discussed below, the size of particle also has a critical effect on the reactivity and selectivity.

Pd K edge spectra provide very valuable information about the composition of the bimetallic catalysts. For the 0.01%Pd+8%Ag/SiO$_2$ catalyst, the coordination number of Pd is 10.5 which is very close to the value of Ag (10.2), and shows that Pd atoms are uniformly distributed and present both in the surface and in the bulk. If Pd atoms had segregated completely to the surface, they should be under-coordinated relative to Ag and the coordination number should be smaller. In contrast, if all Pd atoms are in the bulk the coordination number will be closer to 12 since they would be completely coordinated in a fcc environment. From the above, when the loading of Pd is very low (0.01 wt%) the Pd-Ag alloy forms in a way that silver serves as the host metal and isolated single Pd atoms are inlaid in silver like a raisin bread. In addition, the bond distance of the palladium atoms to the nearest neighbors is 2.82 Å. The Pd-M bond distance is intermediate

83

between the M-M bond distance in bulk silver (2.89 Å) and bulk palladium (2.74 Å). This result implies that Pd is surrounded only by silver atoms, and that the Pd atoms are totally dispersed in Ag nanoparticles. Therefore our materials seem to be nanoparticle analogs to the single crystal models of SAA catalysts described by Kyriakou *et al.* In effect, our work has validated the ideas of Kyriakou *et al.* under real reaction conditions. We suggest that the dilute alloy is actually a SAA catalyst possessing isolated Pd atoms in a Ag matrix which accelerates the activation of H_2 just as in the work of Kyriakou. Hydrogen atoms from dissociated H_2 are then spilled over to the Ag surface where they are only weakly bound and therefore are easily consumed in the hydrogenation reaction. When we examined a higher concentration of Pd, to determine if our synthesis technique could produce selective (and presumably site isolated) catalysts with a higher Pd loading (and therefore a more economical use of the metal), the selectivity advantage was lost.

The results show that the selectivity of $0.01\%Pd+8\%Ag/SiO_2$ is slightly lower than the pure silver catalyst. However, if we consider the particle size effect on selectivity (as shown in Fig. 19), the selectivity is actually not impeded but improved by doping individual Pd atoms. Although $8\%Ag/SiO_2$ shows better selectivity, its particle size is a lot larger than $0.01\%Pd+8\%Ag/SiO_2$ (8.7 nm vs. 5.8 nm). The trend of selectivity vs. particle size over silica supported Ag samples shows that the selectivity of a monometallic silver catalyst having similar particle size to $0.01\%Pd+8\%Ag/SiO_2$ is only around 15%, which is merely half of the selectivity achieved over $0.01\%Pd+8\%Ag/SiO_2$. It seems unlikely that the addition of the Pd is changing the reactivity of Ag itself. Since the Ag-M bond distances are largely unchanged, no strain effect appears to be present. Similarly, changes in the local reactivity of Ag atoms neighboring Pd seems unlikely to

be significant since most Ag atoms would have zero or one Pd neighbors. Another possible effect of the Pd is that the acrolein molecule adsorbs in a more favorable configuration for selective hydrogenation (i.e. C=O bond down to the surface as opposed to adsorbing through its C=C bond). DFT calculations of acrolein adsorbed on a Ag(111) slab with a single atom of Ag replaced by Pd indicate that in fact while acrolein adsorbs weakly to the pure Ag surface in both orientations, the presence of the Pd atom enhances acrolein adsorption through the C=C bond (0.45 eV) more dramatically than the C=O bond.(0.11 eV). Although this would appear that this is counter to our supposition that C=O orientation toward the surface is critical to selective hydrogenation, Sautet and co-workers have previously explained this result by noting that preferential attack of the C=O functionality may be possible even if the acrolein molecule is not bound to the surface by the aldehyde functionality [96].

4.4   Conclusion

By keeping the concentration of Pd very low, a raisin-bread-like Pd-Ag alloy catalyst was synthesized having isolated Pd atoms dispersed in Ag particles. These isolated Pd atoms provided active centers for H_2 dissociation without changing the structure of Ag nanoparticles. The barrier of H_2 dissociation was lowered, and both activity and selectivity were improved accordingly. We believe that doping a very diluted and hydrogen-active second component will facilitate the acrolein hydrogenation.

5   UTILIZING SINGLE SITE HETEROGENEOUS CATALYSTS IN SELECTIVE HYDROGENATION OF ACROLEIN

5.1   Introduction

The creation of atomically uniform sites in heterogeneous catalysis remains a long standing dream of the catalysis community. The term single-site came up after Andresen *et al.* [97] found that some zirconocene-based catalysts exhibited novel and outstanding behavior in ethylene polymerization. More recently, Thomas [98] gave the definition of single site heterogeneous catalysts as follows: "consisting of one or more atoms, the single-sites are spatially isolated from one another, with no spectroscopic or other cross-talk, have the same energy of interaction with reactants, are well-characterized, in the same way as the single-sites are in homogeneous catalysts". Pioneering work on the synthesis of single site heterogeneous catalysts (SSHC) has adopted two strategies either tethering homogeneous catalysts to the support [99-103] or through ligand exchange with active center-support bonds that tune the electronic structure of the active site[98, 104-111].

Heterogeneously catalyzed reactions often suffer from poor selectivity due to the presence of multiple types of sites for adsorption and reaction so while heterogeneous catalysts may be highly active compared to homogeneous catalysts, their selectivity is often lower. The potential for SSHCs to achieve both high activity and high selectivity makes their use attractive when addressing reactions with poor selectivity. One such reaction which requires large improvement of selectivity to achieve greater commercial success is the regioselective hydrogenation of α,β–unsaturated aldehydes. In particular,

the selective hydrogenation of acrolein to allyl alcohol is difficult as the hydrogenation of the olefinic bond is thermodynamically favored over the carbonyl group by ca. 35 kJ/mol [5] and a lack of bulky substituents on the C=C bond makes it easier to be attacked. Different approaches have been tried to promote the selectivity, such as adjusting particle size [19, 67], alloying with a second metal [20, 33, 63] and adjusting reaction conditions or pretreatments [25, 112]. However, all of these approaches are still predicated on a premise of nanoparticle catalysis which possess a variety of sites (terraces, corners, edges, interfaces [113]). If a single-site catalyst with specific active sites anchoring the adsorption of acrolein via C=O bond, a very high selectivity can be potentially achieved. Here we will present some preliminary results about a single-site silica supported zinc catalyst for acrolein hydrogenation.

5.2 Experimental

5.2.1 Preparation of catalysts

Zn/SiO$_2$ catalyst was prepared by strong electrostatic adsorption (SEA). Silica gel (Sigma-Aldrich, 35-60 mesh, 285 m^2/g) was used as the support. The estimated loading of Zn was 4%. An excessive amount of Zn(NO$_3$)$_2$ 6H$_2$O (giving about 5.7% weight percentage of Zn if completely adsorbed on the support) was used to make sure the highest possible loading. The procedure was described as below in a particular case: 50 mL H$_2$O and 5 mL ammonium hydroxide were added in to 10 g of SiO$_2$ and the mixture was vigorously stirred. Zn(NO$_3$)$_2$ 6H$_2$O was dissolved in 25 mL H$_2$O and 2 mL NH$_3$ H$_2$O was added. The solution of Zn was then added to silica suspension liquid and continued

stirring for 10 min to let Zn precursor to adsorb on the silica surface. Then the silica loaded with Zn precursor was filtered and rinsed with water for 3 times. Next, it was dried in the hood for 2 hrs and moved to the drying oven at 125 ℃ for drying overnight. At last, the catalyst was calcined at 300 ℃ for 3 h.

5.2.2 Characterization

ICP The loading of the catalyst was test by inductively coupled plasma (ICP). The result was 5.05%, higher than expected but lower than the total amount of Zn precursor. Thus the maximum adsorption ability of silica was reached.

EXAFS Zn/SiO_2 The Zn K edge EXAFS spectra were taken at Advanced Photon Source (APS) at beamline 10 BM at Argonne national laboratory in transmission mode. The spectra were taken at different temperatures and also when treating the Zn catalyst with various gases (H_2, O_2, He, and CO). The detail of the experiments is given elsewhere [114]. The WINXAS 3.1 program was used to fit the data.

5.2.3 Catalysis

Catalyst testing was performed in a 1/2 inch OD stainless steel fixed-bed continuous gas flow reactor. Mass flow controllers were used to control the gas flow rate. A liquid pump (VICI M6) was used to deliver acrolein (Fluka $\geq$ 95%). Acrolein was delivered into a four way cross heat-traced to 70 ℃, evaporated, and carried in to the system by reaction feed gas (argon and hydrogen). The cross was filled with quartz wool

to enable a constant speed evaporation and also filter the polymerization products. The molar ratio of acrolein:H_2 was kept at 1:20. The concentration of acrolein in gas phase was checked before each run via a reactor bypass line by an on-line gas chromatograph (GC), which was also used for qualification and quantification of productions when reactions were run. The GC (Agilent 6890) was equipped with a dual column formed by a RT-Msieve 5A and a RT-QPLOT (Restek) for lighter gaseous species and a EC-Wax (Alltech) for less volatile species such as alcohols. TCD (thermal conductive detector) and FID (flame ionization detector) were both used for detecting H_2 and other organic/flammable compounds, respectively. About 1 g of catalyst was used for each run because its low activity. The catalyst was brought to 100 ℃ for catalytic testing without any other treatments. Reaction testing was carried out at 100 ℃ and atmospheric pressure. A trap was installed at the exit of testing system to collect condensed products to minimize affection to the environment.

5.3 Results and discussion

5% Zn/SiO_2 has been previously demonstrated to have single-site structure by EXAFS results which are summarized here. By comparing the spectrum of Zn catalyst with Zn foil there was no Zn-Zn bond suggesting Zn atoms were all isolated and do not see each other (as shown in Fig. 20(a)). Using ZnO as reference, the peak observed in the spectrum of Zn catalyst was assigned to Zn-O bond (spectrum not listed). It demonstrated that Zn was present as single atoms on the support by bonding with the surface O of SiO_2.

One can see in Fig. 20(a) that the size of the main peak shrank after the temperature reached 235 ℃, which indicated a decrease in the coordination number of Zn. By fitting the data, the zinc sites was 4-fold coordinated at room temperature. However, when the temperature reached 235 ℃ and above, Zn sites lost a ligand to become 3-fold coordinated. The loss of a ligand also occurred in different gas environment (even in O_2). As shown in Fig. 20(b), the spectra taken under four different gas environment are almost identical. It was not clear why Zn sites lost an oxygen ligand at higher temperature but undercoordinated Zn could potentially become more active for some reactions. For example, we observed that selectivity to allyl alcohol decreased with the increase of reaction temperature. So the undercoordinated Zn sites may favor the hydrogenation of C=C bond. The mechanism of the loss of O ligand for Zn/SiO_2 single site catalyst was proposed as a dehydration mechanism and illustrated in Fig. 20(c).

Another feature we can learn from the EXAFS results is that Zn remained +2 oxidation state no matter what temperature or what gas environment it undergoes. The catalyst mediates a redox process through mechanisms which do not involve electron transfer directly to and from the metal.

This catalyst has shown impressive thermo-stability as well. The catalyst was exposed to H_2 then air and then H_2 again one after another at 400 ℃. The EXAFS spectra under reducing environments did not change, indicating Zn atoms were able to remain as isolated single sites instead of aggregating to nanoparticles even after harsh treatments. Although *in situ* EXAFS experiments of acrolein hydrogenation were not performed, the structure stability of 5% Zn/SiO_2 can be safely assumed under reaction condition (1 atm H_2, 100 ℃) because of its wonderful redox durability at higher temperature.
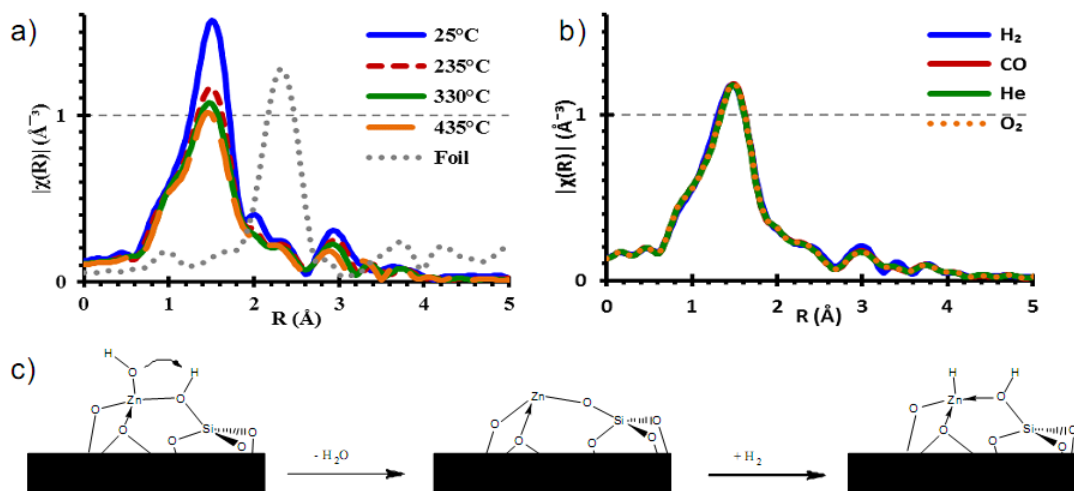
Fig. 20 R space plots of in-situ XAS of Zn@SiO2 as a function of a) temperature and b) atmosphere (250 ℃), c) Proposed mechanism of ligand loss through surface Zn dehydration followed by proposed heterolytic H_2 activation.

The activity of Zn/SiO_2 catalyst is very low, 1.4×10^{-4} mol/(h g_{Zn}), at 100 ℃ and 1 atm. Silver catalyst has 100 times higher activity (1.4×10^{-2} mol/(h g_{Ag})) at 200 ℃ and 1 atm. The activity of silver should have an activity of 8.2×10^{-4} mol/(h g_{Ag}) by using Arrhenius equation obtained previously. The value is still almost 6 times of that of the Zn catalyst. However, the selectivity of Zn catalyst is 45%, slightly higher than that of silver catalyst (41%) tested under optimized condition (200 ℃ and 5 atm). Only propanal and allyl alcohol were observed as products. The low activity may result from the fact that the Zn species exist on the silica surface in ionic state with fully-filled d orbitals. Thus we suggest a different mechanism for Zn single site catalyst that Zn species participate the reaction as Lewis acid sites rather than typical transition metal active centers. Since the C=O bond is electron-rich, Lewis acid sites should favor the adsorption of acrolein through the carbonyl group. Thus the selectivity should be improved. However, H_2

dissociation and activation of acrolein should be very difficult on Zn catalyst. As a result, the activity is extremely low and ideal selectivity cannot be reached.

The catalyst was tested online for 200 min to examine the stability (shown in Fig. 21). The initial selectivity was as high as 85%, but dropped quickly and reached relatively stable plateau around 45% at about 60~100 min but then the selectivity kept decreasing to 12% after 140 min with no change in the conversion. Similar deactivation was observed by Miller and Hock's group on the same catalyst for propane dehydrogenation. It was probably because the trace amount of H_2O in the feed gas poisoned the active and selective Lewis acid sites. In our case, 95% acrolein contains water as stabilizer and alcohol is produced, the Lewis acid sites could be more easily poisoned. This is in fact an intrinsic weakness of this type of catalyst if the reaction does follow the Lewis acid mechanism. Therefore even if anhydrous acrolein is used, there is always allyl alcohol in the products, which may poison the active sites. Given this result, one may suspect that the stability of Zn or other similar single site catalysts will likely be poor for acrolein hydrogenation.
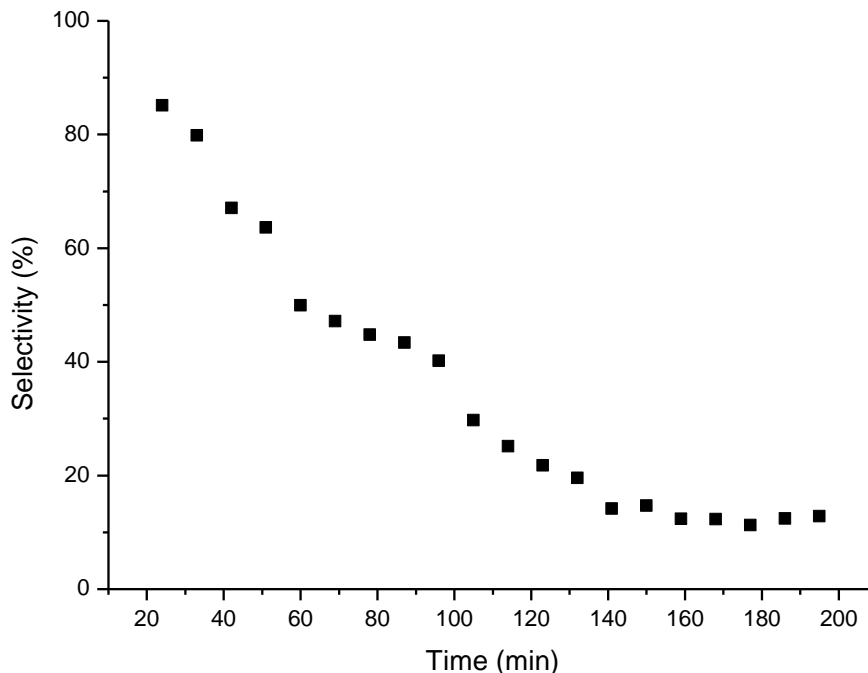
Fig. 21 Stability test on 5% Zn/SiO$_2$.

Lewis acid sites have previously been recognized in hydrogenation reactions. Chase *et al.* [115] conducted a research on B(C$_6$F$_5$)$_3$-mediated reduction of imines and nitriles with H$_2$ and found that B(C$_6$F$_5$)$_3$ was a very efficient catalyst for hydrogenation. For example, *t*BuN=CPh(H) was hydrogenated to *t*BuNH-CPh(H)$_2$ with a yield of 89% and Ph$_2$CHN=CPh(H) was hydrogenated to Ph$_2$CHNH-CPh(H)$_2$ with a yield of 99%. They proposed that B(C$_6$F$_5$)$_3$ could split H$_2$ and open the double bond then lead to a hydrogenation. Although the example given above was in homogeneous catalysis and the reactant was very different from ours, we have reason to believe that Lewis acid sites can be active for hydrogenation reactions. They should be able to activate H$_2$ and favor the adsorption of acrolein via C=O bond so that better selectivity can be obtained. Ultimately

we want to have a water-resistant Lewis acid catalyst because anhydrous acrolein is not stable. Polymerization of acrolein through aldol condensation reactions is a serious concern. In addition, the ideal Lewis acid sites should not interact strongly with allyl alcohol since we want our product to desorb from the surface instead of lingering on the catalyst surface and hindering the reaction.

In addition to our examination of selectivity, the activation energy and reaction orders were extracted from additional kinetic tests. The activation energy is found to be 49 kJ/mol, within 10% of previous values observed for Ag nanoparticle catalysts. The reaction order of acrolein is 0.8, indicating similar behavior to that on Ag catalysts where acrolein is weakly bound to the surface. However, the reaction order of H_2 is -2.0. This surprising result indicates that the mechanism of acrolein hydrogenation for the Zn/SiO_2 SSHC is completely different from the mechanism found on 8% Ag/SiO_2 (where the reaction order is 0.5 a reaction order consistent with dissociative adsorption of hydrogen) . This implies that high partial pressure of H_2 is not helpful to the reaction and actually poisons the surface. It may because H_2 is in competitive adsorption with acrolein. All the catalyst tests were performed at a H_2:acrolein ratio near 20:1 due to the previous success observed for Ag nanoparticle catalysts at these conditions. However, our result here suggests that the change in the mechanism of selective hydrogenation also implies that the optimal reaction conditions are significantly different from what is reported here.

5.4 Conclusion

Our preliminary results show that Zn/SiO_2 SSHC is active and selective for hydrogenation of acrolein. Better selectivity was achieved on Zn/SiO_2 compared to silver

catalyst. Although the activity is low and selectivity decreases with the reaction proceeding for Zn/SiO_2 at this point, this new type SSHC catalysts can be considered promising. Improvement can be made by changing the active metal that may provide a more suitable active center and by modifying or changing the support like modification of ligands in homogeneous catalysis. Thus we expect better performance for hydrogenation of acrolein over SSHC catalysts and more detailed study is required.

6 ALLOYING EFFECT: A COMPARATIVE DENSITY FUNCTIONAL THEORY STUDY OF WATER GAS SHIFT OVER PdZn(111) AND NiZn(111)

6.1 Introduction

The water gas shift (WGS) reaction

$$CO(g)+H_2O(g) \rightleftharpoons CO_2(g)+H_2(g) \qquad\qquad (1)$$
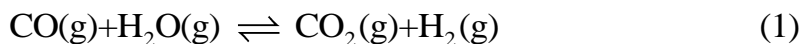
plays an important role in shifting the composition of syngas and in the production of hydrogen. In addition, WGS exists as an important reaction in many industrial processes such as methanol steam reforming, methanol synthesis, and Fischer-Tropsch synthesis [116, 117]. Accordingly, many studies have been directed toward improvement of WGS catalysts [118]. To avoid restrictions of equilibrium, one would prefer to operate at the lowest temperature possible. However, to achieve reasonable kinetics while balancing thermodynamic considerations, industrial processes often rely on a two stage configuration, where a high temperature shift (HTS) process at 310-450 ℃ with an iron-based catalyst promoted by chromium oxide, is followed by a low temperature shift (LTS) process at 210-240 ℃ using $Cu/ZnO/Al_2O_3$ catalyst [52]. Since this two stage process is not suitable for small scale applications, a catalyst with high activity at lower temperature is highly desirable. Consequently, improved Cu-based catalysts have attracted particular attention to fulfill this requirement. Schumacher *et al.* [52] investigated low temperature WGS reaction on various transition metals based on a redox mechanism and they found that Cu was closed to the optimal of the rate calculation, in agreement with Grenoble and his co-workers' experimental result[119]. However, Schumacher *et al*. found that the performance of the copper-based catalysts could still be potentially improved by subtle tuning of the electronic structure of Cu so that the adsorption energies of CO and O

become slightly stronger. Furthermore, it should be recognized that in Schumacher's work the same microkinetic model was assumed to be applicable to all metals, which implies that better WGS catalysts may exist on which the reaction pathways pass through a different mechanism. .

Of course, one route to tuning the reactivity of transition metals is through judicious alloying. Due to the complexity of these systems, alloys often have significant advantages over pure metals in heterogeneous catalysis and substantial improvements in reactivity and selectivity can be made[84]. Iwasa *et al* [53, 54], noticed that a Pd-Zn alloy catalysts have comparable or better performance than Cu-based catalysts for the methanol steam reforming (MSR). Several groups have now linked the activity of Pd/ZnO catalysts to the formation of the alloy [120, 121]. A series of theoretical studies were conducted by Rösch and co-workers using with a density functional method by examining the MSR reaction over PdZn alloy surfaces [122-130]. Rösch *et al*., found that PdZn (111) had the lowest surface energy (0.06 J m^{-2} lower than PdZn(100)) of all the low Miller index planes in the (1:1) PdZn alloy [124]. Segregation of neither Zn nor Pd was favorable in 1:1 PdZn alloy films[127]. Furthermore, Rösch and coworkers found strong similarity between the local valence *d*-band density of states of Pd in the alloy and that of Cu [124]. This result has since been confirmed experimentally using UPS and helps rationalize the similar catalytic performance of these two systems [122]. Methoxy (CH_3O) is considered to be a crucial intermediate during MSR reaction[125, 128, 129]. In an effort to understand the superior performance of PdZn alloy catalysts, methoxide adsorption and decomposition has been investigated on PdZn (111), Pd (111), Cu (111), and PdZn (100) surfaces and PdZn (221) surfaces exposing steps built of Pd atoms, (221)^{Pd}, and steps built of Zn atoms, (221)^{Zn}.

On Pd-Zn alloy surfaces, H atoms and all C-bound species prefer to bond with Pd atoms, while O containing species which bond through O were more stable when located on sites involving Zn atoms. On all surfaces, C-H bond breaking leading to the formation of formaldehyde (CH_2O) proceeded more easily than C-O bond scission, which leads to methyl (CH_3) formation. The calculated results showed that on defect-free flat surfaces, CH_3O decomposition was thermodynamically favored on Pd (111) due to the weaker bonding between CH_3O and Pd(111) surface while decomposition on the PdZn surfaces was actually endothermic. However, C-H bond breaking on steps were greatly facilitated with fairly low barriers (0.5 eV), suggesting the possibility that defects are responsible for the methoxide decomposition on PdZn catalysts.

More recently, Lim *et al.* [123] have combined their DFT results with a microkinetic model to examine the surface composition of PdZn(111) and Cu(111) under typical MSR conditions. H_2 and O_2 adsorb dissociatively with adsorption energies of -58 and -312 kJ mol^{-1} on PdZn(111). Similarly, on Cu(111) dissociative adsorption energy of H_2 and O_2 are -36 and -336 kJ mol^{-1}, respectively at a coverage of 0.25 ML. The clean PdZn(111) surface, the dissociative adsorption of H_2O was almost thermoneutral,, which therefore favored molecular adsoption of water (which adsorbs weakly: -20 kJ mol^{-1}). Dissociative adsorption of H_2O was favored in the presence of O. as the reaction becomes more exothermic (-40 kJ mol^{-1}) than that without O assistance (10 kJ mol^{-1}). Surface free-energy curves of the reactions on PdZn(111) and Cu(111) were plotted vs. the partial pressure of H_2, indicating that for the initial phase of MSR reaction when $p_{H2} \approx 0$ the oxygen-covered surface was stable. However, with a finite partial pressure of H_2, OH dominates the surface. As p_{H2} is further increased, H_2O becomes the most stable species
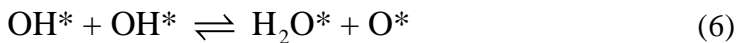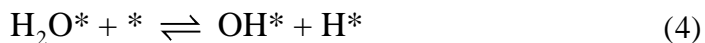
(0.1atm for PdZn(111), 2 atm for Cu(111)). A microkinetic model was then built to predict the equilibrium adsorbate coverages. The analysis was conducted at two different conditions, $T = 500$ K, $p_{H2O} = 1$ atm or 0.01 atm. It revealed that the catalyst surfaces were essentially free of adsorbates at both conditions.

Since water gas shift is highly related to methanol reforming, it is not surprising that Pd/ZnO also works well for WGS. Bollmann *et al*. reported that the formation of PdZn intermetallic compound on alumina and ZnO increased the WGS turnover rate (TOR) greatly [131]. They investigated WGS on 2% Pd/Al$_2$O$_3$ with Zn content varying from 0 to 19%. Compared with Pd/Al$_2$O$_3$, the TOR of the catalyst with 19% loading of Zn raised to 3.6×10^{-2} mol H$_2$ s^{-1} (mol exposed Pd)$^{-1}$ by a factor of 13. In addition, the TOR of an ordered 1:1 PdZn compound on ZnO was boosted to 5.3×10^{-2} mol H$_2$ s^{-1} (mol exposed Pd)$^{-1}$, an increase by a factor of 20. Based on these results, Bollman *et al.* suggested a twofold role of Zn. First, zinc forms an intermetallic with Pd leading to creation of an active site for CO (which otherwise may poison Pd). Second, zinc weakens the Pd-support interaction that is believed to make Pd less effective. Dagle *et al.* studied a series of Pd/ZnO/Al$_2$O$_3$ catalysts and found that WGS activity was dependent on the Pd:Zn ratio with a maximum activity obtained at approximately 0.50 (a conversion of 47.9% at 238 ℃, compared with 78.2% by Cu at the same temperature), surprisingly lower than the ratio of the 1:1 alloy [132].
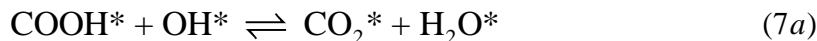
Nickel, which is in the same row of and a period above Pd, has similar properties as palladium. Accordingly, it seems logical to test if Ni-Zn alloy would be an effective, but inexpensive, non-precious metal alloy catalyst for water-gas shift reaction. Ni-Zn alloy catalysts were predicted by Nørskov and co-workers to be active for C$_2$H$_2$ hydrogenation

based upon the strength of which this alloy binds CH_3 [133]. Further experimental examination confirmed that this catalyst was both active and stable under typical C_2H_2 hydrogenation reaction conditions [133, 134]. Both Ni-Zn and Cu fell in the energy window of interest (obtained by plotting adsorption energies of acetylene and ethylene against that of methyl group). Therefore since NiZn should possesses similar reactivity to Cu, NiZn may also be a viable candidate for a WGS catalyst as well.

Although the WGS reaction involves simple adsorbates and a great deal of studies have been devoted to it, the mechanism is still under debate [116, 135-142]. In fact, the reaction appears to be controlled by more than one mechanism depending upon reaction conditions (and choice of catalyst) [135]. One pathway that is generally accepted is a surface redox mechanism. The elementary steps are shown below [136], where asterisk (*) represents a free surface site and X* is adsorbate on the surface:

$$H_2O + * \rightleftharpoons H_2O^* \tag{2}$$
$$CO + * \rightleftharpoons CO^* \tag{3}$$
$$H_2O^* + * \rightleftharpoons OH^* + H^* \tag{4}$$
$$OH^* + * \rightleftharpoons O^* + H^* \tag{5}$$
$$OH^* + OH^* \rightleftharpoons H_2O^* + O^* \tag{6}$$
$$CO^* + O^* \rightleftharpoons CO_2^* + * \tag{7}$$
$$CO_2^* \rightleftharpoons CO_2 + * \tag{8}$$
$$H^* + H^* \rightleftharpoons H_2^* \tag{9}$$
$$H_2^* \rightleftharpoons H_2 + 2^* \tag{10}$$

As an alternative to the redox mechanism, complete dissociation of water may be avoided [137]. In this case, CO^* and OH^* may react to form either a carboxyl or formate intermediate before finally producing CO_2. In the carboxyl mechanism steps (2)-(4) and (8)-(9) are identical with the redox mechanism, while step (5)-(7) vary:

100

$$CO* + OH* \rightleftharpoons COOH* + * \qquad (5a)$$
$$COOH* + * \rightleftharpoons CO_2* + H* \qquad (6a)$$
$$COOH* + OH* \rightleftharpoons CO_2* + H_2O* \qquad (7a)$$
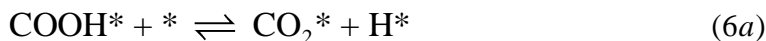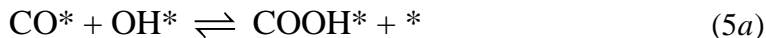
and in an analogous way, HCOO* (formate) could also be formed (this is discussed later.

Questions as which mechanism dominates the surface reaction and which elementary step is the rate limiting (or controlling) step are still unclear and demand systematic investigation. In this present work, we use density functional theory (DFT) to examine the WGS reaction through both redox and carboxyl based mechanisms over PdZn (111) and NiZn (111) alloy surfaces.

6.2 Computational methods

The density functional theory (DFT) calculations are performed using the Vienna Ab Initio Simulation Package (VASP) [143]. A plane-wave basis set with a cut off energy of 400eV and projector-augmented wave (PAW) method [144, 145] are employed. The Perdew Wang (PW-91) form of the generalized gradient approximation (GGA) exchange and correlation functional is used in all calculations reported herein [144]. The Brillouin zone is sampled with a $7 \times 7 \times 1$ k-points grid [146]. The geometries of all structures were located with the conjugate gradient method and were considered to be converged with energy within 0.001 eV and forces of less than 0.025 eV/Å.

A five-layer slab model with 2×2 surface unit cell is adopted to model (111) surfaces of PdZn and NiZn alloy. The top three layers are allowed to relax. A vacuum space of 16 Å was applied to separate the slabs. The transition states (TS) are determined by the climbing nudged elastic band (cNEB) method of Henkelman and Jónsson[147].

6.3 Results

As described earlier, there are two widely-accepted mechanisms for WGS, redox mechanism and carboxyl mechanism. Here we will investigate both of them for both surfaces and have the results compared. Adsorption energies are attained by examining 9 possible adsorption sites on the alloy surfaces. NiZn (111) is taken as an example to illustrate the sites (Fig. 22). The reaction enthalpies of all the elementary steps are listed in Table VI and Table VII. The reaction enthalpies are reported at infinite separation (for all products and reactants) and with the appropriate interaction energies following the example of Mavrikakis and Dumesic [116]. In other words, for the case of H_2O dissociation, the reaction enthalpy is calculated with OH and H coadsorbed and then adjusted to infinite separation by the interaction energy of H and OH.

6.3.1 Redox mechanism

In this mechanism, reactant molecules H_2O and CO first adsorb on the surface. H_2O then dissociates to a hydrogen atom and a hydroxyl group, which may further dissociate into H and O atoms. The surface oxygen reacts with adsorbed CO to form CO_2 and leaves the surface rapidly. O atoms on the surface may also be produced through a disproportionation reaction whereby two hydroxyl groups react to form a water molecule and an oxygen atom. H_2 is formed by simple recombination of two H atoms on the surface leading to desorption.

Table VI. Reaction enthalpy (ΔH) and barrier (E_a) of elementary steps for redox and carboxyl mechanism on PdZn (111)
The enthalpy of elementary step 8 is the inverse adsorption energy of CO_2.
Step 9 is the sum of formation of an adsorbed H_2 and its desorption.

		Elementary steps												
		Redox mechanism						Carboxyl mechanism						
		2	3	4	5	6	7	5a	5.5	6a	7a	8	9	10
ΔH/eV		-0.20	-0.95	0.20	0.96	0.04	-0.78	0.26	0.09	-0.49	-0.62	0	0.43	-0.09
Ea /eV				0.95	1.62	0.53	0.82	0.44	0.54	1.06	0.19		0.91	
Interaction energy/eV	Reactants	-	-	-	-	0.20	-0.04	0.02	-	-	0.03	-	0.00	-
	Products	-	-	0.06	0.37	-0.23	-	-	-	0.05	-0.07	-	-	-

Table VII. Reaction enthalpy (ΔH) and barrier (E_a) of elementary steps for redox and carboxyl mechanism on NiZn (111)
The enthalpy of elementary step 8 is the inverse adsorption energy of CO_2.
Step 9 is the sum of formation of an adsorbed H_2 and its desorption.

		Elementary steps												
		Redox mechanism						Carboxyl mechanism						
		2	3	4	5	6	7	5a	5.5	6a	7a	8	9	10
ΔH/eV		-0.16	-1.66	-0.26	0.28	-0.20	-0.14	0.57	-0.28	-0.16	-0.10	0.03	0.78	0.23
E_a /eV				0.82	1.28	0.40	0.58	0.93	0.73	1.36	0.79		0.93	
Interaction energy/eV	Reactants	-	-	-	-	0.17	0.55	0.21	-	-	0.29	-	-0.01	-
	Products	-	-	0.22	0.35	-0.33	-	-	-	0.00	-0.02	-	-	-
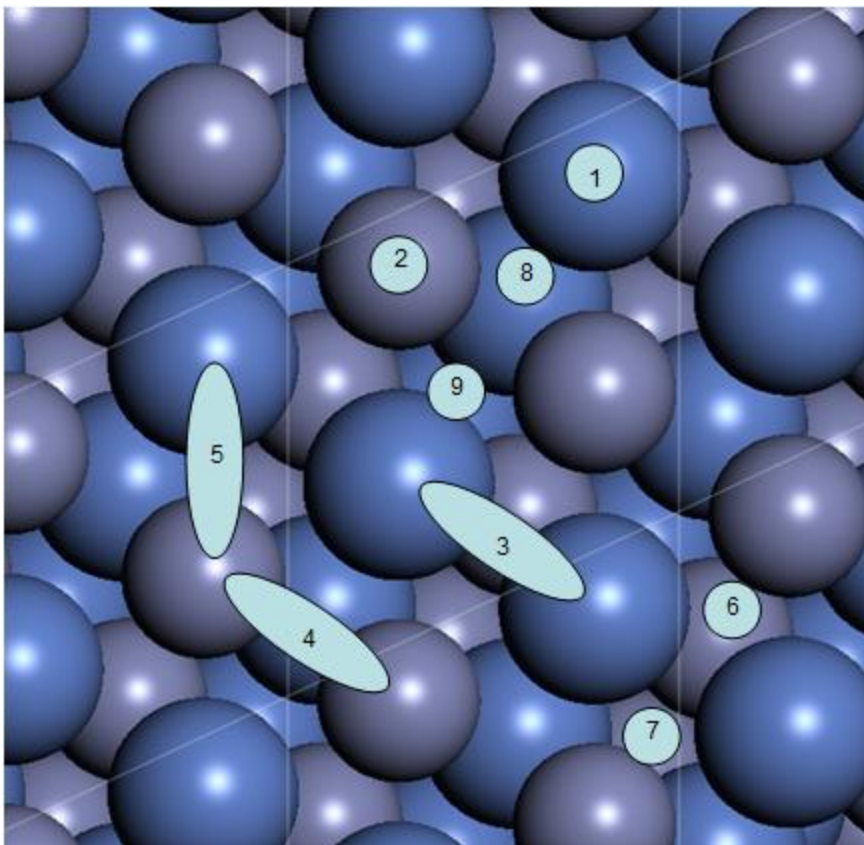
Fig. 22 Adsorption sites on NiZn (111)
1. atop site of Ni (tNi); 2. atop site of Zn (tZn); 3. bridge site of Ni-Ni (bNiNi); 4. bridge site of Zn-Zn (bZnZn); 5. bridge site of Ni-Zn (bNiZn); 6. hcp pseudo hollow site formed by two Ni atoms and one Zn atom (h2NiZn); 7. fcc pseudo hollow site formed by two Ni atoms and one Zn atom (f2NiZn); 8. hcp pseudo hollow site formed by two Zn atoms and one Ni atom (h2ZnNi); 9. fcc pseudo hollow site formed by two Zn atoms and one Ni atom (h2ZnNi);

6.3.1.1 Redox mechanism on PdZn (111) surface

On PdZn (111) CO tends to adsorb on the atop site of Pd with a binding energy of -0.95 eV. H_2O adsorbs weakly (-0.20 eV) atop on Zn and prefers a configuration parallel to the surface, consistent with previous findings of Lim *et al.* [123]. However, when it dissociates, H_2O molecule does so through a configuration where it is vertical at the bZnZn site. Although this vertical orientation is 0.18 eV higher in energy than the parallel

104

one, the barrier to dissociation is significantly lower (0.95 eV compared to 1.35 eV when being placed parallel at tZn). Our result is consistent with a very recent paper published by Huang and Chen[148] although they employed a larger unit cell (4×4). This vertical configuration is important at higher coverage when water forms a two-dimensional ice-like structure on metal surfaces[149], and therefore could potentially be the dominant configuration in the elementary step of water dissociation. The reaction is slightly endothermic with a 0.20 eV reaction enthalpy (0.14 eV at infinite separation). Water dissociates to a hydroxyl group and atomic hydrogen, and OH and H both favor adsorption on site f2ZnPd.

Following water dissociation, the hydroxyl group may further dissociate to generate an oxygen atom and a hydrogen atom. However, this barrier is significantly higher than H_2O dissociation (1.62 eV) and the reaction enthalpy is also significant (0.96 eV), making this reaction difficult.

However, a second path for generation of atomic oxygen on the surface exists through the disproportionation reaction of two adjacent hydroxyl groups. The hydroxyl group moves to bPdZn and tilts to the extent that it almost lies down, a 18° angle is formed between the hydroxyl group and the surface. The generated H_2O prefers to stay atop of Pd and O adsorbs at f2PdZn. Although H_2O at ¼ ML coverage prefers atop Zn, the presence of strong binding O atoms pushes the H_2O molecule (which binds weakly to all sites) to atop Pd. This elementary step is approximately thermoneutral with a reaction enthalpy of 0.04 eV and a barrier of 0.53 eV. Obviously oxygen is more easily generated through this path provided there are OH groups available for reaction.

CO oxidation on PdZn(111) is exothermic with a reaction enthalpy of -0.78 eV and a

barrier is 0.82 eV. CO adsorbed at tPd reacts with an oxygen atom at f2ZnPd and produces a CO_2 molecule lying parallel to the surface. Once created, CO_2 will rapidly desorb since it does not interact with the surface (E_{ads} = -0.04 eV) .

Hydrogen atoms which are created by the dissociations of water and hydroxyl groups will combine to make H_2 molecules on the Pd atop sites. The enthalpy of this reaction is 0.43 eV and the barrier 0.91 eV. H_2 will desorb easily because it does not bind molecularly to the surface.

6.3.1.2 Redox mechanism on NiZn (111)

In contrast to the PdZn(111) surface, the favored adsorption site of CO on NiZn(111) is the bridge site of two Ni atoms. The binding energy is -1.66 eV. Just as on the PdZn(111) surface, H_2O adsorbs weakly (E_{ads} = -0.16 eV) at the Zn atop site and the molecule plane is parallel to the surface too. Nonetheless it does not flip to vertical configuration for dissociation as it does on PdZn(111). Instead, it moves to tNi, which is less stable by 0.11 eV, but in a better position for dissociation. It then dissociates to OH at site h2NiZn and H at bNiNi. The dissociation enthalpy is -0.26 eV (-0.48 eV at infinite separation) and has an activation energy is 0.82 eV, implying that water activation is a little easier on NiZn (111) than on PdZn (111).

Just as in the case of PdZn(111), the dissociation of hydroxyl groups is even more difficult than H_2O dissociation with a barrier of 1.28 eV (but lower than the barrier for OH dissociation on PdZn(111)). Similarly, disproportionation of adjacent hydroxyl groups has a much lower barrier (0.40 eV) on this surface as well, allowing for the facile generation of surface oxygen. Finally, CO at the bNiNi site is oxidized by surface atomic

106

oxygen at h2NiZn to CO_2 with a barrier of 0.58 eV and desorbs very rapidly as it does not bind to NiZn(111). Although the reaction is not as exothermic as on PdZn(111), CO is easier to oxidize on NiZn (111) than on PdZn(111). This suggests that CO oxidation does not follow a traditional BEP relationship on these alloy surfaces. The enthalpy of creating a H_2 molecule on NiZn (111) is 0.78 eV and the barrier is 0.93 eV. Taking the adsorption energy of H_2 (-0.23 eV) into account, the reaction enthalpy of associative hydrogen desorption is 1.01 eV. This result also implies that H_2 dissociates steadily on NiZn(111) while on PdZn(111) it dissociative adsorption requires to overcome a higher barrier.

6.3.2   Carboxyl mechanism

As mentioned above, an alternative mechanism for WGS passes through a carboxyl intermediate. In this case, the initial steps of CO adsorption and H_2O dissociation are the same. However, unlike in the redox mechanism where hydroxyl groups dissociate or disproportionate to water and oxygen, OH reacts with CO to form carboxyl on the surface. COOH can either decompose to CO_2 and H (step 6a) or produce CO_2 and H_2O with the participation of OH (step 7a). Although formate was observed in experiments as an intermediates [141, 150, 151], it was also found too stable to be an active intermediate for LTS WGS and could even be a poison of catalysts. For example, on Pt/CeO_2 catalyst it is stable up to 433 K [150]. On the other hand, Rodriguez *et al.* [139] detected the rapid reaction of CO and OH on Au (111) surface at low temperatures (90 K and 120 K), consistent with the formation of unstable carboxyl. Hence, we have focused on carboxyl as a key intermediate in WGS.

107

6.3.2.1 Carboxyl mechanism on PdZn (111)

With the co-adsorption of OH at f2ZnPd, CO does not change its favorite adsorption site and remains atop of Pd. Cis-COOH (Fig. 23a) then is produced adsorbed to the tPd site. The reaction is mildly endothermic with an enthalpy of 0.26 eV and a fairly low barrier 0.44 eV.

Yet an additional step (5.5) whereby cis-COOH transforms into trans-COOH (Fig. 23b) is necessary for the next two steps (step (6a) and (7a)).

$$\text{cis-COOH} \rightleftharpoons \text{trans-COOH} \tag{5.5}$$

H atom rotates on the side of COO plan from a position pointing away from the surface to a position heading towards the surface. The reaction enthalpy for rotation of the OH is 0.09 eV with a barrier of 0.54 eV.

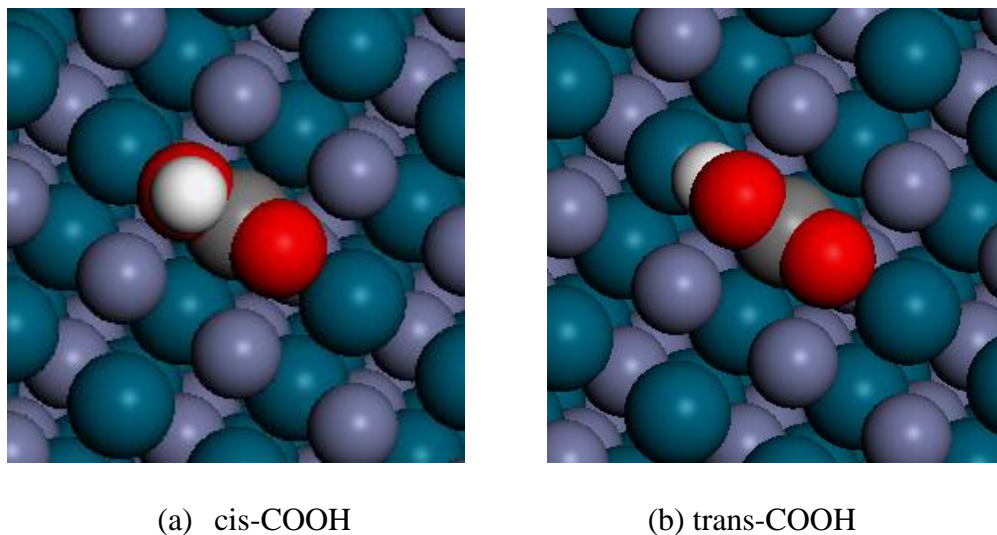(a) cis-COOH   (b) trans-COOH

Fig. 23 (a) cis-COOH and (b) tran-COOH on PdZn(111).

Although the dissociation of trans-COOH is an exothermic reaction with an enthalpy of -0.49 eV, the barrier is 1.06 eV. However, the reaction of COOH with OH (step 7a) has a small barrier of 0.19 eV and reaction enthalpy of -0.62 eV. Thus production of CO_2 is apparently easier through the later pathway provided the OH coverage on the surface is high enough.

Generally carboxyl mechanism seems the dominant mechanism on PdZn (111) surface, while redox mechanism is less favored because step 6 and 7 clearly have higher overall barrier than step 5a and 7a.
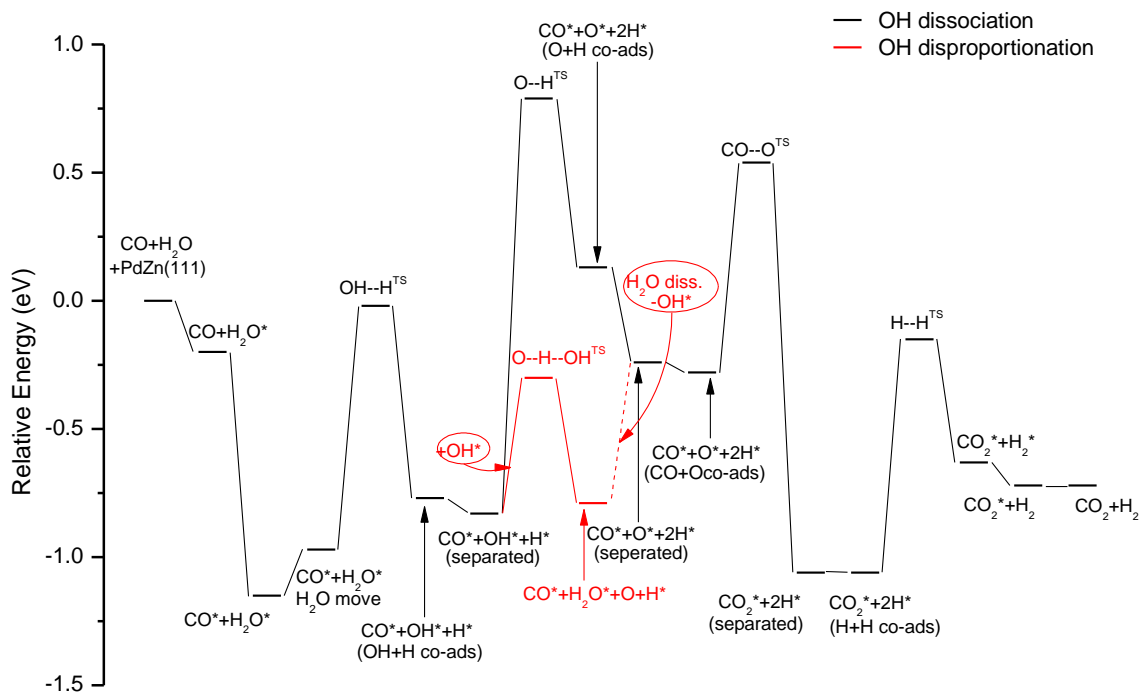
6.3.2.2 Carboxyl mechanism on NiZn (111)

CO and OH favor the sites tNi and f2ZnNi, respectively. They form a cis-COOH and move a little towards the bridge site of two nickel atoms. Both the enthalpy of reaction (0.57 eV) and barrier (0.93 eV) are larger on NiZn (111) than on PdZn (111).

The transformation of cis- to trans-COOH is more difficult on NiZn (111) with an activation energy of 0.73 eV, but is slightly exothermic with a reaction enthalpy of -0.28eV. We have previously determined that the barrier for the conformation change of COOH is not particularly sensitive to the identity of the surface. However, the geometry of COOH on PdZn(111) and NiZn(111) are not identical.

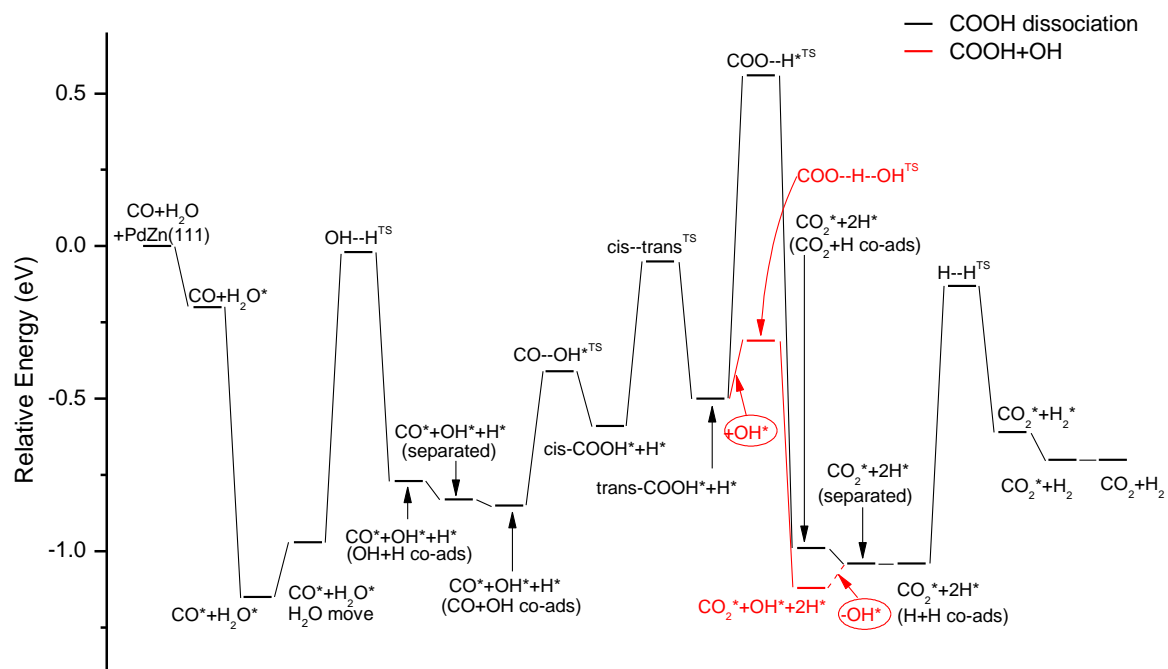On the other hand, both the dissociation of trans-COOH to CO_2 on NiZn (111) ($E_a =$ 1.36 eV) and its reaction with OH become more difficult ($E_a = 0.79$ eV) as well. Carboxyl dissociation leads to CO_2 production which immediately desorbs. In the meantime, when H breaks off and it will move to site h2NiZn. Alternatively, when trans-COOH reacts with hydroxyl group, the oxygen of OH is tilted and the plan of COOH

rotates so that its hydrogen locates closer to hydroxyl group. H₂O is then formed at the Zn atop site. Unlike the case for PdZn (111), the redox mechanism becomes a little more favored than carboxyl mechanism.

To sum up, the potential energies of all reaction pathways are presented in Fig.24. Fig. 24(a) and Fig. 24(b) illustrate the redox mechanism and carboxyl mechanism on PdZn(111) surface, respectively. Fig.24(c) and 24(d) are for NiZn(111). In the redox mechanism the participation of OH group in step 6 lowers the difficulty of surface oxygen generation. This pathway is marked by red to distinguish from and compare with OH dissociation. Likewise, the reaction between trans-COOH and OH eases the production of CO_2 as well.

(a)

Relative Energy (eV)

COOH dissociation
COOH+OH

0.5

0.0

-0.5

-1.0

CO+H$_2$O
+PdZn(111)

CO+H$_2$O*

OH--H^{TS}

CO*+H$_2$O*

CO*+H$_2$O*
H$_2$O move

CO*+OH*+H*
(separated)

CO*+OH*+H*
(OH+H co-ads)

CO--OH*^{TS}

cis-COOH*+H*

CO*+OH*+H*
(CO+OH co-ads)

cis--trans^{TS}

trans-COOH*+H*

COO--H*^{TS}

COO--H--OH^{TS}

CO$_2$*+2H*
(CO$_2$+H co-ads)

+OH*

CO$_2$*+2H*
(separated)

CO$_2$*+OH*+2H*

-OH*

CO$_2$*+2H*
(H+H co-ads)

H--H^{TS}

CO$_2$*+H$_2$*

CO$_2$*+H$_2$

CO$_2$+H$_2$
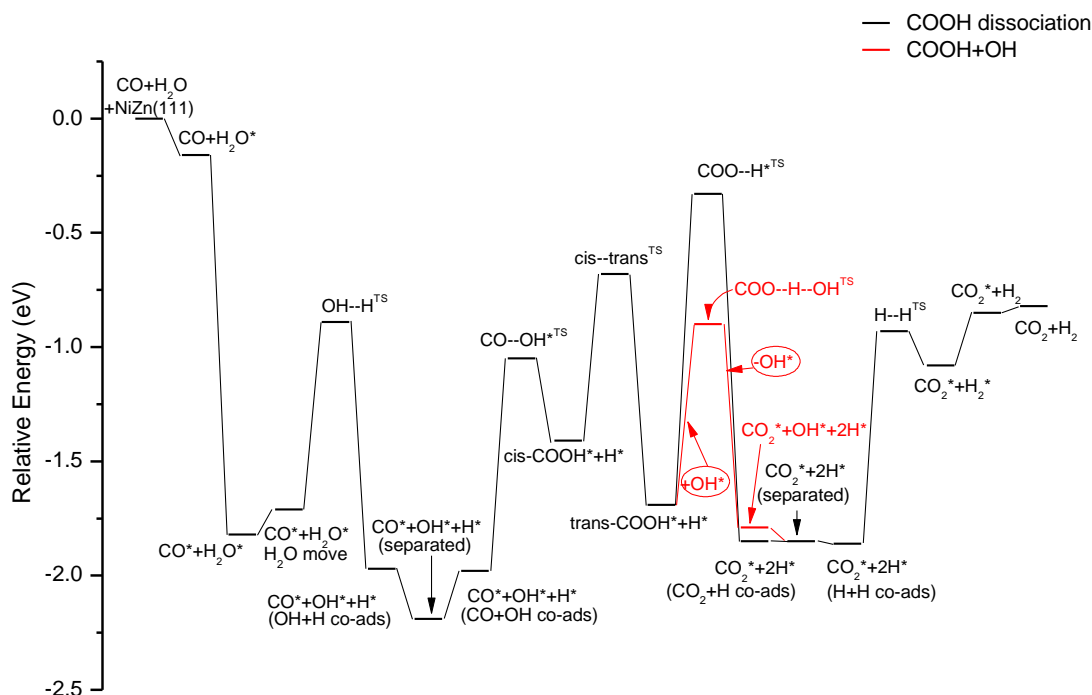
(b)

(c)

Fig. 24 Reaction pathway figure of two different mechanisms on two surfaces. (a) redox mechanism on PdZn(111); carboxyl mechanism on PdZn(111); (c) redox mechanism on NiZn(111); (d) carboxyl mechanism on NiZn(111). The total energy of reactants and clean surface is set to zero. In the pathway of OH disproportionation OH* is added to reaction and removed following an additional step of H_2O dissociation

6.3.3 Formate mechanism

Although we ruled out the possibility of formate to be an active intermediate in the water gas shift reaction according to previous research results as indicated in the last section (3.2), there is still a need to confirm it for our system as several of the observations for the intermetallic alloys studied here do not conform to our previous picture of WGS on monometallic surfaces. In this case we only investigated the related

mechanism on NiZn(111).

Chen *et al.* [121] divided the formation of formate into two elementary steps:
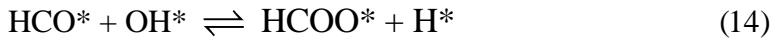
$$CO* + OH* \rightleftharpoons HCO* + O* \qquad\qquad (11)$$
$$HCO* + O* \rightleftharpoons HCOO* + * \qquad\qquad (12)$$
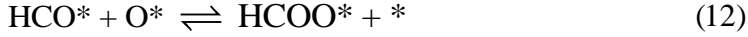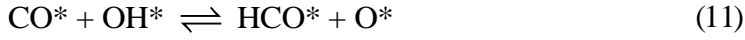
found that the reaction barrier of the formyl formation reaction (step 11) on ceria

supported gold cluster $Au_{10}/CeO_2(111)$ was about 1 eV and the barrier on $Au_3/CeO_2(111)$

was 1.80 eV.

In addition to steps 11 and 12, we also considered the following two reactions 13 and

14 as additional possible channels to produce formate.

$$CO* + H* \rightleftharpoons HCO* \qquad\qquad (13)$$
$$HCO* + OH* \rightleftharpoons HCOO* + H* \qquad\qquad (14)$$
$$HCOO* + * \rightleftharpoons CO_2* + H* \qquad\qquad (15)$$

Here we calculate all of these four formate production steps and the dissociation step

(reaction 15) to check the feasibility of formate mechanism on NiZn(111) surface.

From our calculation results it does not seem possible to form formate through either

channel (11)-(12) or (13)-(14), because the energy barriers of reaction (11) and (13) for

C-H bond formation (2.11 eV and 1.71 eV, respectively). Futhermore, Step (15) has an

extremely high activation energy (2.80 eV) indicating that once formate is produced on

the surface it will not dissociate, thus the further reaction will be impossible and formate

itself could be poison for the metal surface. Our results coincide with experimental results

[139, 150] which stated that formate was too stable on the surfaces and therefore, formate

is very unlikely to be an active species in the WGS reaction.

6.4 Discussion

In this work we investigated two mechanisms on two different alloy surfaces by DFT calculation. To properly define the rate limiting step, a full degree of rate control analysis of a microkinetic model would have to be undertaken [152-154] (This has be done recently for WGS on Cu(111) [155]). However, we can naively probe the important kinetic steps in each mechanism by simply tracing the highest barriers for each path. The highest barrier for a single step in both mechanisms on the PdZn(111) surface along the simplest path is the activation of H_2O (Eact = 0.95 eV). However, if the concentration of OH on the surface is too low (as has been suggested by Schneider et al [156]), then the redox pathway requires the difficult direct dissociation of OH (1.62 eV) whereas the carboxyl mechanism decomposition has a barrier of only 1.06 eV. This would imply that the carboxyl is likely to be favored in the absence of a large number of hydroxyl groups on the metal surface (although it is worth mentioning that hydroxyl groups on the support surface may be available at the metal/support interface).

In contrast, for NiZn(111) the barrier for H_2O dissociation is lowered to 0.82 eV and in this case, the barrier for hydrogen association would actually be the single step with the largerst barrier if all pathways are available. Otherwise, the barrier for OH dissociation is somewhat lower than that on PdZn(111) (only 1.28 eV) whereas the carboxyl decomposition barrier rises to 1.36 eV, shifting the mechanism from the carboxyl route to the the redox pathway. In addition we have confirmed formate to be an inactive and unimportant species on NiZn(111) for WGS reaction. Based on the calculations above, NiZn(111) should show reasonable activity for WGS which supports our original proposal that it is possible to be a low-priced and active substitute for WGS

catalysts. When compared to the work of Mavrikakis on Cu(111), we find that the highest barriers for the carboxyl path involve water dissociation (1.36 eV) and carboxyl decomposition (1.41 eV), suggesting that in our naïve analysis that PdZn and NiZn should both be competitive with Cu[116]. Critical to the success of NiZn will be its ability to resist oxidation. Although WGS is a essentially a reducing environment, its not clear that NiZn(111) will remain stable under reaction conditions. In addition, sintering remains a concern for NiZn as the melting point of NiZn is certainly significantly lower than PdZn: 1057 C [157] vs. 1550 C (it should be noted that the melting point of Cu is 1084 C).

6.5 Conclusions

We have examined the water gas shift reaction over PdZn(111) and NiZn(111) using density functional theory to probe their suitability for replacement of Cu as low temperature WGS catalysts. We have found that while the WGS reaction on PdZn(111) is likely to proceed through a carboxyl mechanism, on NiZn(111) both pathways are likely to be important kinetically. In addition, both surfaces show behavior that would suggest that they should be competitive with Cu. However, while PdZn stability has been already demonstrated, NiZn may suffer from some of the same issues as Cu catalysts.

7   FUTURE WORK

To this point, we have investigated some important factors affecting the selectivity in the selective hydrogenation of α, β-aldehydes to α, β-unsaturated alcohols using acrolein as a model compound over supported silver catalysts. We made several key observations through our study.

1) The selectivity to allyl alcohol is better over a catalyst having larger silver nanoparticles. It is most likely because larger particles have more terrace sites that favor the adsorption of acrolein, especially via the carbonyl group. Therefore the catalysts with larger particle sizes have not only better selectivity but also higher activity;

2) TiO_2 is the best support among SiO_2, Al_2O_3 and TiO_2. Ag/TiO_2 provides higher activity and selectivity to allyl alcohol. An important difference between TiO_2 and the other two support is that TiO_2 is partially reducible. Ti^{3+} species is considered to play an crucial role in the reaction. We speculate that Ti^{3+} sites (especially the ones locating at the interface with silver particles) are apt to adsorb acrolein via the C=O bond so better selectivity towards the hydrogenation of C=O is obtained.

To summarize, our study suggests that the adsorption manner of acrolein is critical to the selectivity. Since acrolein tends to adsorb parallel to the surface at low coverage on metal surfaces and C=C bond is easier to be activated, it is hard to hydrogenate C=O bond only and leave C=C bond intact. Stronger interaction via C=O bond with the catalytic surface will facilitate its hydrogenation and improve the selectivity to allyl alcohol. Thus a configuration with C=O bond attached to the surface and C=C bond tilting away from the surface will be ideal to avoid the hydrogenation of the olefinic

group. As mentioned in Chapter 5, the intrinsic complexity of supported nanoparticle catalysts may prevent a high selectivity towards a specific product. In contrast, a single site catalyst with uniform active sites can be well tailored to suit the need of a certain reaction pathway.

One of our goals in the future is to find a SSHC that adsorbs acrolein only via the C=O bond so that the selectivity to allyl alcohol can be significantly improved. Besides $Zn@SiO_2$ discussed in Chapter 5, we have tried a few other metals for the selective hydrogenation of acrolein and some of them showed fairly good selectivity. Their synthesis and testing conditions and performances are listed in Table VIII. $Fe@SiO_2$ and $Pt@SiO_2$ are the second and the third best catalysts in terms of selectivity that we have made so far, showing a selectivity of 38% and 34%, respectively. $Pt@SiO_2$ not only showed promising selectivity but also exhibited much higher activity than $Zn@SiO_2$ and $Fe@SiO_2$. We have reasons to believe that we can improve upon these results and that we can synthesize a SSHC having both higher selectivity and activity than any of our current candidates. Due to our lack of understanding of the SSHC mechanism, it is difficult to predict which metal or which support will serve the hydrogenation of C=O bond better at this point. In the immediate future we will have to try more combinations of different metals (W, Ru, Mn) and supports (eg. TiO_2, Al_2O_3). Ultimately, a SSHC providing water resisting Lewis acid sites (such as Mo) is favored because water exists in commercial acrolein as a stabilizer to prevent polymerization in a level of several percent. At the same time, the group is beginning with density functional theory calculations to examine

Catalyst	Loading (wt%)	Precursor	Synthesis condition	Reaction Temperature ($^{\circ}$C)	P (atm)	Selectivity to allyl alcohol (%)	TOF (s^{-1})
Pt@SiO$_2$	0.99	Pt(NH$_3$)$_4$(NO$_3$)$_2$	-	100	5	34	3.2×10^{-4}
Pd@SiO$_2$	3	Pd(NH$_3$)$_4$(NO$_3$)$_2$	Dried at 125 $^{\circ}$C	30	1	0.9	4.0×10^{-3}
Fe@SiO$_2$	5	2, 4-dimethyl-1,3-pentadienide Fe	Reduced at 350 $^{\circ}$C	100	1	38	1.6×10^{-6}
Ni@SiO$_2$	4	Ni(NH$_3$)$_6$Cl$_2$	Dried at 25 $^{\circ}$C Calcined at 300 $^{\circ}$C	100	1	12	2.0×10^{-6}
Co@SiO$_2$	4	Co(NH$_3$)$_6$(NO$_3$)$_3$	Dried at 25 $^{\circ}$C Calcined at 300 $^{\circ}$C	75	1	6	3.4×10^{-5}
Rh@SiO$_2$	2	Rh(NH$_3$)$_4$Cl$_2$	Dried at 125 $^{\circ}$C	100	5	4	1.2×10^{-4}
Ru@SiO$_2$	2	Ru(NH$_3$)$_4$Cl$_3$	Dried at 125 $^{\circ}$C	30	1	0.7	6.7×10^{-4}
Ir@SiO$_2$	2	Ir(NH$_3$)$_4$Cl$_3$	Dried at 125 $^{\circ}$C	100	5	0.6	1.9×10^{-4}
Zn@SiO$_2$	4	Zn(NO$_3$)$_2$ 6H$_2$O	Dried at 125 $^{\circ}$C Calcined at 300 $^{\circ}$C	100	1	45	3.3×10^{-6}
Pt@sulfate Al$_2$O$_3$	2	Pt(NH$_3$)$_4$(NO$_3$)$_2$	Dried at 125 $^{\circ}$C Calcined at 550 $^{\circ}$C	75	1	12	3.5×10^{-4}

Table VIII   Tested single site catalysts, their synthesis and testing condition and performance.

the mechanism of acrolein adsorption over a single site $Zn@SiO_2$ to determine if our hypotheses regarding the adsorption modes of hydrogen and acrolein are correct.

Another way to improve both the selectivity and activity of the catalysts is to employ alloys. Cu and Au were tried because of their similarity in chemistry to Ag and comparable performance reported for Au [5, 20, 158]. Unfortunately, neither the monometallic Cu and Au catalysts or their alloys with silver are as good as silver from the standpoint of selectivity. In Fig. 25, two Cu catalysts (one supported on SiO_2, one supported on CeO_2) and one Cu-Ag bimetallic
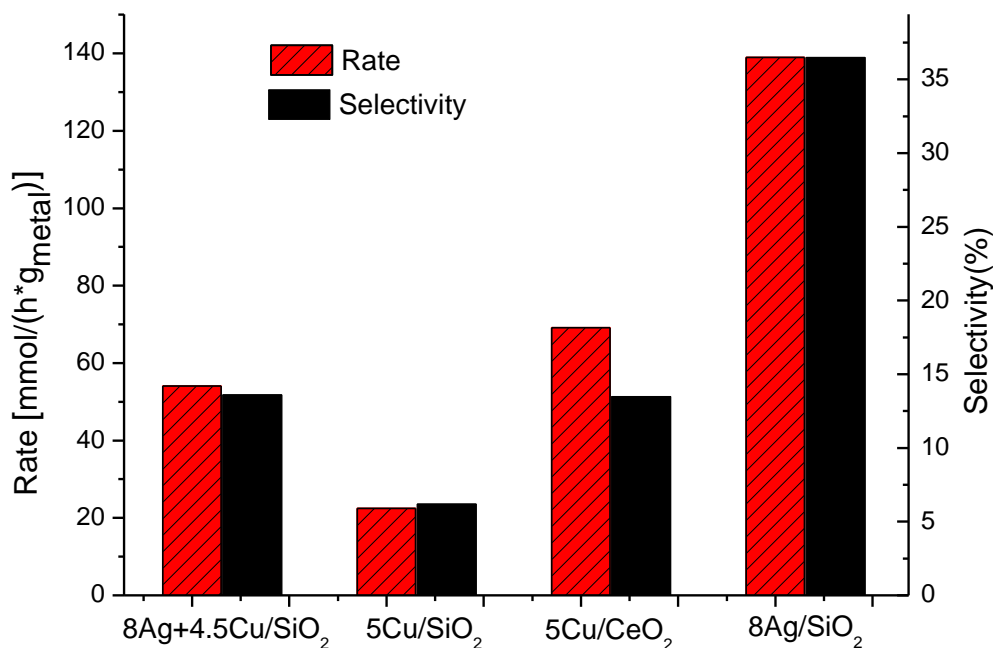

Fig. 25 The reaction rate and selectivity to allyl alcohol of a Cu-Ag/SiO_2 catalyst and two copper catalysts compared to a silver catalyst. (The numbers before the element symbols represent the weight percentage of that metal).

catalyst with a 1:1 molar ratio of Cu to Ag are compared with a Ag/SiO$_2$ having the largest particle size. Cu/SiO$_2$ merely has 6% selectivity to allyl alcohol. Ag-Cu/SiO$_2$ has 15% selectivity, in between pure Cu and pure Ag. A support effect is observed as well. The ceria supported Cu has about 14% selectivity that is much better than the silica supported one, making CeO$_2$ a promising support. The gold catalyst has poorer selectivity and activity than the silver catalyst. As shown in Fig. 26, the selectivity over the silica supported gold catalyst is similar selectivity to that over Cu/SiO$_2$. Two Au-Ag catalysts
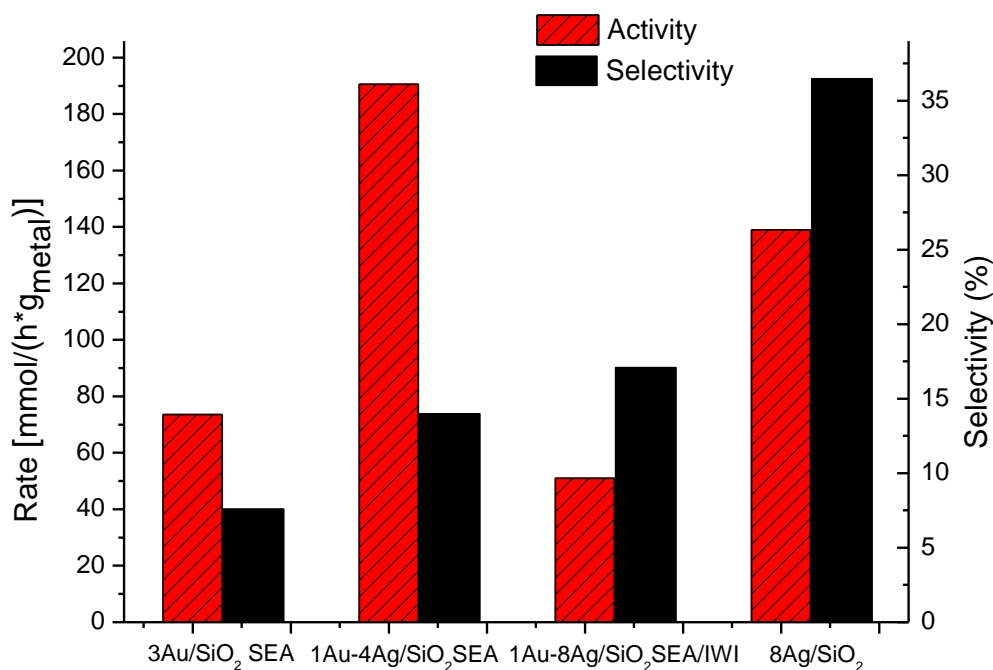

Fig. 26 The reaction rate and selectivity to allyl alcohol of a Au/SiO$_2$ catalyst and two Au-Ag/SiO$_2$ catalysts compared to a silver catalyst. (The numbers before the element symbols represent the weight percentage of that metal).

(with different Ag loadings) both have around 15% selectivity and the one with high loading of Ag is slightly more selective than the other by about 3%.

Ag-In bimetallic catalyst was reported to be better than silver with an exceeding selectivity of 60% [33]. However, in our experiments Ag-In catalysts only have comparable selectivity to monometallic silver catalyst and the activity is much lower (showed in Fig. 27). An issue with In is that In is very difficult to reduce from the oxidation state to metal. Thus the catalyst is air sensitive after reduction. Two Ag-In
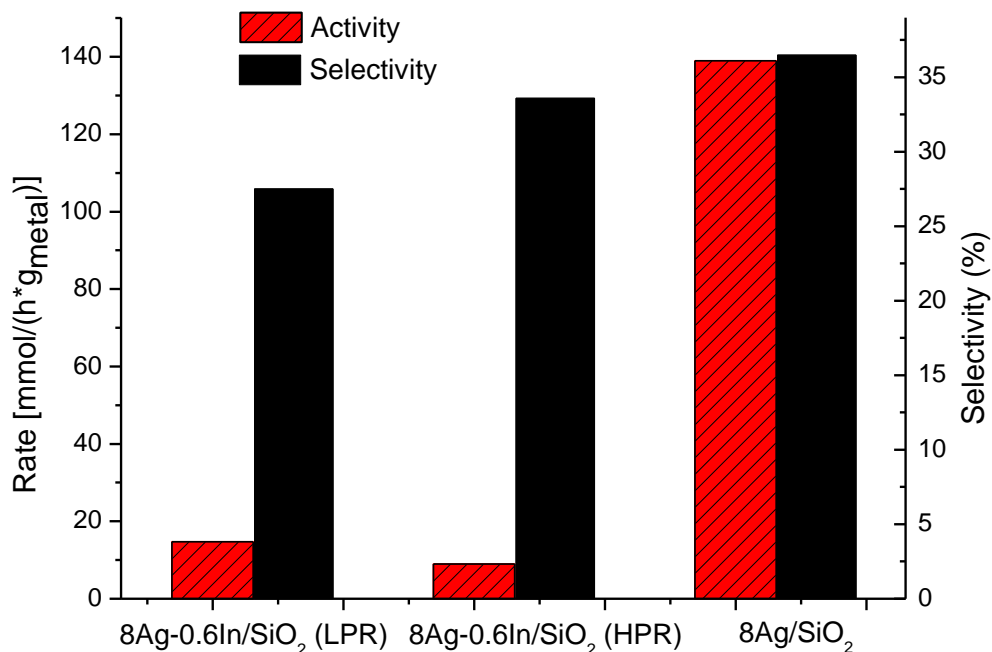

Fig. 27 The reaction rate and selectivity to allyl alcohol of two Ag-In/SiO$_2$ catalysts compared to a silver catalyst. (The numbers before the element symbols represent the weight percentage of that metal, LPR: low pressure reduction, HPR: high pressure reduction).

catalysts were made and the only difference was the reduction pressure. One was reduced at 290 psia and the other at 75 psia, both at 325 ℃. Higher pressure seemed to help the reduction of In and increase the selectivity to allyl alcohol. The former has higher selectivity (34% vs. 28%) but the activity is even lower.

Compared to conventional alloys, single atom alloys are more promising as shown in Chapter 4. Our initial results show that the selectivity and activity were both enhanced on 0.01%Pd+8%Ag/SiO$_2$ by adding a very small amount of Pd into silver catalyst. Other hydrogen active metal, such as Pt, Rh and Ru, have also been screened. The precursors and synthesis conditions are described in Table IX and their selectivity and activity were compared with the best performing silver catalyst in Fig. 28. In Fig. 28 (b), the activities of all bimetallic catalysts are higher than monometallic silver catalyst. The Rh-Ag catalyst showed the highest activity (about 9 times of that of pure silver) but (perhaps not coincidentally) the lowest selectivity (only 14%). Pd-Ag and Ni-Ag have around 30% selectivity which is comparable to Ag for the same particle size. Ru-Ag and Ir-Ag showed selectivities above 40% which are the best two among all of them.

Catalyst	Dilute metal precursor	Silver precursor	Synthesis condition	Particle size (nm)
0.01%Rh-8%Ag	Rh(NO$_3$)$_3$		1st IWI: Dried at 125 ℃	6.1
0.02%Pt-8%Ag	Pt(NH$_3$)$_4$(NO$_3$)$_2$			6.1
0.01%Pd-8%Ag	Pd(NO$_3$)$_2$	AgNO$_3$	Calcined at 250 ℃	5.8
0.01%Ru-8%Ag	Ru(acac)$_3$		2nd IWI: Dried at 125 ℃	6.4
0.01%Ir-8%Ag	Ir(acac)$_3$			6.1
0.01%Ni-8%Ag	Ni(NO$_3$)$_2$		Reduced at 325 ℃	6.5

Table IX Precursors and synthesis condition for all SAAs
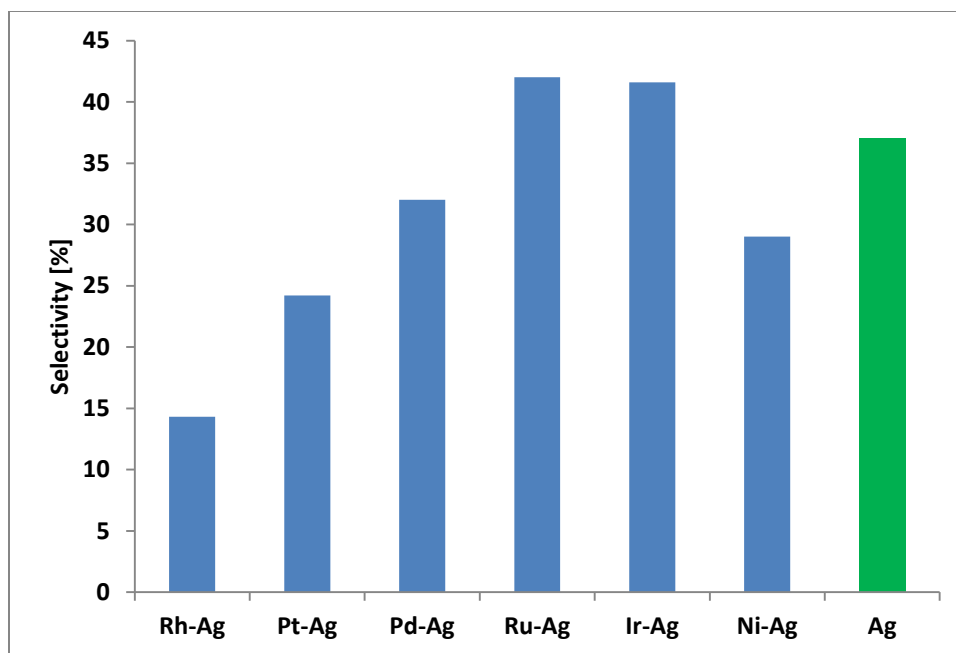
(a)
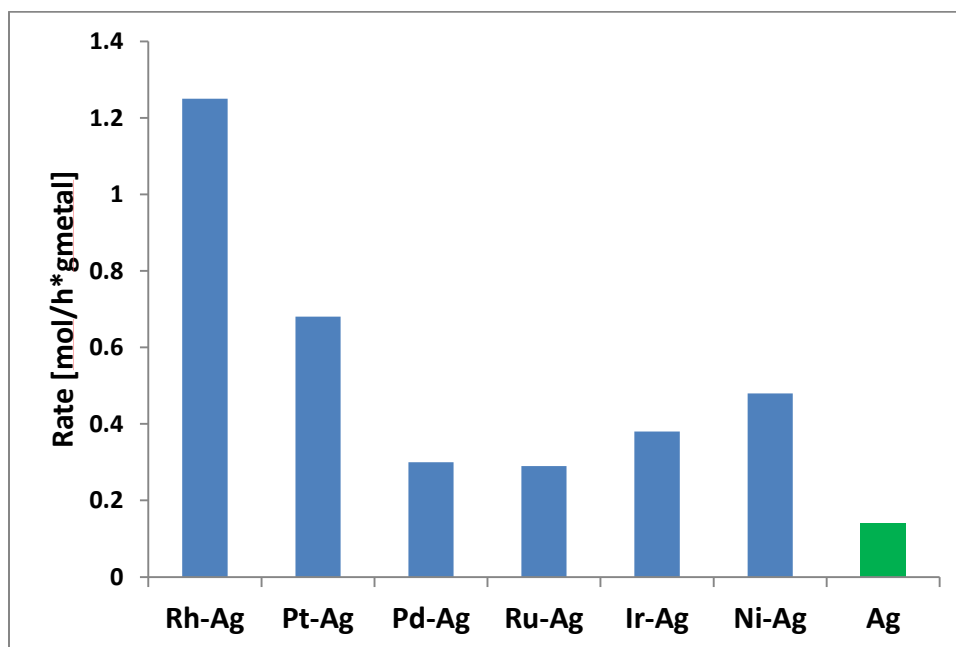
(b)

Fig. 28 The selectivities (a) and reaction rates (b) of all SAA catalysts (silica supported) compared to best-performing Ag/SiO₂.

124

According to our preliminary results, adding a small amount of a hydrogen active metal can definitely improve the activity of silver catalysts. However, a detailed study is demanded because we have noticed that several parameters in catalyst synthesis have important influences on the selectivity and activity of the catalysts. First of all, the synthesis method could potentially be improved. All the bimetallic catalysts were synthesized by sequential impregnation. However, our goal is to make the second metal well dispersed in silver and sequential impregnation should be less conducive to obtain a highly dispersed alloying metal compared to co-impregnation. We expect that the alloying metal can exist as isolated atoms in the Ag matrix at much higher loadings than merely 0.01 wt% by using co-impregnation. Thus there will be more active centers for H_2 dissociation and the activity will be improved accordingly and maybe the selectivity as well. In addition, sequential impregnation seems to limit the particle growth as the alloying metal acts to provide a nucleation center for the Ag. This is unfavorable because larger Ag particles have better selectivity and activity according to our results in Chapter 2. Secondly, the suitable amount of the second metals was not examined. We expect the activity will increase with increasing the amount of the doped hydrogen active metals and the high selectivity can be maintained. There should be a point that both high selectivity and activity can be achieved but the selectivity will drop beyond that point because of segregation leading to the presence of contiguous M-M bonds in the Ag matrix which may ultimately lead to C-C cleavage. A systematic study on the effect the concentration of the doped metals for at least one system must be performed (although it should be clear that not all systems will behave the same.

Thirdly, the precursor of the alloying metal seems to have an effect on the selectivity to allyl alcohol as well. Ru-Ag and Ir-Ag catalysts having the best selectivity were all made from organic precursors. Although it is not clear why using organic precursors has positive effect on selectivity at this point, we believe it is not coincidence and we would like to try using organic precursors for other metals too.

In all, there are many issues left to explore in this system. Although acrolein hydrogenation is a fairly simple reaction, it provides a rich canvas upon which we can illustrate many key concepts related to catalysis (particle size effects, support effects etc.). Future efforts will be pursued with regard to the two unique types of single site catalysts, focusing on optimizing the adsorption manner of acrolein and facilitating the dissociation of H_2. Eventually, we hope that a very selectivity and active catalyst for gas phase selective hydrogenation of acrolein should be able to be synthesized and this process can an optional process for commercial use.

CITED LITERATURE

[1] G.A. Somorjai, C.J. Kliewer, React. Kinet. Catal. Lett. 96 (2009) 191.

[2] P. Gallezot, D. Richard, Catal. Rev. Sci. Eng. 40 (1998) 81.

[3] P. Mäki-Arvela, J. Hájek, T. Salmi, D.Y. Murzin, Appl. Catal. A 292 (2005) 1.

[4] Ullmann's Encyclopedia of Industrial Chemistry, 5th ed., Weinheim, 1985

[5] C. Mohr, H. Hofmeister, J. Radnik, P. Claus, J. Am. Chem. Soc. 125 (2003) 1905.

[6] A. Daimon, T. Kamitanaka, N. Kishida, T. Matsuda, T. Harada, J. of Supercritical Fluids 37 (2006) 215.

[7] Y. Zhu, G.-K. Chuah, S. Jaenicke, J. Catal. 241 (2006) 25.

[8] K. Weissermel, H.J. Arpe, Industrial Organic Chemistry, Wiley-VCH, 2003

[9] T.H. Vanderspurt, 1978, Celanese Corporation, US 4127508

[10] F. Delbecq, P. Sautet, J. Catal. 152 (1995) 217.

[11] R.A.V. Santena, H.P.C.E. Kuipersa, Adv. Catal. 35 (1987) 265.

[12] P. Claus, Topics Catal. 5 (1998) 51.

[13] R. Hirschl, F. Delbecq, P. Sautet, J. Hafner, J. Catal. 217 (2003) 354.

[14] T.J. Thibodeau, A.S. Canney, W.J. DeSisto, M.C. Wheeler, F.G. Amar, B.G. Frederick, Appl. Catal. A 388 (2010) 86.

[15] T.B.L.W. Marinelli, S. Nabuurs, V. Ponec, J. Catal. 151 (1995) 431.

[16] C. Hoang-Van, O. Zegaoui, Appl. Catal. A 164 (1997) 91.

[17] B. Coq, F. Figueras, P. Geneste, C. Moreau, P. Moreau, M. Warawdekar, J. Mol. Catal. 78 (1993) 211.

[18] N. Gyorffy, Z. Paál, J. Mol. Catal. A: Chem 295 (2008) 24.

[19] P. Claus, A. Bruckner, C. Mohr, H. Hofmeister, J. Am. Chem. Soc. 122 (2000) 11430.

[20] P. Claus, H. Hofmeister, C. Mohr, Gold Bulletin 37 (2004) 181.

[21] C. Mohr, H. Hofmeister, P. Claus, J. Catal. 213 (2003) 86.

[22] C. Mohr, H. Hofmeister, M. Lucas, P. Claus, Chem. Eng. Technol. 23 (2000) 324.

[23] W. Grünert, A. Bruckner, H. Hofmeister, P. Claus, J. Phys. Chem. B 108 (2004) 5709.

[24] M. Bron, D. Teschner, A. Knop-Gericke, F.C. Jentoft, J. Kröhnert, J. Hohmeyer, C. Volckmar, B. Steinhauer, R. Schlögl, P. Claus, Phys. Chem. Chem. Phys. 9 (2007) 3559.

[25] M. Bron, D. Teschner, A. Knop-Gericke, B. Steinhauer, A. Scheybal, M. Hävecker, D. Wang, R. Födisch, D. Hönicke, A. Wootsch, R. Schlögl, P. Claus, J. Catal. 234 (2005) 37.

[26] R.I. Masel, Principles of adsorption and reaction on solid surfaces, John Wiley & Sons, Inc., New York, 1996, p762.

[27] C.E. Volckmar, M. Bron, U. Bentrup, A. Martin, P. Claus, J. Catal. 261 (2009) 1.

[28] T.B.L.W. Marinelli, J.H. Vleeming, V. Ponec, Stud. Surf. Sci. Catal. 78 (1993) 195.

[29] Z. Poltarzewski, S. Galvagno, R. Pietropaolo, P. Staiti, J. Catal. 102 (1986) 190.

[30] F. Coloma, A. Sepúlveda-Escribano, J.L.G. Fierro, F. Rodríguez-Reinoso, Appl. Catal. A 136 (1996) 231.

[31] B. Coq, F. Figueras, C. Moreau, P. Moreau, M. Warawdekar, Catal. Lett. 22 (1993) 189.

[32] A. Taylor, B. Kagle, Crystallographic Data on Metal and Alloy Structures, Dover Publishing, New York, 1962

[33] M. Lucas, P. Claus, Chem. Eng. Technol. 28 (2005) 867.

[34] F. Haass, M. Bron, H. Fuess, P. Claus, Appl. Catal. A 318 (2007).

[35] N.F. Brown, M.A. Barteau, J. Am. Chem. Soc. 114 (1992) 4258.

[36] J.L. Davis, M.A. Barteau, J. Mol. Catal. 77 (1992) 109.

[37] J.C.d. Jesús, F. Zaera, Surf. Sci. 430 (1999) 99.

[38] M. Akita, N. Osaka, K. Itoh, Surf. Sci. 405 (1998) 172.

[39] K. Brandt, M.E. Chiu, D.J. Watson, M.S. Tikhov, R.M. Lambert, J. Am. Chem. Soc. 131 (2009) 17286.

[40] F. Delbecq, P. Sautet, J. Catal. 211 (2002) 398.

[41] K.H. Lim, Z.-X. Chen, K.M. Neyman, N. Rösch, Chem. Phys. Lett. 420 (2006) 60.

[42] K.H. Lim, A.B. Mohammad, I.V. Yudanov, K.M. Neyman, M. Bron, P. Claus, N. Rösch, J. Phys. Chem. C 113 (2009) 13231.

[43] R. Ferullo, M.M. Branda, F. Illas, J. Phys. Chem. Lett. 1 (2010) 2546.

[44] N.A. Bhore, M.T. Klein, K.B. Bischoff, Ind. Eng. Chem. Res. 29 (1990) 313.

[45] P. Claus, H. Hofmeister, J. Phys. Chem. B 103 (1999) 2766.

[46] R. Malathi, R.P. Viswanath, Appl. Catal. A 208 (2001) 323.

[47] G. Kyriakou, M.B. Boucher, A.D. Jewell, E.A. Lewis, T.J. Lawton, A.E. Baber, H.L. Tierney, M. Flytzani-Stephanopoulos, E.C.H. Sykes, Science 335 (2012) 1209.

[48] Y.Y. Yeo, L. Vattuone, D.A. King, J. Chem. Phys. 106 (1997) 392.

[49] H. Wei, C. Gomez, R. Meyer, Top. Catal. 55 (2012) 313.

[50] W.O. Haag, R.M. Lago, P.B. Weisz, Nature 309 (1984) 589.

[51] I.J. Shannon, T. Maschmeyer, R.D. Oldroyd, G. Sankar, J.M. Thomas, H. Pernot, J.-P. Balikdjian, M. Che, J. Chem. Soc., Faraday Trans. 94 (1998) 1495.

[52] N. Schumacher, A. Boisen, S. Dahl, A.A. Gokhale, S. Kandoi, L.C. Grabow, J.A. Dumesic, M. Mavrikakis, I. Chorkendorff, J. Catal. 229 (2005) 265.

[53] N. Iwasa, S. Kudo, H. Takahashi, S. Masuda, N. Takezawa, Catal. Lett. 19 (1993).

[54] N. Iwasa, S. Masuda, N. Ogawa, N. Takezawa, Appl. Catal. A 125 (1995).

[55] Z.-X. Chen, K.M. Neyman, A.B. Gordienko, N. Rösch, Phys. Rev. B 68 (2003) 075417.

[56] J. Regalbuto, Catalyst Preparation: Science and Engineering CRC Press, Boca Raton, Fl, 2006, p279.

[57] Y. Lei, J. Jelic, L.C. Nitsche, R. Meyer, J. Miller, Top. Catal. 54 (2011) 334.

[58] T. Miyamoto, H. Niimi, Y. Kitajima, T. Naito, K. Asakura, J. Phys. Chem. A 114 (2010) 4093.

[59] J. Hohmeyer, E.V. Kondratenko, M. Bron, J. Kröhnert, F.C. Jentoft, R. Schlögl, P. Claus, J. Catal. 269 (2010) 5.

[60] A.B. Mohammad, K.H. Lim, I.V. Yudanov, K.M. Neyman, N. Rösch, Phys. Chem. Chem. Phys. 9 (2007) 1247.

[61] A.B. Mohammad, I.V. Yudanov, K.H. Lim, K.M. Neyman, N. Rösch, J. Phys. Chem. C 112 (2008) 1628.

[62] N.A. Bhore, M.T. Klein, K.B. Bischoff, Chem. Eng. Sci. 45 (1990) 2109.

[63] T.B.L.W. Marinelli, V. Ponec, J. Catal. 156 (1995) 51.

[64] N.A. Khan, S. Shaikhutdinov, H.J. Freund, Catal. Lett. 108 (2006) 159.

[65] Y.M. Jin, A.K. Datye, E. Rightor, R. Gulotty, W. Waterman, M. Smith, M. Holbrook, J. Maj, J. Blackson, J. Catal. 203 (2001) 292.

[66] A. Borodzinski, G.C. Bond, Cat. Rev. Sci. Eng. 48 (2006) 91.

[67] H. Wei, C. Gomez, J. Liu, N. Guo, T. Wu, R. Lobo, C.L. Marshall, J.T. Miller, R. Meyer, J. Catal. accepted (2012).

[68] S.J. Tauster, S.C. Fung, R.L. Garten, J. Am. Chem. Soc. 100 (1978) 170.

[69] B. Coq, P.S. Kumbhar, C. Moreau, P. Moreau, M.G. Warawdekar, J. Mol. Catal. 85 (1993) 215.

[70] M.A. Vannice, C. Sudhakar, J. Phys. Chem. 88 (1984) 2429.

[71] B. Sen, M.A. Vannice, J. Catal. 113 (1988) 52.

[72] M.A. Vannice, B. SEN, J. Catal. 115 (1989) 65.

[73] M.A. Vannice, J. Vasco-Jara, Metal-Support and Metal Additive Effects in Catalysis, Elsevier, Amsterdam, 1982, p. 185.

[74] J. Hidalgo-Carrill, M.A. Aramend á, A. Marinas, J.M. Marinas, F.J. Urbano, Appl. Catal. A 385 (2010) 190.

[75] M. Englisch, A. Jentys, J.A. Lercher, J. Catal. 166 (1997) 25.

[76] A. Chambers, S.D. Jackson, D. Stirling, G. Webbz, J. Catal. 168 (1997) 301.

[77] M. Consonni, D. Jokic, D.Y. Murzin, R. Touroude, J. Catal. 188 (1999) 165.

[78] C. Milone, R. Ingoglia, L. Schipilliti, C. Crisafulli, G. Neri, S. Galvagno, J. Catal. 236 (2005) 80.

[79] C. Milone, C. Crisafulli, R. Ingoglia, L. Schipilliti, S. Galvagno, Catal. Today 122 (2007) 341.

[80] J.H. Larsen, J.T. Ranney, D.E. Starr, J.E. Musgrove, C.T. Campbell, Phys. Rev. B 63 (2001) 195410.

[81] J.A. Farmer, J.H. Baricuatro, C.T. Campbell, J. Phys. Chem. C 114 (2010) 17166.

[82] C.T. Campbell, J.C. Sharp, Y.X. Yao, E.M. Karpb, T.L. Silbaughb, Faraday Discuss. 152 (2011) 227.

[83] C. Gomez, H. Wei, R.J. Meyer, in preparation.

[84] J.H. Sinfelt, Sci. Am. 253 (1985) 90.

[85] A. Gross, Top. Catal. 37 (2006) 29.

[86] N. Schweitzer, H. Xin, E. Nikolla, S. Linic, J. Miller, 53 (2010) 348.

[87] P. Reyes, G. Pecchi, J.L.G. Fierro, Langmuir 17 (2001) 522.

[88] F. Delbecq, P. Sautet, J. Catal. 220 (2003) 115.

[89] J. Haubrich, D. Loffreda, F. Delbecq, P. Sautet, A. Krupski, C. Becker, K. Wandelt, J. Phys. Chem. C 113 (2009) 13947.

[90] L.E. Murillo, A.M. Goda, J.G. Chen, J. Am. Chem. Soc. 129 (2007) 7101.

[91] L.E. Murillo, C.A. Menning, J.G. Chen, J. Catal. (2009) 335.

[92] H.L. Tierney, A.E. Baber, E.C.H. Sykes, J. Phys. Chem. C 113 (2009) 7246.

[93] H.L. Tierney, A.E. Baber, J.R. Kitchin, E.C.H. Sykes, Phys. Rev. Lett. 103 (2009) 246102.

[94] A.E. Baber, H.L. Tierney, T.J. Lawton, E.C.H. Sykes, Chem. Cat. Chem. 3 (2011) 607.

[95] L. Jiao, J.R. Regalbuto, J. Catal. 260 (2008) 329.

[96] D. Loffreda, F. Delbecq, F. Vigne, P. Sautet, J. Am. Chem. Soc. 128 (2006) 1316.

[97] A. Andresen, H.G. Cordes, J. Herwig, W. Kaminsky, A. Merk, R. Mottweiler, J. Pein, H. Sinn, H.J. Vollmer, Angew. Chem. Int. Ed. Engl. 15 (1976) 630.

[98] J.M. Thomas, R. Raja, D.W. Lewis, Angew. Chem. Int. Ed. 44 (2005) 6456.

[99] P. McMorn, G.J. Hutchings, Chemical Society Reviews 33 (2004) 108.

[100] P.R. Likhar, M. Roy, S. Roy, M.S. Subhas, M.L. Kantam, B. Sreedhar, Adv. Synth. Catal 350 (2008) 1968.

[101] B.V. Berlo, K. Houthoofd, B.F. Sels, P.A. Jacobs, Adv. Synth. Catal 350 (2008) 1949.

[102] I. Karamé, M. Boualleg, J.-M. Camus, T.K. Maishal, J. Alauzun, J.-M. Basset, C. Copéret, R.J.P. Corriu, E. Jeanneau, A. Mehdi, C. Reyé, L. Veyre, C. Thieuleux, Chem. Eur. J. 15 (2009) 11802.

[103] H. Yang, H. Gao, R.J. Angelici, Organometallics 19 (2000) 622.

[104] J.M. Thomas, Z. Saghi, P.L. Gai, Top. Catal. 54 (2011) 588.

[105] C. Copéret, M. Chabanas, R.P. Saint-Arroman, J.-M. Basset, Angew. Chem. Int. Ed. 42 (2003) 156.

[106] M.W. McKittrick, C.W. Jones, J. Am. Chem. Soc. 126 (2004) 3052.

[107] S. Dzwigaj, M. Che, Catal. Today 169 (2011) 232.

[108] A. Corma, H. Garcia, Adv. Synth. Catal 348 (2006) 1391.

[109] C.P. Nicholas, H.S. Ahn, T.J. Marks, J. Am. Chem. Soc. 125 (2003) 4325.

[110] D. Gajan, C. Copéret, New. J. Chem. 35 (2011) 2403.

[111] M.A. Barteau, J.E. Lyons, I.K. Song, J. Catal. 216 (2003) 236.

[112] M. Bron, D. Teschner, U. Wild, B. Steinhauer, A. Knop-Gericke, C. Volckmar, A. Wootsch, R. Schlögl, P. Claus, Appl. Catal. A 341 (2008) 127.

[113] H.-J. Freund, M. Bäumer, J. Libuda, T. Risse, G. Rupprechter, S. Shaikhutdinov, J. Catal. 216 (2003) 223.

[114] A. Hock, in preparation.

[115] P.A. Chase, T. Jurca, D.W. Stephan, Chem. Comm. (2008) 1701.

[116] A.A. Gokhale, J.A. Dumesic, M. Mavrikakis, J. Am. Chem. Soc. 130 (2008) 1402.

[117] R. Farrauto, S. Hwang, L. Shore, W. Ruettinger, J. Lampert, T. Giroux, Y. Liu, O. Ilinich, Annu. Rev. Mater. Res. 33 (2003) 1.

[118] C. Ratnasamy, J.P. Wagner, Catal. Rev. 51 (2009) 325.

[119] D.C. Grenoble, M.M. Estadt, D.F. Ollis, J. Catal. 67 (1981) 90.

[120] M.L. Cubeiro, J.L.G. Fierro, J. Catal. 179 (1998) 150.

[121] Y.-H. Chin, R. Dagle, J. Hu, A.C. Dohnalkova, Y. Wang, Catal. Today 77 (2002) 79.

[122] K.M. Neyman, K.H. Lim, Z.-X. Chen, L.V. Moskaleva, A. Bayer, A. Reindl, D. Borgmann, R. Denecke, H.-P. Steinrück, N. Rösch, Phys.Chem.Chem.Phys. 9 (2007) 3470.

[123] K.H. Lim, Z.-X. Chen, K.M. Neyman, N. Rösch, J. Phys. Chem. B 110 (2006) 14890.

[124] Z.-X. Chen, K.M. Neyman, A.B. Gordienko, N. Rösch, Phys. Rev. B 68 (2003) 075417.

[125] Z.-X. Chen, K.H. Lim, K.M. Neyman, N. Rösch, Phys. Chem. Chem. Phys. 6 (2004) 4499.

[126] K.M. Neyman, R. Sahnoun, C. Inntam, S. Hengrasmee, N. Rösch, J. Phys. Chem. B 108 (2004) 5424.

[127] Z.-X. Chen, K.M. Neyman, N. Rösch, Surf. Sci. 548 (2004) 291.

[128] Z.-X. Chen, K.M. Neyman, K.H. Lim, N. Rösch, Langmuir 20 (2004) 8068.

[129] Z.-X. Chen, K.H. Lim, K.M. Neyman, N. Rösch, J. Phys. Chem. B 109 (2005) 4568.

[130] K.H. Lim, L.V. Moskaleva, N. Rösch, Chem. Phys. Chem. 7 (2006) 1802.

[131] L. Bollmann, J. Ratts, A.M. Joshi, W.D. Williams, J. Pazmino, Y.V. Joshi, J.T. Miller, A.J. Kropf, W.N. Delgass, F.H. Ribeiro, J. Catal. 257 (2008) 43.

[132] R.A. Dagle, A. Platon, D.R. Palo, A.K. Datye, J.M. Vohs, Y. Wang, Appl. Catal. A 342 (2008) 63.

[133] F. Studt, F. Abild-Pedersen, T. Bligaard, R.Z. Sørensen, C.H. Christensen, J.K. Nørskov, Science 320 (2008) 1320.

[134] J.K. Nørskov, T. Bligaard, J. Rossmeisl, C.H. Christensen, Nature Chem. 1 (2009) 37.

[135] C. Rhodes, G.J. Hutchings, A.M. Ward, Catal. Today 23 (1995) 43.

[136] L.C. Grabow, A.A. Gokhale, S.T. Evans, J.A. Dumesic, M. Mavrikakis, J. Phys. Chem. C 112 (2008) 4608.

[137] P. Liu, J.A. Rodriguez, J. Chem. Phys. 126 (2007) 164705.

[138] Y. Chen, J. Cheng, P. Hu, H.F. Wang, Surf. Sci. 602 (2008) 2828.

[139] S.D. Senanayake, D. Stacchiola, P. Liu, C.B. Mullins, J. Hrbek, J.A. Rodriguez, J. Phys. Chem. C 113 (2009) 19536.

[140] R. Burch, Phys. Chem. Chem. Phys. 8 (2006) 5483.

[141] F.C. Meunier, D. Tibiletti, A. Goguet, S. Shekhtman, C. Hardacre, R. Burch, Catal. Today 126 (2007) 143.

[142] D. Tibiletti, F.C. Meunier, A. Goguet, D. Reid, R. Burch, M. Boaro, M. Vicario, A. Trovarelli, J. Catal. 244 (2006) 183.

[143] G. Kresse, J. Furthmuller, Phys. Rev. B 54 (1996) 11169.

[144] J.P. Perdew, Y. Wang, Phys. Rev. B 45 (1992) 13244.

[145] P.E. Blöchl, Phys. Rev. B 45 (1994) 17953.

[146] H.J. Monkhorst, J.D. Pack, J. Phys. Chem. B 13 (1976) 5188.

[147] G. Henkelman, B.P. Uberuaga, H. Jónsson, J. Chem. Phys. 113 (2000) 9901.

[148] Y. Huang, Z.-X. Chen, J. phys. Chem. C 115 (2011) 18752.

[149] P.J. Feibelman, Science 295 (2002) 99.

[150] F.C. Meunier, D. Reid, A. Goguey, S. Shekhtman, C. Hardacre, R. Burch, W. Deng, M.F. Stephanopoulos, J. Catal. 247 (2007) 277.

[151] F.C. Meunier, A. Goguet, C. Hardacre, R. Burch, D. Thompsett, J. Catal. 252 (2007) 18.

[152] C. Stegelmann, A. Andreasen, C.T. Campbell, J. Am. Chem. Soc. 131 (2009) 8077.

[153] C.T. Campbell, J. Catal. 204 (2001) 520.

[154] C. Stegelmann, N.C. Schiodt, C.T. Campbell, P. Stoltze, J. Catal. 221 (2004) 630.

[155] R.J. Madon, D. Braden, S. Kandoi, P. Nagel, M. Mavrikakis, J.A. Dumesic, J. Catal. 281 (2011) 1.

[156] A.A. Phatak, W.N. Delgass, F.H. Ribeiro, W.F. Schneider, J. Phys. Chem. C 113 (2009) 7269.

[157] P. Nash, Y.Y. Pan, Bull Alloy Phase Diagr 8 (1987) 422.

[158] P. Claus, Appl. Catal. A 291 (2005) 229.

NAME: Haojuan Wei

EDUCATION: Ph.D., Chemical Engineering, University of Illinois at Chicago, Chicago, Illinois, 2013

M.S., Physical Chemistry, Nanjing University, Nanjing, Jiangsu, China, 2007

B.S., Chemistry, Nanjing University, Nanjing, Jiangsu, China, 2004

PRESENTATIONS: 243rd ACS National Meeting, San Diego, CA, 2012.

22nd North American Catalysis Society Meeting, Detroit, MI, 2011.

Symposium of Catalysis Club of Chicago, Chicago, IL, 2011.

13th National Conference on Catalysis of China, Lanzhou, Gansu, China, 2006.

PROFESSIONAL   American institute of chemical engineers (AICHE)

MEMBERSHIP: American chemical society (ACS)

Catalysis club of Chicago (CCC)

PUBLICATIONS: H. Wei, C. Gomez, J. Liu, R. Meyer, N. Guo, T. Wu, R. Lobo, C.L. Marshall and J.T. Miller, Selective hydrogenation of acrolein on supported silver catalysts: a kinetic study of particle size effect, 298 (2013) 18.

C.-K. Lin, Y.-G. Lin, T. Wu, H.M. Barkholtz, Q. lin, H. Wei, D.L. Brewe, J.T. Miller, D.J. Liu, Y. Ren, Y. Ito, T. Xu, Direct synthesis of bimetallic Pd_3Ag nanoalloys from bulk Pd_3Ag alloy, Inorganic Chemistry, 51 (2012) 13281.

H. Wei, C. Gomez and R. Meyer, A comparative density functional theory study of water gas shift over PdZn(111) and NiZn(111), Topics in Catalysis, 55 (2012) 313.

H.-J. Wei, Y. Cao, W.-J. Ji, and C. T. Au, Lattice oxygen of $La_{1-x}Sr_xMO_3$ (M = Mn, Ni) and $LaMnO_{3-\alpha}F_\beta$ perovskite oxides for the partial oxidation of methane to synthesis gas, Catalysis Communications, 9 (2008) 2509.